



National Library
of Canada

Acquisitions and
Bibliographic Services Branch

395 Wellington Street
Ottawa, Ontario
K1A 0N4

Bibliothèque nationale
du Canada

Direction des acquisitions et
des services bibliographiques

395, rue Wellington
Ottawa (Ontario)
K1A 0N4

Your file *Votre référence*

Our file *Notre référence*

NOTICE

The quality of this microform is heavily dependent upon the quality of the original thesis submitted for microfilming. Every effort has been made to ensure the highest quality of reproduction possible.

If pages are missing, contact the university which granted the degree.

Some pages may have indistinct print especially if the original pages were typed with a poor typewriter ribbon or if the university sent us an inferior photocopy.

Reproduction in full or in part of this microform is governed by the Canadian Copyright Act, R.S.C. 1970, c. C-30, and subsequent amendments.

AVIS

La qualité de cette microforme dépend grandement de la qualité de la thèse soumise au microfilmage. Nous avons tout fait pour assurer une qualité supérieure de reproduction.

S'il manque des pages, veuillez communiquer avec l'université qui a conféré le grade.

La qualité d'impression de certaines pages peut laisser à désirer, surtout si les pages originales ont été dactylographiées à l'aide d'un ruban usé ou si l'université nous a fait parvenir une photocopie de qualité inférieure.

La reproduction, même partielle, de cette microforme est soumise à la Loi canadienne sur le droit d'auteur, SRC 1970, c. C-30, et ses amendements subséquents.

University of Alberta

Fatigue of Riveted Tension Members

by

Jeffrey David DiBattista



A thesis submitted to the Faculty of Graduate Studies and Research in partial fulfillment of
the requirements for the degree of Master of Science

in

Structural Engineering

Department of Civil Engineering

Edmonton, Alberta

Fall 1995



National Library
of Canada

Bibliothèque nationale
du Canada

Acquisitions and
Bibliographic Services Branch

Direction des acquisitions et
des services bibliographiques

395 Wellington Street
Ottawa, Ontario
K1A 0N4

395, rue Wellington
Ottawa (Ontario)
K1A 0N4

Your file *Votre référence*

Our file *Notre référence*

THE AUTHOR HAS GRANTED AN IRREVOCABLE NON-EXCLUSIVE LICENCE ALLOWING THE NATIONAL LIBRARY OF CANADA TO REPRODUCE, LOAN, DISTRIBUTE OR SELL COPIES OF HIS/HER THESIS BY ANY MEANS AND IN ANY FORM OR FORMAT, MAKING THIS THESIS AVAILABLE TO INTERESTED PERSONS.

L'AUTEUR A ACCORDE UNE LICENCE IRREVOCABLE ET NON EXCLUSIVE PERMETTANT A LA BIBLIOTHEQUE NATIONALE DU CANADA DE REPRODUIRE, PRETER, DISTRIBUER OU VENDRE DES COPIES DE SA THESE DE QUELQUE MANIERE ET SOUS QUELQUE FORME QUE CE SOIT POUR METTRE DES EXEMPLAIRES DE CETTE THESE A LA DISPOSITION DES PERSONNE INTERESSEES.

THE AUTHOR RETAINS OWNERSHIP OF THE COPYRIGHT IN HIS/HER THESIS. NEITHER THE THESIS NOR SUBSTANTIAL EXTRACTS FROM IT MAY BE PRINTED OR OTHERWISE REPRODUCED WITHOUT HIS/HER PERMISSION.

L'AUTEUR CONSERVE LA PROPRIETE DU DROIT D'AUTEUR QUI PROTEGE SA THESE. NI LA THESE NI DES EXTRAITS SUBSTANTIELS DE CELLE-CI NE DOIVENT ETRE IMPRIMES OU AUTREMENT REPRODUITS SANS SON AUTORISATION.

ISBN 0-612-06464-6

Canada


University of Alberta

Library Release Form

Name of Author: Jeffrey D. DiBattista
Title of Thesis: Fatigue of Riveted Tension Members
Degree: Master of Science
Year This Degree Granted: 1995

Permission is hereby granted to the University of Alberta Library to reproduce single copies of this thesis and to lend or sell such copies for private, scholarly, or scientific research purposes only.

The author reserves all other publication and other rights in association with the copyright in the thesis, and except as hereinbefore provided, neither the thesis nor any substantial portion thereof may be printed or otherwise reproduced in any material form whatever without the author's prior written permission.




53 Baxter Crescent
Thorold, Ontario
Canada
L2V 4S1

September 29/95


University of Alberta

Faculty of Graduate Studies and Research

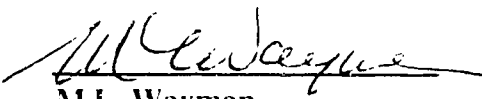
The undersigned certify that they have read, and recommended to the Faculty of Graduate Studies and Research for acceptance, a thesis entitled Fatigue of Riveted Tension Members submitted by Jeffrey David DiBattista in partial fulfillment of the requirements for the degree of Master of Science in Structural Engineering.



G.L. Kulak, Supervisor



G.Y. Grondin



M.L. Wayman

1995.09.26

To my family

Abstract

Economic factors often require that old riveted bridges function longer than originally anticipated. Although current standards indicate that many riveted bridges have exceeded their theoretical fatigue design lives, it is known that this conclusion is often conservative. An improved understanding of the fatigue behaviour of riveted connections is required so that costly premature bridge repairs can be avoided and an appropriate level of safety can be maintained.

Fatigue tests were conducted on full-scale riveted tension diagonals taken from a railway bridge. The experimentation showed that connections in which rivets are subject to bearing have reduced fatigue strength, and that the effect of staggered rivet patterns is significant. The members tested exceeded the fatigue strength of the American Railway Engineering Association Category D. Structural models for the bridge, assessed through comparison with measured strains, showed that a simple truss model can be used to provide an adequate description of the behaviour of the diagonals for use in the calculation of remaining fatigue life. An effective technique for the repair of fatigue cracks in this type of member was also developed.

Acknowledgements

This study was conducted with the financial assistance of the Natural Sciences and Engineering Research Council of Canada.

The author acknowledges financial support from the Natural Sciences and Engineering Research Council of Canada, the Canadian Institute for Steel Construction, Alberta Region, the Department of Civil Engineering of the University of Alberta, and the Faculty of Graduate Studies of the University of Alberta.

The technicians of the Department of Civil Engineering of the University of Alberta have been instrumental in the successful completion of this study.

Thanks are extended to Dr. Panagiotis Papanikolas, of Waiward Steel Limited, Edmonton, who helped to develop the conceptual design for the loading system. Dr. Peter Kunz, a Post-Doctoral Fellow in the Department of Civil Engineering of the University of Alberta, gave valuable insight for the design of the loading system. Mr. Daniel Adamson provided continual advice related to all aspects of the experimentation. Dr. Gilbert Grondin gave valuable assistance in the analysis of the crack surfaces, and made revisions to both the technical content and style of the report. Dr. Michael Yam was a valuable consultant. and my discussions with him on many topics led to the generation of new ideas. My fellow graduate student Mr. Andrew Boucher was tireless in his enthusiasm to help remove and install the specimens in the load frame.

I would like to thank my advisor, Dr. Geoffrey Kulak, who spent long hours reviewing my work. Finally, I want to thank my wife, Traci, who provided encouragement and support throughout.

Table of Contents

1. Introduction	1
1.1 Fatigue of Metal	1
1.2 Statement of the Problem.....	2
1.3 Research Needs	3
1.3.1 Study of Fatigue Strength	3
1.3.2 Methods of Predicting Remaining Fatigue Life	4
1.4 Scope and Objectives	4
2. Literature Survey.....	6
2.1 Introduction to Fatigue.....	6
2.1.1 History of Fatigue and Riveted Connections.....	6
2.1.2 Principal Variables Controlling Fatigue Life	6
2.2 Field Strain Measurements and Analytical Models.....	8
2.3 Fatigue Testing of Riveted Connections and Members	11
2.3.1 Tests of Small-Scale Specimens.....	11
2.3.2 Tests of Full-Scale Specimens.....	13
2.3.2.1 Tension Tests.....	14
2.3.2.2 Flexural Tests	15
2.4 Remaining Fatigue Life of Existing Structures	18
2.4.1 Standard Methods of Calculating Fatigue Damage	18
2.4.2 Current Code Requirements	21
2.4.3 Alternative Methods of Fatigue Evaluation.....	26
3. Development of Structural Models.....	34
3.1 The Need for Models.....	34
3.2 Description of the Case Study Bridge.....	34
3.3 Field Strain Measurements	35
3.4 Structural Models	37
3.4.1 <i>Simple Truss Model</i>	37
3.4.2 <i>Space Frame Model</i>	37
3.5 Simulation of Trains	38
3.5.1 <i>Train Simulation Algorithm</i>	38
3.6 Method of Comparison of Measured Strains with Simulated Strains	39
3.6.1 <i>Effective Strain Range Algorithm</i>	41
3.7 Results of Comparison of Measured Strains with Simulated Strains.....	42
3.7.1 Importance of Filtering	42
3.7.2 Comparison of Filtered Records	43

4. Experimental Program.....	65
4.1 Goals of the Test Program.....	65
4.2 Description of Test Specimens	65
4.3 Preparation of Test Specimens	67
4.3.1 Locations of Critical Details	67
4.3.2 Preparation of Specimens	68
4.3.3 Ancillary Tests.....	69
4.4 Load System.....	70
4.4.1 End Connections.....	70
4.4.2 Control and Data Acquisition	71
4.5 Test Procedure.....	72
4.5.1 Inspection for Cracks	73
4.5.2 Repair of Cracks	73
4.6 Post Test Examination	74
4.6.1 Examination of Fatigue Crack Surfaces.....	74
4.6.2 Examination of Rivets.....	74
5. Experimental Results.....	84
5.1 General Observations from Fatigue Tests.....	84
5.2 Fatigue Test Results	85
5.2.1 Behaviour of BD Series Specimens.....	86
5.2.2 Behaviour of TD Series Specimens	88
5.3 Discussion of Results	90
5.3.1 BD Series	90
5.3.2 TD Series.....	91
5.3.2.1 Effect of Web-Angle Rivet Holes	91
5.3.2.2 Effect of Clamping Force.....	94
5.4 Examination of Crack Surfaces	94
5.5 Examination of Riveted Joints	95
6. Prediction of Remaining Fatigue Life.....	103
6.1 Scope.....	103
6.2 Methods used to Evaluate Remaining Fatigue Life	104
6.3 Method of Calculation	105
6.4 Calculation of Remaining Fatigue Life for Diagonals.....	107
6.4.i Traffic Model.....	108
6.5 Results of Evaluation of Remaining Fatigue Life	109
7. Discussion	114
7.1 Literature and Current Standards.....	114

7.1.1 Experimental Studies of Full-Scale Riveted Specimens	114
7.2 Interpretation of Experimental Results	114
7.3 Performance of Structural Models	115
7.3.1 <i>Simple Truss</i> and <i>Space Frame</i> Models	115
7.3.2 Comparison with Results of Others	117
7.4 Fatigue Tests of Full-Scale Riveted Members	118
7.4.1 Experimental Results	118
7.4.2 Suitability of Failure Criterion	121
7.4.3 Effectiveness of Repair	121
7.4.4 Comparison of Results with the Work of Others	122
7.5 Prediction of Remaining Fatigue Life	124
8. Summary, Conclusions, and Recommendations	130
8.1 Summary	130
8.2 Conclusions	131
8.3 Recommendations	132
Appendix A - Details of Trains T730, F430, F658, and F717	137
Appendix B - Space Frame Model Details	146
Appendix C - Train Simulation Algorithm, Effective Strain Range Algorithm	151
Appendix D - Results of Tension Coupon Tests	157
Appendix E - Crack Tip Location Observations	159

List of Tables

Table 3.1 Comparison of Measured Strains to Predicted Strains for Diagonal D1	45
Table 5.1 Experimental Results.....	97
Table 6.1 Composition of Typical Trains	111
Table 6.2 Typical Traffic Patterns in Trains per Year	111
Table 6.3 Summary of Remaining Fatigue Life Calculation Parameters	112
Table 7.1 Prediction of Fatigue Test Results by AREA and Kunz Methods	126
Table D.1 Tension Coupon Test Results	158

List of Figures

Figure 2.1 Typical Fatigue Strength Curves.....	29
Figure 2.2 Results from Literature	30
Figure 2.3 AREA Fatigue Strength Curves for Riveted Details.....	31
Figure 2.4 AASHTO Variable Amplitude Fatigue Strength Curves	31
Figure 2.5 Eurocode 3 Fatigue Strength Curves for Detail Category 69	32
Figure 2.6 Crack Propagation Rate versus Stress Intensity Factor Range	32
Figure 2.7 Typical Fatigue Strength Curve with Transition Region for Kunz Method.....	33
Figure 3.1 Bridge in Service.....	46
Figure 3.2 Elevations of Trusses	47
Figure 3.3 Views of Diagonal D1	48
Figure 3.4 Locations of Strain Gauges	49
Figure 3.5 Influence Line for Axial Force in Diagonal D1 (Eastbound Unit Load).....	50
Figure 3.6 <i>Space Frame</i> Model.....	51
Figure 3.7 Influence Line for Bending Moment in Diagonal D1 (Eastbound Unit Load) Calculated Using the <i>Space Frame</i> Model.....	52
Figure 3.8 Measured and Predicted Strains in Diagonal D1, South Flange (Train T720)	53
Figure 3.9 Measured and Predicted Strains in Diagonal D1, North Flange (Train F430)	54
Figure 3.10 Measured and Predicted Strains in Diagonal D1, South Flange (Train F430)	55
Figure 3.11 Measured and Predicted Strains in Diagonal D1, North Flange (Train F430)	56
Figure 3.12 Measured and Predicted Strains in Diagonal D1, Web (Train F658).....	57
Figure 3.13 Measured and Predicted Strains in Diagonal D1, North Flange (Train F658)	58
Figure 3.14 Measured and Predicted Strains in Diagonal D1, Web (Train F658).....	59
Figure 3.15 Measured and Predicted Strains in Diagonal D1, North Flange (Train F658)	60
Figure 3.16 Measured and Predicted Strains in Diagonal D1, Web (Train F717).....	61
Figure 3.17 Measured and Predicted Strains in Diagonal D1, North Flange (Train F717)	62
Figure 3.18 Measured and Predicted Strains in Diagonal D1, Web (Train F717).....	63
Figure 3.19 Measured and Predicted Strains in Diagonal D1, North Flange (Train F717)	64
Figure 4.1 Potential Locations of Fatigue Cracking.....	75
Figure 4.2 Critical Net Cross-Sectional Areas.....	76
Figure 4.3 Typical Fabrication Details, BD Series	77
Figure 4.4 Typical Fabrication Details, TD Series	78
Figure 4.5 Schematic of Load Frame	79
Figure 4.6 Details of Load Frame	80
Figure 4.7 Overall Test Setup	81
Figure 4.8 Rivets Replaced with Bolts to Prevent Cracking at Connection to Load Frame.....	82
Figure 4.9 Repair of Specimen BD3	83

Figure 5.1 Results of Experimental Program	98
Figure 5.2 Specimen BD2, Typical Severed Element at Failure, BD series	99
Figure 5.3 Specimen BD4, After Failure to Carry Applied Load	99
Figure 5.4 Specimen TD1, Typical Severed Element at Failure, TD series	100
Figure 5.5 Specimen TD1, Crack in Second Element	100
Figure 5.6 Gap Between Angle and Gusset Plate, Specimen TD3.....	101
Figure 5.7 Photomicrograph Showing Striations on Fracture Surface, Specimen BD2.....	102
Figure 5.8 Cross-section of Gusset-Angle Rivet	102
Figure 6.1 Influence Lines for Remaining Fatigue Life Calculations	113
Figure 7.1 Results from Literature Survey and Experimental Program.....	127
Figure 7.2 Results of Connections with Rivets Theoretically in Bearing	128
Figure 7.3 Results of Connections with Rivets Theoretically not in Bearing	129
Figure B.1 Node and Element Numbers	147
Figure E.1 Specimen BD1	160
Figure E.2 Specimen BD2	161
Figure E.3 Specimen BD3	162
Figure E.4 Specimen BD4	163
Figure E.5 Specimen TD1.....	164
Figure E.6 Specimen TD2.....	165
Figure E.7 Specimen TD3.....	166

List of Abbreviations and Symbols

Abbreviations

AASHTO	American Association of State Highway and Transportation Officials
AREA	American Railway Engineering Association
ASTM	American Society for Testing and Materials
ATLSS	Center for Advanced Technology of Large Structural Systems
CAFL	Constant Amplitude Fatigue Limit
CEN	European Committee for Standardisation
FCM	Fracture Critical Member
OFCM	Other than Fracture Critical Member
RMC	Root-Mean-Cube
RMS	Root-Mean-Square

Symbols

a	crack size
D	total fatigue damage
k	number of stress or strain ranges
m	slope of the fatigue strength curve
M	constant
n_i	number of cycles at stress or strain range level i
N	number of stress cycles
N_i	total number of variable amplitude stress or strain cycles
$Y(a)$	geometric factor
α	AREA effective stress range factor
ΔK	stress intensity factor range
ΔK_{th}	threshold stress intensity factor range
$\Delta \epsilon$	strain range
$\Delta \epsilon_e$	effective strain range
$\Delta \epsilon_i$	strain range at level i
$\Delta \sigma$	stress range
$\Delta \sigma_c$	constant amplitude fatigue limit stress range
$\Delta \sigma_e$	effective stress range
$\Delta \sigma_i$	stress range at level i
$\Delta \sigma_{th}$	threshold stress range

1. Introduction

1.1 Fatigue of Metal

Repeated application of stress can initiate and cause the propagation of microcracks in metal. These cracks can grow to macroscopic proportions with continued application of stress, and the whole process is known as fatigue. As fatigue cracks continue to propagate, the remaining cross-section of metal may eventually be reduced to such an extent that failure occurs.

Fatigue cracking is possible even if the maximum applied stress is below the elastic limit of the metal. A fatigue crack usually originates at a stress concentration, such as an existing flaw or an abrupt geometrical discontinuity in the material. While almost all metals can exhibit fatigue cracking, structural engineers are most often concerned with the fatigue properties of structural steel. The dominant variables that influence the fatigue strength of structural steel are the applied stress range, the number of cycles of applied stress, and the type of structural detail [Fisher, 1977].

Fatigue failures typically involve minimal amounts of plastic deformation. Consequently, it can be difficult to detect fatigue cracks before fracture of the remaining cross-section occurs. Many examples of catastrophic failures caused by fatigue cracking have been documented [Fisher, 1984], illustrating that structural engineers must have a firm understanding of the phenomenon of fatigue.

A fatigue fracture surface normally has three regions, each characteristic of distinct stages of the crack propagation [Fuchs and Stephens, 1980]. The first region, characterised by slow, stable crack growth, is typically smooth, possibly with a series of concentric striations known as “beach marks” centred at the crack nucleus. The second region is that of rapid crack growth, and the surface is less smooth. Finally, the third region is that of fracture, when the cross-section can no longer carry the applied load.

Many civil engineering structures, such as bridges or cranes, are required to withstand the effects of fatigue because of the nature of the moving or repeated loads that they must carry. Recent studies have provided the basis for the development of satisfactory procedures for the fatigue design of welded structural steel details. Procedures for the design of riveted and bolted connections have also been established, although less experimental research information is available. Generally, satisfactory rules exist for the design of new structural connections, but guidelines to account for fatigue in existing structures have not been as well established.

1.2 Statement of the Problem

From the middle of the nineteenth century until approximately 1960, most wrought iron and steel railway and highway bridges were constructed using rivets as the structural fastener. Many of these old bridges have endured millions of cycles of stress, and it is often essential that they continue to function for many years to come. The effects of fatigue damage in these structures must be considered in order to make the continued safe use of these bridges possible.

Riveted bridges often suffer from the effects of corrosion as they age. At the same time, the total number of cycles of applied stress to which they have been exposed increases. Additionally, riveted bridges must often carry increasing volumes of traffic and vehicles heavier than anticipated in their original designs. Consequently, many riveted structures are approaching or have reached the end of their theoretical fatigue design lives, requiring their replacement or renovation. This is most significant for railway bridges, which are generally subject to higher live loads than are highway bridges. It would be prohibitively expensive to attempt to replace or renovate all of these old bridges, as they number in the thousands in North America alone. Bridge owners, therefore, look to research for information enabling more accurate predictions of the remaining fatigue lives of their structures so that premature bridge repairs or replacements can be avoided, while at the same time maintaining adequate margins of safety.

1.3 Research Needs

Two primary areas of research are necessary in order to make accurate predictions of the fatigue life of riveted structures. First, experimental and theoretical knowledge of the fatigue strength of various steel details is required. Second, methods of predicting remaining fatigue life must be developed, including both consideration of existing damage due to past loads and future damage caused by forecasted loads.

1.3.1 Study of Fatigue Strength

Despite the large number of riveted bridges still in service, only limited research has been performed on riveted connections as compared to research on welded or bolted connections. Until recently, the absence of research can be attributed to a lack of appreciation for fatigue as a failure mode in the design of civil engineering structures. It was not until the 1960's that fatigue failure in welded structures prompted major interest in the study of fatigue. At the same time, the use of rivets in structural connections was ending, so riveted connections attracted minimal interest with researchers. More fatigue research of full-scale riveted specimens is required.

There are generally two categories into which riveted connections may be separated. The first category encompasses rivets that are principally loaded in shear, such as those in riveted shear splice connections or built-up flexural members that must carry moving loads. The rivets will likely impose substantial bearing stresses directly on the edges of their holes in these situations, although some load transfer between the joined parts might be through friction. The second category involves rivets that are not subject to substantial bearing, such as those that simply fasten the components of the cross-section of a built-up riveted tension member or a built-up riveted flexural member having a constant moment region. In this situation, the rivet is only nominally in shear, and the detail is simply one of a hole filled by a rivet. Most of the research performed to date has involved tests of built-up flexural members that have a constant moment region, where the rivets were theoretically not in bearing. However, in most real structures, rivets are generally subject

to shear stresses, so many of the tests performed to date do not correspond with most real riveted details. Consequently, more research on connections where the rivets are in bearing is required.

1.3.2 Methods of Predicting Remaining Fatigue Life

In order to be able to predict remaining fatigue life of a structure, it is necessary to estimate the stress history and to predict future stresses on critical details. This can only be accomplished by developing structural models and then calibrating these models with field strain measurements. Issues such as the degree of continuity of connections can greatly influence the stresses predicted at critical details, and these issues are often not easily addressed in structural models. There is a need to improve modelling techniques in order to better account for these effects.

Once stress ranges at critical details have been identified, several methods exist that allow an estimate of existing fatigue damage to be made and enable the prediction of the remaining fatigue lives of riveted structures. These include the equivalent stress range technique and the Kunz damage accumulation method, both of which are discussed later in this report. Results from these predictions of remaining fatigue life are generally very sensitive to small variations of input variables. More experimental data will improve both the quality of the predictions and the ability to assess the accuracy of methods of predicting remaining fatigue life.

1.4 Scope and Objectives

The scope and objectives of this study are to:

1. Review the existing literature on fatigue of riveted connections and on methods of predicting remaining fatigue life.
2. Develop a good structural model of a case study bridge, and verify the model with field strain measurements.

3. Investigate the fatigue strength of full-scale riveted shear splice connections.
4. Investigate the fatigue strength of full-scale riveted built-up members, in which the rivets are theoretically not in shear.
5. Establish appropriate failure criteria for the fatigue tests.
6. Develop a technique to repair cracked riveted steel shear splices and document the effectiveness of the technique.
7. Improve the database of information on which theoretical models of fatigue life expectancy are based.
8. Assess current methods of accounting for existing fatigue damage and predicting remaining fatigue life, using information obtained in this study.

2. Literature Survey

2.1 Introduction to Fatigue

2.1.1 History of Fatigue and Riveted Connections

The Industrial Revolution of the nineteenth century saw a rapid increase in the use of iron in many new applications. The use of iron in machines and civil engineering structures brought to light the problem of fatigue failure, and several examples have been documented by Petroski [1985]. These failures inspired the first classical studies of fatigue, which were carried out in the middle of the nineteenth century by Wöhler [Gordon, 1978]. Since then the importance of fatigue as a failure mode has become better understood, but it is only in about the last half century that significant research has led to reliable methods that account for fatigue in the design of structures.

Rivets were most commonly used as fasteners in the iron and steel structures of the nineteenth century and first half of the twentieth century. A significant investigation of fatigue of riveted connections began in 1938 with a study by Wilson and Thomas, which is one of several studies discussed later in this chapter. Results from these studies have generally indicated that the fatigue life expectancy of a riveted steel connection depends on the net section stress range, number of cycles of applied stress, and the geometric characteristics of the riveted detail.

2.1.2 Principal Variables Controlling Fatigue Life

Regardless of the type of connection or detail, the dominant variables related to the applied loads are the net section stress range and the number of cycles of applied stress [Fisher, 1977]. In general, the fatigue design rules and many of the formulas that model the behaviour of steel subject to fatigue loads are based on research of welded details. Experimental investigation of fatigue of riveted connections has generally shown that the behaviour of riveted connections is similar enough to that of welded details that the same set of design rules can be used for both types of details. Statements made in this chapter

about the behaviour of riveted connections are based on the underlying assumption that their behaviour is similar to that of welded details.

Net section stress range is defined as the algebraic difference between the maximum and minimum stress acting on the net area of the cross-section. As net section stress range increases, the number of cycles of load that may be applied decreases. This relationship is linear when each of stress range and number of cycles is expressed logarithmically, and the slope of this line is generally three.[†] A worst case condition occurs when both the maximum and minimum applied stresses are tensile, since it is tensile stress that promotes crack propagation. Various means are used to account for situations in which the minimum applied stress is compressive or both minimum and maximum applied stresses are compressive, as discussed by Kulak and Smith [1993].

In North American practice [American Railway Engineering Association, 1994; American Association of State Highway and Transportation Officials, 1990; Canadian Standards Association, 1989], the various structural details are categorized alphabetically: Category A has the greatest fatigue strength and Category F has the lowest fatigue strength. Within a given category, the relationship between log stress range and log number of cycles is linear with a slope of three, until a certain stress range is reached, below which there is no fatigue crack growth. Thus, there is also a horizontal portion in a plot of log stress range vs. log number of cycles. The stress range below which there is no fatigue crack growth is known as the *constant amplitude fatigue limit*. Typical fatigue strength design curves are presented in Figure 2.1, and they allow visualization of the relationship between the variables. These design curves and others will be described in more detail later in this chapter. The remainder of the chapter discusses the literature related to analytical structural modelling, fatigue tests of riveted specimens, and methods of predicting remaining fatigue life.

[†]Fatigue strength curves are typically plotted with log stress range on the vertical axis and log number of cycles until failure plotted on the horizontal axis. The resulting linear curves have a slope of negative 1/3. However, for simplicity, standard practice in the field of fatigue generally refers to the slope of this line as either negative 3, or, more simply, as 3. To maintain consistency with standard practice, the slope of a standard fatigue curve will be referred to as 3 for the remainder of this report.

2.2 Field Strain Measurements and Analytical Models

In order to evaluate the remaining fatigue life of a bridge, it is first necessary to make estimates of the past and future vehicle loads. Analytical structural models are then required that will enable the determination of the stress ranges at critical details. It is desirable to verify analytical results with actual bridge strain measurements, so as to calibrate the models and to ensure their accuracy. It has been shown in several studies that the results from analytical models can be extremely sensitive to factors such as the degree of continuity of connections, boundary conditions, and out-of-plane effects [Fisher and Daniels, 1976; Adamson, 1995].

Fisher and Daniels [1976] presented a case study of the stresses in a riveted railway bridge. The investigation principally involved analysis of stresses at hanger and stringer locations in the bridge, and the results were compared to measurements taken using strain gauges. A prediction of remaining fatigue life was also made.

Two analytical models were developed. The first model was a simple plane truss, that is, all truss connections were assumed to be pinned. Transfer of bending moment from the floorbeam to the hanger was included in the model to account for the interaction between the floor system and the truss. This type of simple model normally gives an upper bound solution to overall member stress resultants because the benefits of continuity of bending resistance in the system are ignored. The second model was a three-dimensional frame that used "...only major load-carrying members believed to have a significant influence on MILL [hanger] stress resultants..." All gusset joints were assumed to be continuous, and all actual pin connections were modelled as pinned. Loads applied to the structure in the analytical model were equivalent to those loads applied by special work trains that crossed the bridge during measurement of strains in the field.

Fisher and Daniels did not tabulate their results for the plane truss model, but they did present a chart in which strains predicted by the model are compared to measured strains. Although a quantitative comparison is not possible, the chart indicates that the predicted strain values were greater than the measured strain values. Results for the three-

dimensional model were tabulated, and the ratio of measured axial strains in the hangers to those strains predicted by the three-dimensional model ranged from 0.96 to 1.02. Although the correlation for axial strain was good, the ratio of measured major axis bending stress to predicted major axis bending stress was poor, with values ranging from 0.97 to 2.71. This generally poor correlation was attributed by the researchers to an eccentricity in the applied load on the hanger. The hangers were fastened by pins to the panel points of the truss, and it was found that the gussets were not bearing evenly on the pins, thereby causing eccentric loading. The authors advised that caution must be used when estimating stresses in elements with pin connections because of the possibility of uneven bearing.

The behaviour of a riveted railway truss bridge was also studied by Szeliski and Elkholy [1984]. Their study included measurement of strains in various portions of the bridge, including locations in the top and bottom chords, end posts, hangers, bracing, stringers, and floor beams. The hangers were gauged with as many as ten strain gauges so as to determine the influence of bending stresses. Three theoretical models were developed for the prediction of strains in the gauged members. These models were a plane simple truss model, a plane frame model with all joints assumed to be continuous, and a three-dimensional frame model in which all joints were assumed to be continuous. Results from the three models gave measured-to-predicted strain ratios of 0.913 to 1.142. This indicates that all three models yielded reasonably accurate results, regardless of the amount of continuity assumed to be present in the connections.

Adamson [1995] reported on the correlation between measured strains and analytical models of a riveted railway truss bridge built in 1911. Strains were measured in one diagonal and in one stringer for several trains that crossed the bridge. The loading and configuration of the trains were obtained from records kept by the railway. Three models, containing only the primary structural elements of the bridge, were developed, and these were designated *Pinned*, *Continuous*, and *Continuous-with-Springs*. Predicted strains from the models were compared to measurements made in the field through the

calculation of effective strain ranges. The calculation of effective strain ranges was based on a root-mean-cube effective stress range formulation, as described later in this chapter.

The *Pinned* model presented by Adamson [1995] was a simple plane truss, and it gave results for strains in the stringer significantly greater than those measured in the field. Because of the absence of the beneficial effects of continuity of bending resistance between members, it was considered to be an upper bound on the predicted strains. The ratio of measured effective strain range to predicted effective strain range varied from 0.66 to 0.86 for five different trains.

The *Continuous* model was a three-dimensional frame with all connections treated as completely continuous. This model also predicted strains in the stringer greater than those measured. The ratios of measured-to-predicted effective strain range ranged from 0.81 to 0.86. Adamson concluded that there was additional stiffness present in the system that was not present in the model, especially in the rails, ties, and bracing. Furthermore, the model tends to overestimate peak strains in the stringer, because axles were applied as concentrated loads in the model, but in the real structure axle loads tend to be distributed by the rails and ties.

The *Continuous-with-Springs* model was developed to try to account for the effects of additional stiffness in the system. This model incorporated rotational spring supports at the stringer to floorbeam connections as a way of representing the additional stiffness in the system caused by the minor structural elements that did not otherwise appear in the model. All springs had the same spring constant, which was adjusted to calibrate the model with strains measured in the field. The spring constant was adjusted so that the measured-to-predicted ratio for one of the five trains reached unity, and at the same time ratios for the other four trains did not exceed unity. The rotational spring stiffness chosen was 271 160 kN•m/radian, and this added stiffness gave measured-to-predicted effective strain range ratios of 0.92 to 1.00 for the five trains.

The same three models were also used by Adamson to predict strains in the diagonals of the bridge, although the *Continuous-with-Springs* model was developed specifically for

the stringers and is not applicable to the diagonal. It was concluded that the *Pinned* model gave satisfactory solutions for the values of strain in the diagonal, hence, the amount of continuity in the stringer–floorbeam connection in the models did not significantly influence the results for strain in the diagonal. Measured-to-predicted effective strain range ratios ranged from 0.72 to 1.01 for the *Pinned* model, and from 0.86 to 1.11 for the *Continuous* model. The models developed by Adamson did not consider the effects of bending of the diagonals, so all models predicted only average axial strain. Because the bridge in the study by Adamson is the same structure that is investigated in this report, modelling of the diagonals, including the effects of bending, will be examined further (Chapter 3).

2.3 Fatigue Testing of Riveted Connections and Members

There have been many studies that have investigated the fatigue behaviour of riveted connections, but only a small proportion of this research has involved full-scale specimens. These studies have been conducted to explore the effect of parameters such as rivet bearing ratio, rivet clamping force, and rivet grip length. However, almost all of these tests have been conducted using new, small-scale specimens. Few studies of large scale specimens have been identified, and there is only one study that specifically investigated the fatigue behaviour of full-scale riveted shear splices.

2.3.1 Tests of Small-Scale Specimens

An early study of small-scale riveted specimens was carried out by Wilson and Thomas [1938]. The effects of rivet grip length, clamping force, method of hole preparation, ratio of maximum stress to minimum stress, bearing ratio, and several other variables were investigated. The recommendations from this report led to further studies that identified the significance of these variables, some of which are discussed below.

It can be expected that a clamping force exists in connections containing pretensioned bolts or rivets. Clamping force is defined as the force between the contact surfaces of two fastened elements resulting from the presence of rivets or bolts. Equivalently, it is the

residual longitudinal tension in the rivets or bolts after installation. In riveted connections, clamping force is introduced during the rivet installation process. Structural rivets are produced with one preformed head and a cylindrical shank. To install a rivet, it is heated and the shank is then inserted into a hole. While the rivet still hot, the head is held to prevent movement and the protruding shank is driven to form a second head. As the rivet cools, shrinkage of the shank introduces tension in the rivet shank and compression in the pieces being joined. It has been found that the clamping force produced in this process can vary considerably, even among rivets in the same connection, because of variations of rivet installation temperature and driving pressure [Kulak *et al.*, 1987].

Lenzen [1950] found that the fatigue resistance of a riveted joint is directly proportional to the clamping force. Because of the variability in the installation process, the clamping force is considered to be a primary source of scatter in fatigue test data for riveted connections. In the study conducted by Lenzen, the fatigue strength of connections with high-strength pretensioned bolts, hot-driven rivets, and cold-driven rivets were compared. The study concluded that high clamping forces present in the bolted connections allowed more load to be transferred by friction between the joined parts rather than by bearing, and that this reduction in load transfer by bearing decreased the effect of stress concentrations. The clamping force also produces local compressive stresses around the hole, which discourages fatigue crack growth. High-strength pretensioned bolted connections had the highest fatigue strength, while connections made with cold-driven rivets, which have no appreciable clamping force, had the lowest.

Grip length is defined as the distance between the undersides of the heads of a rivet or bolt, or, equivalently, as the total thickness of the joined plies. A study conducted by Baron and Larson [1953] indicated that rivet grip length influences clamping force, and, thereby, fatigue strength. For hot-driven rivets, increased grip lengths led to higher average clamping forces, and, thus, higher fatigue strength. For long grip lengths, the deformation of the rivet head is a smaller portion of the total cooling shrinkage. Consequently, longer rivets generally have higher clamping forces. However, because of

variations in the riveting process as described above, the use of long grip lengths does not ensure high clamping forces.

The effect of bearing ratio was investigated by Parola *et al.* [1964]. Bearing ratio is defined as the bearing stress on the rivet shank divided by the average tensile stress on the net section of the connected element. These researchers found that fatigue strength increased as bearing ratio decreased. The explanation for this relationship was that the stress concentration caused by a bolt or rivet transferring load to a plate may be up to twice that caused by the hole alone, at least when stresses are in the elastic range. Local increases of stress due to bearing promote the formation and propagation of cracks.

Although clamping force, grip length, and bearing ratio are characteristics of riveted details that affect fatigue strength, other factors have been identified [Parola *et al.*, 1964; Wyly and Scott, 1956]. The degree to which a rivet fills its hole can affect local stress concentrations caused by bearing [Parola *et al.*, 1964]. If a rivet substantially fills a hole, the load transferred through the rivet to the plates is distributed more or less uniformly along sides of the hole. In cases where the rivet does not fill the hole well, greater stress concentrations, and thus greater bearing stresses, are present, thereby reducing fatigue strength. The erection process is another factor that may influence fatigue strength, as described by Wyly and Scott [1956]. When holes in parts that are to be joined by rivets are not in proper alignment, often a drift pin is used to bring the parts forcefully into alignment. Wyly and Scott concluded that use of a drift pin could be a potential cause of initial cracks at the hole, thereby reducing the fatigue strength.

2.3.2 Tests of Full-Scale Specimens

Only a few experimental studies have been performed to investigate the fatigue strength of full-scale riveted specimens. Two test programs on tension specimens and five test programs on flexural members have been identified. Of the tension tests, one was a study of rived shear splice connections and the other was a study of riveted details where the rivets were not in shear.

2.3.2.1 Tension Tests

Reemsnyder [1975] conducted full-scale fatigue tests on truss chords that had riveted gusset plate connections. The primary purpose of the investigation was to determine the effectiveness of repairs to cracked elements by means of replacement of rivets with pretensioned high-strength bolts. The members were built-up riveted box-beams composed of two channels, a flange plate on one side, and lattice bars on the fourth side. The web of each channel was riveted to a gusset plate. The critical detail (the detail having the highest net section stress range) was the web of the channel at the first line of rivets where it was connected to the gusset plate. The connection acted as a lap splice that transferred load primarily by shear in the rivets, although some load transfer undoubtedly occurred through friction. Sixteen tests were conducted on newly constructed full-scale models, and two tests were conducted on specimens removed from service from a riveted steel truss bridge. Most specimens were tested in constant amplitude loading with a stress that ranged from tension to compression. Two of the newly constructed specimens were subjected to variable amplitude loading. The failure criterion for the tests was the severing of one channel flange, and this occurred near the connection of the flange to the lattice bars. Of particular interest are the five tests that were conducted without any bolted repairs being made, and these results are presented in Figure 2.2. It should be noted that the stress range values for the Reemsnyder study in Figure 2.2 are calculated based on 60 % of the compressive stress and 100 % of the tensile stress. This was done in order to be consistent with the way Reemsnyder's results have been presented by others [Adamson, 1995; Fisher *et al.*, 1987; Fisher *et al.*, 1990].

Baker and Kulak [1982] examined hangers that were taken from a seventy-year-old riveted highway bridge. The hangers were built-up I-shaped members in which the flanges were two unequal leg angles (short legs back-to-back) and the web was a lattice of flat bars. Each lattice bar was fastened at each end to the pair of flange angles with a single rivet. In order to simplify testing, each hanger was first cut in half longitudinally through the lattice bars, giving two specimens. The specimens were tested in constant amplitude axial tension. Because the outstanding lattice bars remained free, the rivets were not

subjected to any shear force. An analysis of the history of the bridge determined that prior fatigue damage from service loads was negligible. The failure criterion was the complete severing of one of the flange angles. After each failure, testing of the remaining uncracked portion of the specimen was continued to allow cracking to develop at another location. The results are presented in Figure 2.2.

2.3.2.2 Flexural Tests

All of the tests discussed in this section were conducted in four-point bending, thereby creating a constant moment region. Generally, fatigue cracks started in the constant moment region, meaning the rivets in the region were not loaded in shear.

Out *et al.* [1984] published the results of tests on four built-up riveted railway bridge stringers. The configuration typically consisted of a web plate continuously riveted to a pair of angles that formed each flange. All stringers were tested in constant amplitude four-point bending, and the critical detail was the riveted connection joining the angles to the web. The stringers were significantly corroded, especially where cross-frames were riveted to the tension flanges. It was assumed that no existing fatigue damage was present in the specimens because strains measured in the stringers while the bridge was in service indicated that only about 1 % of the stresses were above the Category D endurance limit. While this assumption may not have been completely accurate, it should produce conservative results. Any existing damage caused by service loads would simply reduce the fatigue life recorded in a test. Failures were categorized into two groups, those caused primarily by the riveted detail and those caused primarily by corrosion. Of interest here are the three tests where failure was caused primarily by a riveted detail. For one of these tests, failure at a rivet detail was defined as severing of a flange angle by the fatigue crack. For the other two tests, a crack existed but was repaired before the angle was severed. The results are presented in Figure 2.2, and correspond to a net section stress range calculated taking into account the effect of corrosion upon the section properties.

Results of fatigue tests on stringers from a riveted railway bridge were reported by Fisher *et al.* [1987]. The report also included an extensive review of existing literature for data

from both small-scale and full-scale fatigue tests. Based on the literature review, it was concluded that most riveted details have approximately the same fatigue resistance, that Category D is a reasonable lower bound for the detection of cracks, and that Category C is a reasonable estimate of failure of the section as reflected by the loss of load-carrying capacity.

The stringers tested in fatigue by Fisher *et al.* had flanges made of angles continuously riveted to a web plate. The flanges also had riveted coverplates. The stringers were tested in constant amplitude four-point bending, and several of the tests were conducted at reduced temperatures. The coldest test took place at $-73\text{ }^{\circ}\text{C}$, and it was found that the low temperatures did not significantly affect the fatigue strength. Generally, the end of a coverplate causes a stress concentration, so one of the goals of the study was to determine the effect of cover plate terminations on fatigue strength. Terminations were created in the constant moment region by using an abrasive saw to cut gaps in the continuous cover plates. The testing revealed that most cracks originated at the web-to-angle riveted details, not at rivet holes at cover plate terminations. The tests corresponded well with comparable results taken from the literature review, and, again, Category D was judged to be appropriate for estimating initial crack detection and Category C appropriate as an estimate of loss of load-carrying capacity of the member. These data are also presented in Figure 2.2.

Brühwiler *et al.* [1990] tested riveted built-up plate girders, riveted lattice girders, and rolled mild steel girders. The rolled girders had coverplates riveted to the tension flange, and all of the tests were conducted in four-point bending. Unlike the failure criterion used in other full-scale flexural tests described in this literature review, Brühwiler *et al.* used one based on a deflection limit. When the maximum deflection of the girder increased by 0.2 mm, failure of the cross-section was assumed to be imminent and the test was stopped. In some of the tests, the load was changed if a fatigue crack had not appeared after 6 to 20 million cycles, in order to increase the stress range at the critical detail. The results from tests that were conducted at constant stress ranges are included in Figure 2.2.

Fisher *et al.* [1990] published a paper that reviewed fatigue data compiled in the Fisher *et al.* [1987] study and included new data from the Brühwiler *et al.* [1990] study. The conclusions in the Fisher *et al.* [1990] paper remained substantially the same as those in the 1987 report. Again, it was judged that Category D is a reasonable lower bound for the detection of cracks and that Category C is appropriate as the fatigue strength criterion for riveted members. All of the data reviewed generally indicated that cracking only occurred when net section stress ranges exceeded those described by Category D. Even after initial cracking or severing of elements, members were able to continue to carry the applied load because of redistribution of loads to other elements of the built-up cross-sections. It was also concluded that most fatigue problems experienced with bridges in service occurred because of secondary stresses or from out-of-plane bending, since field measurements of strains most often indicated that stresses rarely exceeded the Category D endurance limit.

Testing of riveted bridge girders was still in progress at the Center for Advanced Technology for Large Structural Systems (ATLSS) at Lehigh University at the time this literature survey was conducted. The results discussed herein are based on a draft report prepared for the sponsor of the project, Canadian National Railways [ATLSS, 1993]. Riveted built-up stringers from a riveted railway bridge were tested with either constant or variable amplitude fatigue loads. The stringers were tested in the inverted position, so that the flange that was in compression in the actual structure became the tension flange in the tests. Because the top and bottom flanges had identical riveted details, the inverted position gives the best assurance that prior fatigue damage, if any, will not affect the experimental results. The preliminary results for the constant amplitude tests from this study are included in Figure 2.2. The results plotted correspond to a condition in which a crack resulted in the severing of a component of the built-up cross-section. In some cases, several results were obtained from a single specimen, since cracks formed at different locations along the girder.

Six stringers from a riveted railway bridge were tested by Adamson [1995]. The members, which were taken from the interior panels of the bridge, came from a riveted through-truss structure that was dismantled after approximately eighty years in service. The stringers,

which were a built-up section consisting of a web plate and riveted flange angles, were tested in four-point bending. All six stringers were initially tested in the normal orientation, that is, with the flange that was principally in tension while the bridge was in service also in tension in the experiment. After consideration of the loading history and review of strain measurements made while the bridge was in service, it was concluded that prior fatigue damage was negligible. Corrosion of the stringers was relatively light and did not appear to influence the experimental results, although reduction of cross-section dimensions was considered in the calculation of section properties. The critical detail was a horizontal gusset plate riveted to the underside of the tension flange, where horizontal bracing between the stringers had been connected. In one case, the stringer was repaired after cracking so that it could be tested in the inverted position. Two of the specimens experienced cracking in the shear region at a detail where cross-bracing was once attached, and these data were also reported. For all tests, the failure criterion used was the complete severing of one of the components of the cross-section followed by first detection of a crack in a second element. The data are presented in Figure 2.2.

2.4 Remaining Fatigue Life of Existing Structures

Most North American and international standards regulating the use of steel in structures use similar techniques to account for fatigue in existing structures. This section contains a description of standards from the American Railway Engineering Association (AREA), American Association of State Highway and Transportation Officials (AASHTO), and the European Committee for Standardisation (CEN). In addition, a new technique to account for fatigue damage accumulation will be discussed.

2.4.1 Standard Methods of Calculating Fatigue Damage

In order to predict the fatigue life of a structure, critical details must first be identified so that stress ranges and the number of cycles to which they are exposed can be estimated. Second, the fatigue damage caused by variable stress cycles must be accumulated. Typically, this is done through the calculation of an equivalent stress range. Finally, the remaining fatigue life can be predicted, taking into consideration the estimate of previous

damage and forecasts of future loads. All of the design standards reviewed in this paper use these three basic steps.

The number and magnitude of the variable stress ranges at critical details of a bridge can be estimated using field measurements under normal traffic conditions. Alternatively, stress ranges and number of cycles can be calculated using traffic survey information and a structural analysis of the bridge. The individual variable stress ranges can be converted into a constant amplitude effective stress range by a standard method of damage accumulation.

To explain how to account for fatigue damage in structures subject to variable loads, it is logical to consider first the simpler case of constant amplitude fatigue loading. Experimental data show that the relationship between stress range and number of cycles until failure is linear when plotted on a log-log scale, and, for most types of details, this linear relation has a slope of three. It is convenient to start with a standard equation for a straight line in order to mathematically develop the relationship between fatigue strength and number of cycles until failure. From a bi-logarithmic plot of stress range, $\Delta\sigma$, versus fatigue life, N , this relationship takes the form:

$$N = M(\Delta\sigma^{-m}) \quad (2.1)$$

where m is the slope of the fatigue curve and M is a constant obtained from experimental data. This basic equation for a straight line takes the same form as the theoretical fracture mechanics formulation [Kulak and Smith, 1993]. Hence, both experimental results and theory predict the same relationship for this case of constant amplitude stress range loading.

For situations in which variable amplitude loading does occur, a linear technique for accumulating damage was proposed by Palmgren in 1924 and developed further by Miner [1945]. The method, commonly known as the Palmgren-Miner rule or Miner summation, assumes that the damage that results from any particular stress range is a

linear function of the number of cycles that take place at that stress range. With the Palmgren-Miner rule, failure occurs when the following criterion is met:

$$\sum_{i=1}^k \frac{n_i}{N_i} = 1 \quad (2.2)$$

where

n_i = number of cycles at stress range level i

N_i = number of cycles to cause failure at stress range level i

k = total number of different stress ranges

Equations 2.1 and 2.2 can be combined into a more practical form so that variable stress ranges can be converted into an effective constant amplitude stress range [Schilling *et al.*, 1978]. The resulting equation for effective stress range takes the following form:

$$\Delta\sigma_e = \left[\sum_{i=1}^k \frac{\Delta\sigma_i^m n_i}{N} \right]^{\frac{1}{m}} \quad (2.3)$$

where

$\Delta\sigma_e$ = effective stress range

$\Delta\sigma_i$ = stress range i

n_i = number of cycles at stress range i

N = fatigue life under $\Delta\sigma_e$

m = either 2 or 3

k = number of different stress ranges

Two forms of this equation have been investigated by Schilling *et al.* [1978]. In Equation 2.3, m represents the slope of the fatigue curve described in Equation 2.1, which has been found to be three for a large number of structural steel details. If m is taken as three, the equation gives the so-called root-mean-cube (RMC) effective stress range, and it will predict the same fatigue life as given by the Miner summation (Equation 2.2). Schilling *et al.* also found that it is possible to improve correlation of the prediction of remaining fatigue life to actual test data by using the value $m = 2$ in Equation 2.3. This is called the root-mean-square (RMS) effective stress range. The RMS equation tends to match experimental data better, but is not as conservative as the RMC equation. Results from the two equations are generally within 10 %, however.

The standards reviewed all recommend use of the more conservative root-mean-cube method for the calculation of effective stress range. In order to calculate the remaining fatigue life, a point ($\Delta\sigma_e$, N) can be plotted on a fatigue strength design curve, such as shown in Figure 2.1. The effective stress range, $\Delta\sigma_e$, is calculated according to Equation 2.3. However, in this case the effective stress range does not, in general, describe the failure criterion. Therefore, the term N in Equation 2.3 is now understood to be the actual number of cycles to which the detail is subjected. The remaining fatigue life of the detail is then the horizontal distance measured from the plotted point to the intersection of the equivalent stress range with the appropriate detail category curve. To convert the number of cycles of remaining life to time, an estimate of the frequency of future loading must be made.

2.4.2 Current Code Requirements

All of the standards reviewed use similar techniques to evaluate the fatigue life of riveted structures. The discussion herein is limited to fatigue of riveted connections and members.

The American Railway Engineering Association requirements for the evaluation of fatigue in existing riveted railway bridges [AREA, 1994] divide members being evaluated for fatigue into two categories. The categories are: Fracture Critical Members (FCM), and Other Than Fracture Critical Members (OFCM). FCM's are defined as, "...those tension members or tension components of members whose failure would be expected to result in collapse of the bridge or inability of the bridge to perform its design function." In the fatigue evaluations methods described below, fracture critical members are treated more conservatively than those that are not fracture critical.

To rate existing bridges, the requirements used for the design of new bridges are first checked. If these requirements, which are conservative, are met, then the bridge is assumed to have satisfactory fatigue strength. To estimate the number of cycles of stress that a member must resist, members are classified into two groups. For Classification I (longitudinal flexural members and their connections, truss chord members, end posts, and others), 2 000 000 cycles are to be considered for member span lengths less than 30.5 m

(100 feet), and more than 2 000 000 cycles are to be considered for longer spans. For Classification II members (floorbeams and their connections, hangers, truss web members, and others), 2 000 000 cycles are to be considered for cases where two tracks are loaded, and more than 2 000 000 cycles are to be considered for cases where only one track is loaded. The use of these classifications is further described below.

The AREA standard indicates that members with riveted or bolted connections that have low slip resistance should be considered as Category D. However, in the design of new bridges, Category D is defined differently for FCM's and OFCM's. The standard states that for a Category D FCM, the maximum allowable fatigue stress range is 55.1 MPa (8 ksi) if 2 000 000 cycles or fewer constant stress cycles are applied, while it is 34.5 MPa (5 ksi) if more than 2 000 000 constant stress cycles are applied. For an OFCM, the allowable fatigue stress ranges are 68.9 MPa (10 ksi) and 48.3 MPa (7 ksi) for these same two cases. It is the responsibility of the engineer to calculate or measure the stress ranges at the critical details and to then compare them with the prescribed stress ranges.

These requirements for new bridges can be waived for the evaluation of existing structures. In this case, Category D, which has value 69 MPa (10 ksi) at two million cycles and a constant amplitude fatigue limit at 48.3 MPa (7 ksi), may be used for riveted connections. However, according to the AREA Manual [1994], "Where the Engineer can verify that the fasteners are tight and have developed a normal level of clamping force fatigue Category C may be used provided the Root-Mean-Cube (RMC) stress range has not and will not exceed 12 ksi [82.7 MPa]." The standard also states that if Category C is used, the constant amplitude fatigue limit shall still be that of Category D, namely 48.3 MPa (7 ksi). These requirements apply to both the FCM's and OFCM's in existing structures. The fatigue design curves for riveted connections proposed in the AREA standard are presented in Figure 2.3.

Where riveted members do not meet any of the above requirements but are fabricated from multiple elements, another option exists. There is a certain redundancy in a member built up of multiple elements because a crack that starts in one element is not able to

propagate into the next. All of the requirements given above may be waived providing several conditions are met. The root-mean-cube effective stress range must be below 82.7 MPa (12 ksi) and the members must have sufficient structural capacity so that a crack in one component of the cross section would be detected by inspection before the development of more serious damage. Additionally, there must be sufficient bracing so that out-of-plane or similar behaviour would not have any adverse effects. Remaining fatigue life is calculated by the root-mean-cube method, using an equation similar in form and identical in results to Equation 2.3. Either field strain measurements or traffic records with analytical models can be used to obtain stress histories for the equivalent stress range calculation. If theoretical models are used to obtain the stress history, the equivalent stress range is then to be multiplied by a tabulated factor α , which represents the beneficial effects of such variables as bracing, the floor system, three-dimensional response of the structure, and the fact that full impact does not occur for every stress cycle. The value of α given by the AREA Manual for the bridge considered in this study is 0.85 (member span length less than 50 feet (15.2 m)). The Manual also states that an appropriate analysis can also be used to obtain a more accurate estimate of α , but no guidelines are given for the use of this option.

The American Association of State Highway and Transportation Officials standard (AASHTO) is the Guide Specifications for Fatigue Evaluation of Existing Steel Bridges [1990], which focuses on highway bridges and traffic loadings. While railway bridges are of primary interest in the report presented herein, methods of evaluating fatigue life are similar regardless of the use of the bridge involved. A description of the AASHTO standard is therefore appropriate.

In the AASHTO Specification, fatigue life is defined in two ways. One of these is the *Remaining Fatigue Life*, used when the best estimate of the actual fatigue life of the structure is required. The other is the *Remaining Safe Fatigue Life*, which is an estimate of the duration for which the bridge can be safely used with an acceptably low probability of fatigue failure. *Remaining Fatigue Life* is defined as the duration of time corresponding to a 50 % probability of failure, that is, the mean fatigue life of the detail is used. The

Remaining Safe Fatigue Life is defined as the duration for which the detail has a 97.7 % probability of survival for redundant members, or a 99.9 % probability of survival for non-redundant members. In order to obtain the desired level of safety against fatigue failure, the *Remaining Safe Fatigue Life* is taken as the *Remaining Fatigue Life* less a given number of standard deviations of fatigue life (2 for redundant members and 3 for non-redundant members).

The AASHTO Specification contains three primary sections: Stress Range, Remaining Life, and Options to be Considered if Remaining Life is Inadequate. The Stress Range section outlines two methods for obtaining stress range data. Data may be obtained through field strain measurements, which will give the best estimate of actual stress conditions in the structure. If strain measurements are not possible, several equations are given for the calculation of stresses based on traffic frequency data, assumed or known truck weights, and impact.

The stress range data obtained is then used in the root-mean-cube version of Equation 2.3. Once the effective stress range is known, fatigue life can be calculated for the appropriate detail category. The AASHTO design curves consist of detail categories very similar to those used in the AREA standard discussed above, and, for riveted connections, Category D is again recommended. However, the curves in the AASHTO Specification differ from those in the AREA Manual, because the constant amplitude fatigue limits are replaced by variable amplitude fatigue limits. The variable amplitude fatigue limits are 0.367 times the constant amplitude fatigue limit for each different fatigue detail category. The standard states that if the effective stress range is below the variable amplitude fatigue limit, then all ranges are likely to be below the constant amplitude fatigue limit, so no fatigue damage occurs. Any individual ranges below the variable amplitude fatigue limit are to be neglected in the calculation of effective stress range. These fatigue design curves are presented in Figure 2.4.

If the Remaining Safe Fatigue Life is inadequate, various measures are proposed. The remaining life can be recalculated using one or more alternative methods described in the

Specification, or restrictions can be placed on the weight or frequency of vehicles crossing the bridge. The bridge can also be strengthened or modified to improve its fatigue strength, or the frequency of inspections can be increased so that problems can be addressed if cracks begin to develop.

The European Committee for Standardisation (CEN) uses a different method for identifying detail categories in Eurocode 3 [CEN, 1992]. Rather than a letter designation, fatigue details are identified by the value of a particular fatigue curve at two million cycles. The constant amplitude fatigue limit starts at five million cycles for all detail categories. If all stress ranges on a detail are below the constant amplitude fatigue limit, then it is assumed that no damage occurs and that the fatigue life is infinite. If any stress range exceeds the constant amplitude fatigue limit, then all cycles are assumed to contribute to damage, including those below the limit. Variable amplitude stress ranges are accommodated through the use of an equivalent stress range calculation. Three different choices are available for the calculation of the fatigue life: a fatigue strength curve with a single slope of 3; a fatigue strength curve with a double slope, changing from slope 3 to slope 5 at 5 million cycles; or a fatigue strength curve with a double slope, changing from slope 3 to slope 5 at 5 million cycles and then a cut-off limit at 100 million cycles. The cut-off limit is a value below which it is assumed that applied stress ranges of the stress history do not contribute to the cumulative damage calculation.

For the case where two slopes are used, the equation for equivalent stress range still has the same form as Equation 2.3, but it must be modified to account for the change in slope:

$$\Delta\sigma_e = \left[\sum_{i=1}^k \frac{\Delta\sigma_i^3 n_i}{N} \right]^{\frac{1}{3}} + \left[\sum_{i=1}^k \frac{\Delta\sigma_i^5 n_i}{N} \right]^{\frac{1}{5}} \quad (2.4)$$

The first term is used for stress ranges above the value of the fatigue strength curve at 5 million cycles, and the second is for stress ranges below the value of the fatigue curve at 5 million cycles.

Eurocode 3 does not give a specific detail category for new or existing riveted construction. The standard does indicate that it may be used for assessing the fatigue life of existing structures, but there is no guidance as to how this may be done. A Eurocode 3 detail category 69 would be approximately equivalent to the North American Category D, which is the standard detail for riveted members and connections. The Eurocode 3 fatigue design curves corresponding to riveted details are presented in Figure 2.5.

2.4.3 Alternative Methods of Fatigue Evaluation

Prediction of remaining fatigue life is particularly difficult when the stress ranges are near the endurance limit. A technique has been developed by Kunz [1992] to more accurately model the endurance limit and the transition from a slope of three to a slope of zero on a fatigue resistance curve. The technique will be referred to herein as the Kunz method. The model is based on fracture mechanics, and uses a new damage accumulation method and a modified form of the AREA fatigue resistance curve. This damage accumulation method attempts to reproduce more accurately the effect of variable amplitude stress ranges that straddle the constant amplitude fatigue limit.

Because the Kunz method is based on fracture mechanics, it is appropriate to describe the relevant aspects of fracture mechanics. The stress field at the tip of a stable crack subjected to cyclic loading can be characterised by the following factor:

$$\Delta K = Y(a)\Delta\sigma\sqrt{\pi a} \quad (2.5)$$

where

ΔK = stress intensity factor range

$Y(a)$ = geometric factor

$\Delta\sigma$ = applied stress range

a = crack size

This equation can be derived by considering an elastic model of the stress field near the crack tip [see, for example, Kulak and Smith, 1993]. The stress intensity factor is a description of both stress and crack geometry in a single parameter. A crack will propagate under a stress cycle provided that ΔK is greater than the threshold stress intensity factor range, ΔK_{th} . Figure 2.6 shows a graph of stress intensity factor range

plotted versus crack growth rate (both plotted logarithmically), based on typical experimental data. The curve has three distinct portions: Region I, which contains a vertical portion known as the threshold stress intensity factor range (below which cracks do not propagate under cyclic stress); Region II, a linear sloping portion of stable crack propagation that can be described by the Paris law; and Region III, which contains a vertical portion at high stress intensity factor ranges and indicates that fracture is imminent [Fuchs and Stephens, 1980].

The similarity between the shape of a typical fatigue resistance curve and Regions I and II of a crack growth curve is apparent. If the curve in Figure 2.6 is rotated 90 degrees counter-clockwise, it is clear that its shape is similar to a typical fatigue resistance curve. The threshold stress intensity factor range is analogous to the constant amplitude fatigue limit, and the Paris law portion is analogous to the sloping portion of the fatigue curve.

Equation 2.5 can be written to represent the threshold stress intensity factor range in the following form:

$$\Delta K_{th} = Y(a)\Delta\sigma_{th}\sqrt{\pi a} \quad (2.6)$$

where

ΔK_{th} = threshold stress intensity factor range

$Y(a)$ = geometric factor

$\Delta\sigma_{th}$ = threshold stress range (damage limit)

a = crack size

The threshold stress intensity factor range, ΔK_{th} , is essentially a constant for a particular type of steel. Cracks will not propagate unless the applied stress intensity factor range, ΔK , exceeds ΔK_{th} . Similarly, cracking will not occur unless the applied stress range, $\Delta\sigma$, exceeds the threshold stress range, $\Delta\sigma_{th}$. The Kunz method uses Equation 2.6 in the damage accumulation process and assumes that $\Delta\sigma_{th}$ is initially equal to the constant amplitude fatigue limit. As soon as the ΔK of one cycle exceeds ΔK_{th} , then crack propagation will occur, and the term “a” in Equation 2.6 becomes larger. Therefore, for a crack of constant geometry (i.e. $Y(a)$ is constant during crack propagation), $\Delta\sigma_{th}$ must

decrease in order that the equation still be satisfied, and, consequently, $\Delta\sigma_{th}$ is no longer equal to the constant amplitude fatigue limit. The constant amplitude fatigue limit on the fatigue resistance curve is replaced with the new value of $\Delta\sigma_{th}$, and it is called the damage limit. The damage limit is set based on the crack length, or damage, at any time. The new damage limit is used until it is exceeded by one cycle of stress, and then another new damage limit is calculated based on the new amount of total damage, and so on. The Kunz method applies this technique by calculating a new damage limit each time a stress range causes damage with the following formula:

$$\Delta\sigma_{th} = \Delta\sigma_c(1 - D) \quad (2.7)$$

where:

$\Delta\sigma_{th}$ = threshold stress range (damage limit)

$\Delta\sigma_c$ = constant amplitude fatigue limit

D = existing damage

This method is relatively easy to apply because it does not incorporate complex variables, such as $Y(a)$, from fracture mechanics. Existing damage is calculated using the Palmgren-Miner rule from Equation 2.2. The difference between the Kunz method and conventional techniques lies in the fact that the damage limit moves downward, as shown in Figure 2.7, and its location is based on the amount of fatigue damage present at a given stress cycle.

Another characteristic of the Kunz evaluation procedure is that a transition region is identified between the region of constant slope and the horizontal damage limit line. This transition region is also shown in Figure 2.7. It reflects the gradual transition in crack propagation rate observed between the Paris linear crack propagation curve and the threshold stress intensity factor range (see Figure 2.6). The formulation of the function describing the curve can be found elsewhere [Kunz, 1992]. The use of the transition region in calculation of fatigue life is expected to improve the accuracy of predictions when stress ranges are slightly above the damage limit.

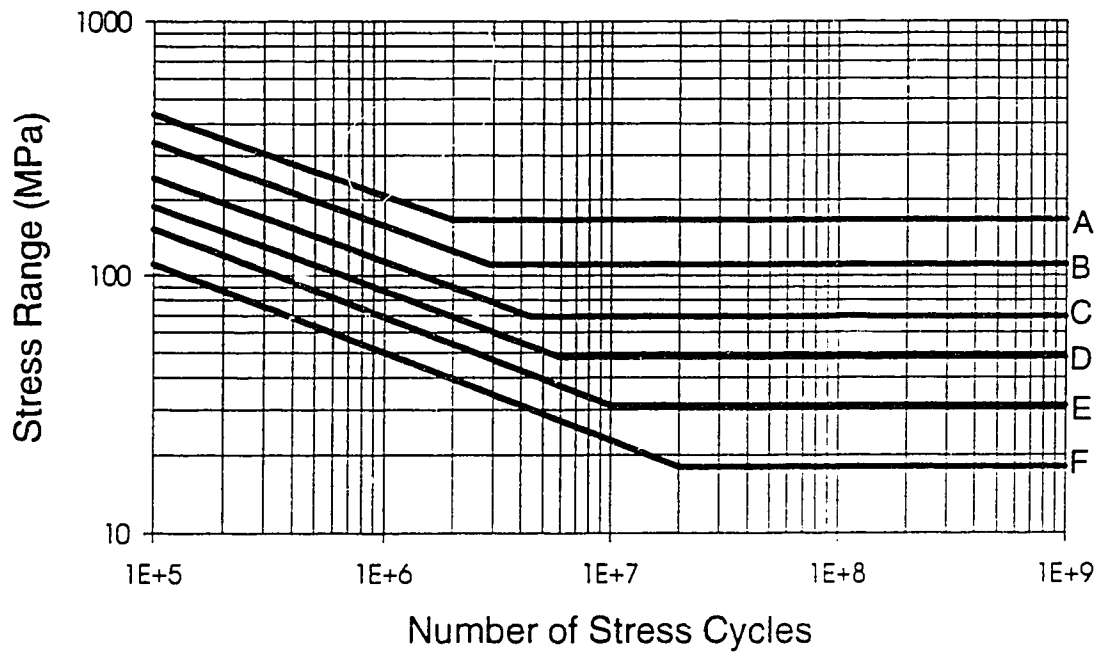


Figure 2.1 Typical Fatigue Strength Curves

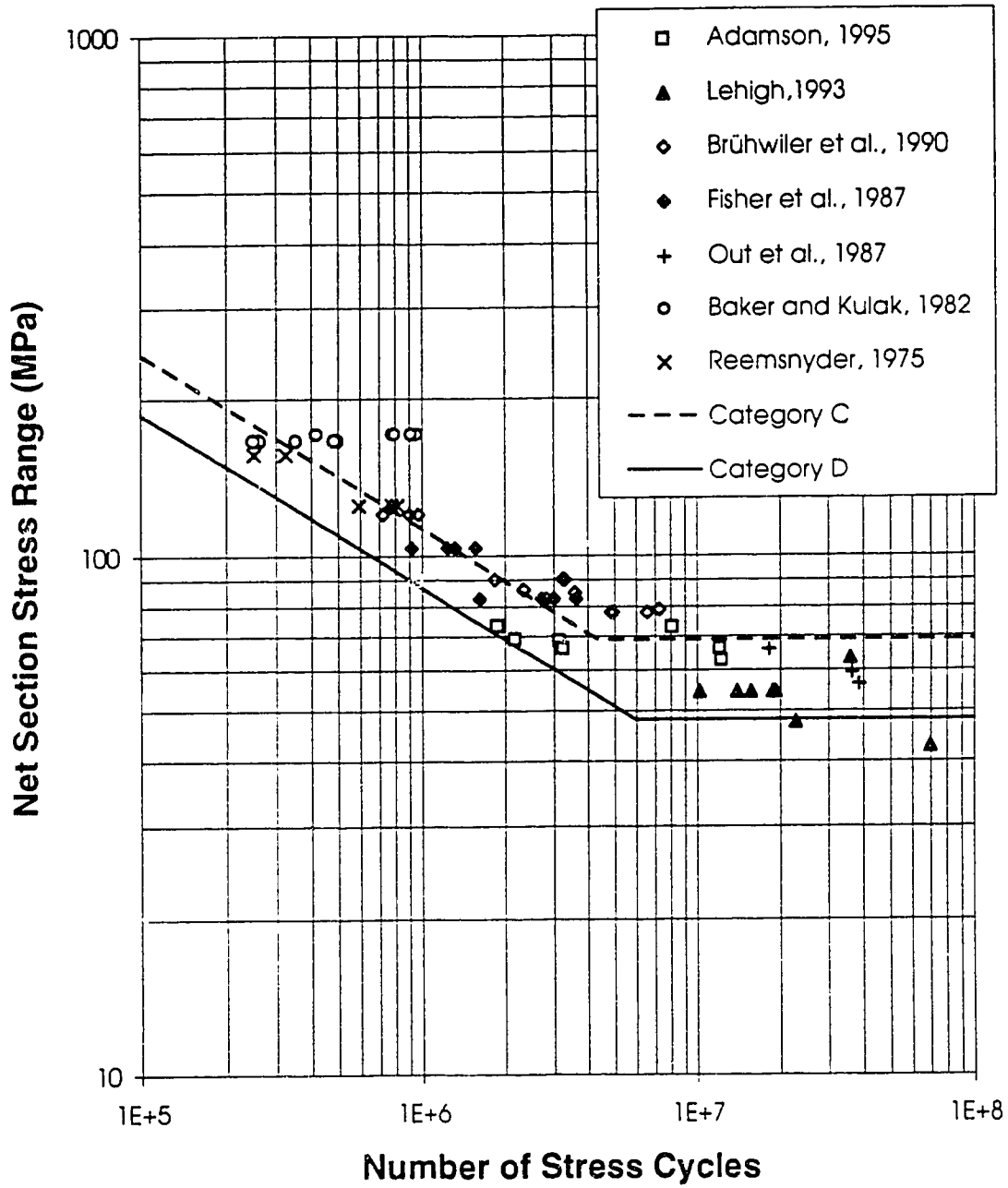


Figure 2.2 Results from Literature

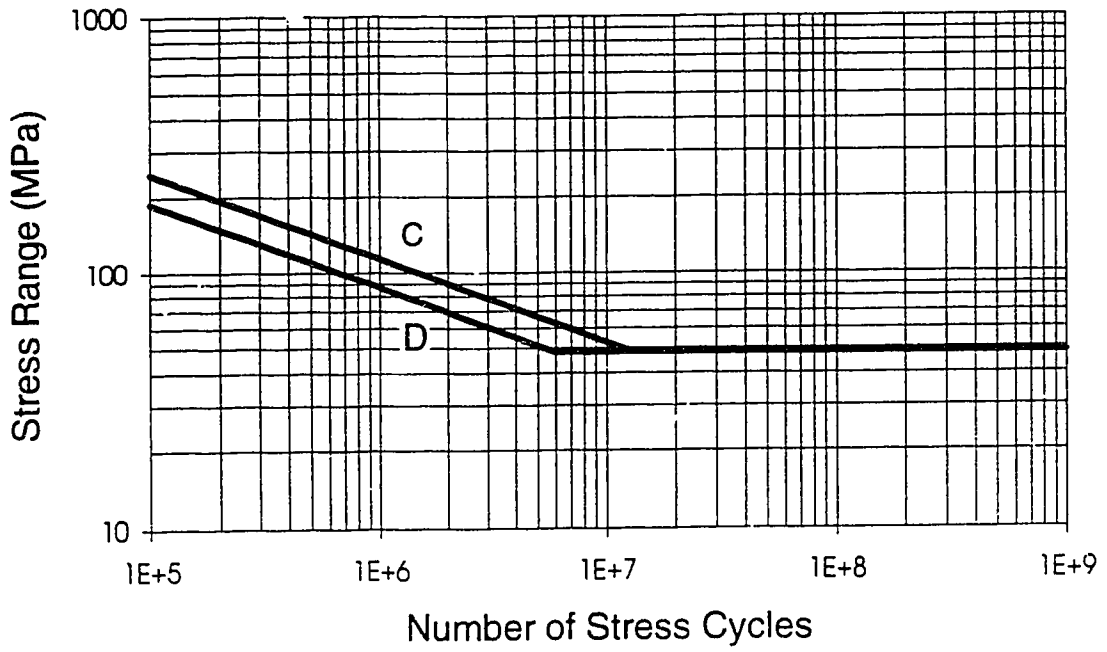


Figure 2.3 AREA Fatigue Strength Curves for Riveted Details

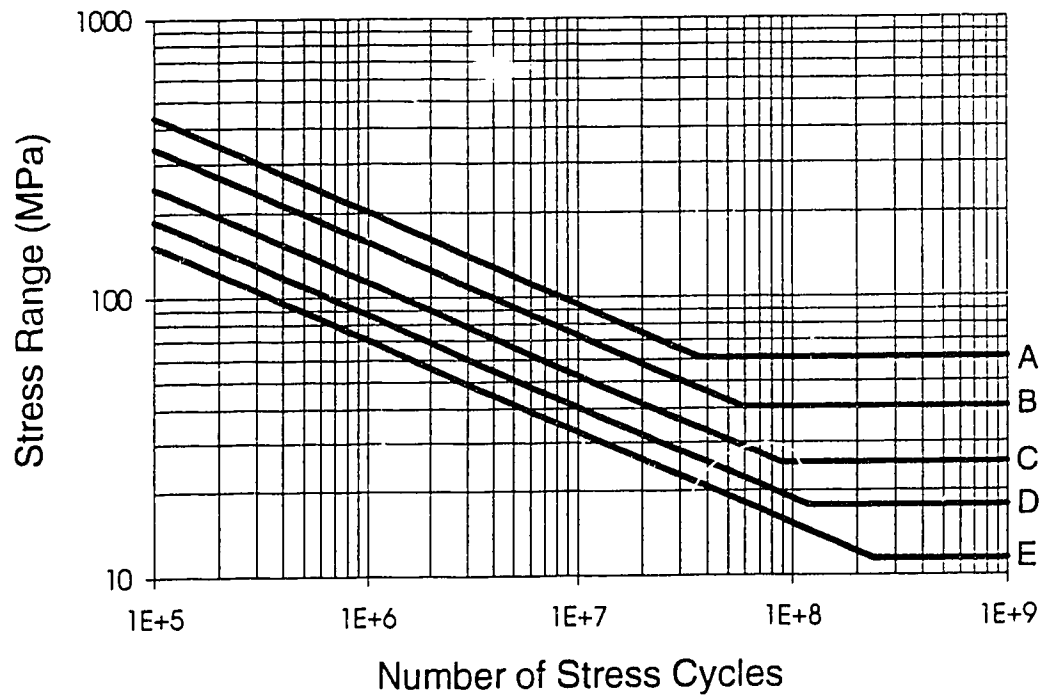


Figure 2.4 AASHTO Variable Amplitude Fatigue Strength Curves

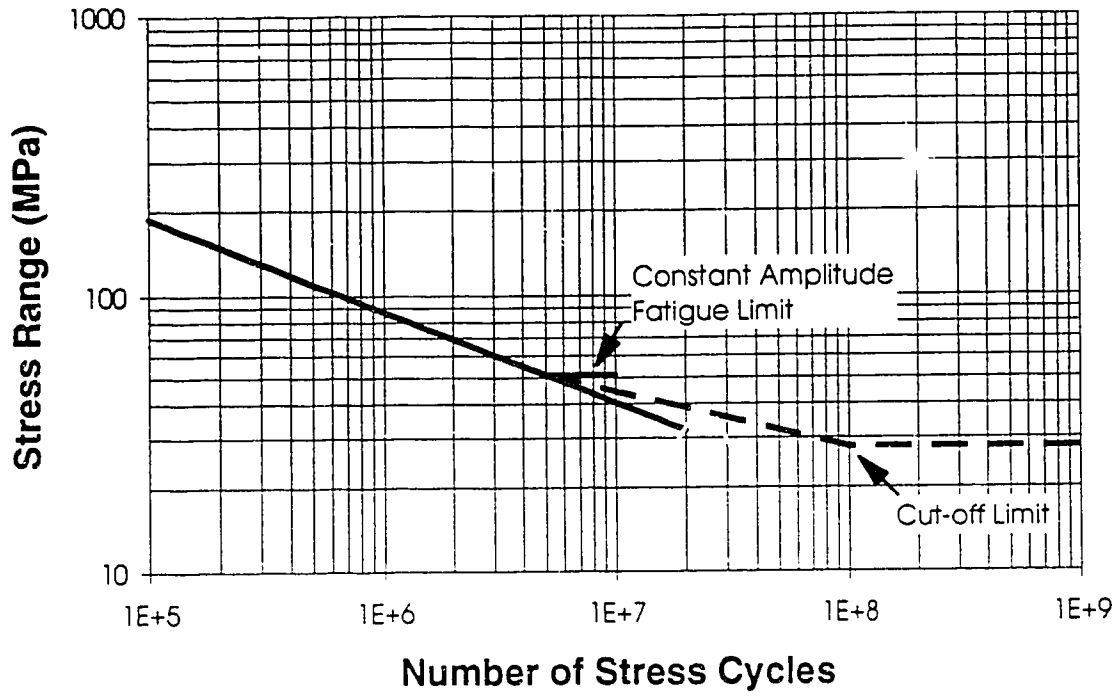


Figure 2.5 Eurocode 3 Fatigue Strength Curves for Detail Category 69

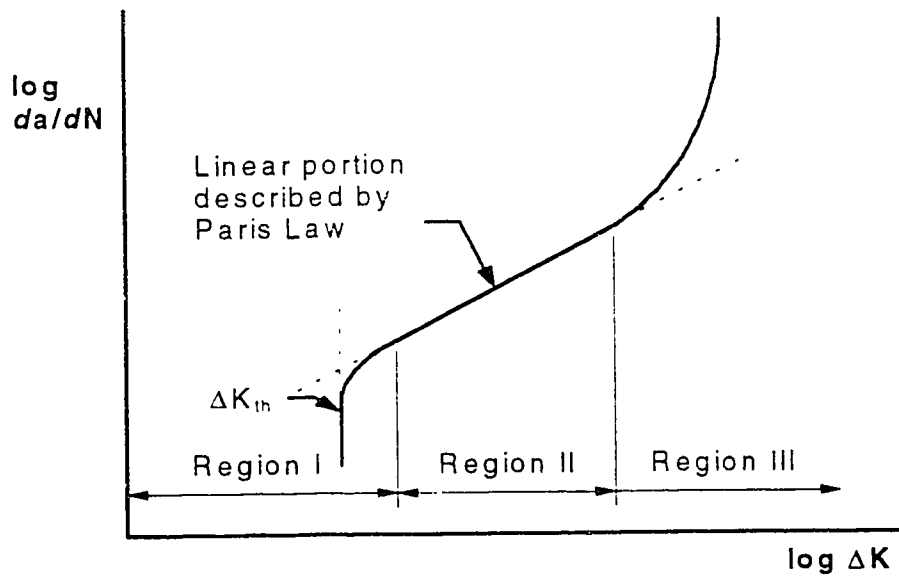


Figure 2.6 Crack Propagation Rate versus Stress Intensity Factor Range

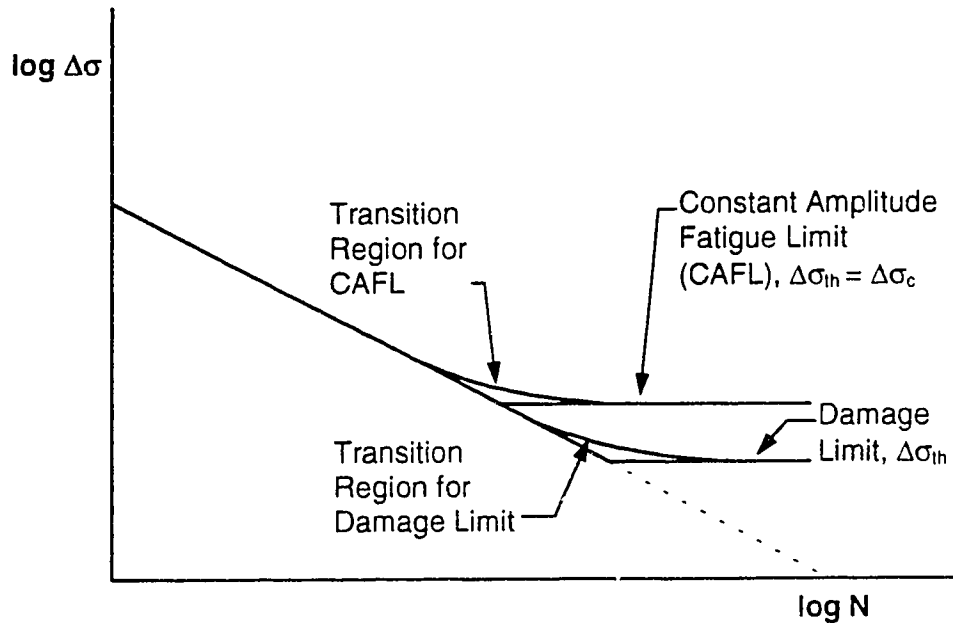


Figure 2.7 Typical Fatigue Strength Curve with Transition Region for Kunz Method

3. Development of Structural Models

3.1 The Need for Models

In order to provide an evaluation of the remaining fatigue life of a bridge, it is necessary that an estimate of the stress history be available for all critical details in the structure. This estimate can be based on measured strains or an analytical model can be used so as to allow calculation of stresses at critical details. When these stresses are to be determined analytically, vehicle loads, both historical and predicted, are needed in conjunction with an accurate structural model.

This chapter contains a discussion of live-load strain measurements taken from one stringer and one tension diagonal of a case study railway bridge. Analytical predictions of live-load strains, and thus stresses, are also made for the tension diagonal. The analysis in this report is limited to the diagonal: an investigation of the behaviour of the stringer can be found elsewhere [Adamson, 1995]. Two structural models are used to obtain the influence lines for the bridge, and strain records for the diagonal are predicted for the passage of several simulated trains. The predicted strains from the models are compared with actual measured strains to determine which of the models best represents the true behaviour of the bridge.

3.2 Description of the Case Study Bridge

The bridge studied in this report was a straight, single track, steel railway bridge built in 1911. It was part of the Canadian National Railways (CN Rail) mainline system, and was located over the Miette River, Albreda Subdivision Mile 7.8, west of Jasper, Alberta. The structure, which will hereafter be referred to as the Miette River Bridge, was a five-panel through-truss with a single span of 31 800 mm (125 feet). It had a fixed simple support at the east abutment and a roller simple support at the west abutment. The bridge had a width of 5 485 mm (18 feet) between truss centrelines, and the floor system consisted of transverse floorbeams and longitudinal stringers. All connections for both truss and floor

members were riveted, and all primary structural members were built-up riveted sections. The track was centred along the longitudinal axis of the bridge and was not ballasted, that is, the timber sleepers rested directly on the stringers. A photograph of the bridge in service is shown in Figure 3.1, and elevations of the trusses are shown in Figure 3.2.

The Miette River Bridge was designed by the Canadian Bridge Company Limited, of Walkerville, Ontario, for the Grand Trunk Pacific Railway Company. The original drawings show that the structure was designed in accordance with 1908 Dominion Government Standards for railway bridges. It was used for traffic in both directions until 1981, when a second, parallel rail line was added. The bridge was replaced in October of 1991 with a structure that does not limit the height of railcars.

Of specific interest for this study are the four primary tension diagonals, designated D1 through D4 in this report. These diagonals were removed from the bridge and have been tested in fatigue as part of this study, and they are discussed further in Chapter 4. The diagonals were riveted built-up I-sections that used 152 mm x 89 mm x 11 mm (6 in. x 3.5 in. x 7/16 in.) angles and a 356 mm x 9.5 mm (14 in. x 3/8 in.) web plate. The short legs of the angles were riveted to opposite sides of the web so as to form an I-shape. These rivets were 22 mm (7/8 in.) in diameter, and their holes were sub-punched at a diameter of 21 mm (13/16 in.) and then reamed to 24 mm (15/16 in.) diameter. The rivets were spaced at 152 mm (6 in.) on centre, except near the end connections, where the spacing was decreased to approximately 76 mm (3 in.). Two gusset plates, each 12.7 mm (1/2 in.) thick, connected each end of the diagonals to other members at the top and bottom panel points. Each gusset plate was attached to the diagonal with twenty-six 22 mm (7/8 in.) diameter rivets. Detail drawings of Diagonal D1 are presented in Figure 3.3.

3.3 Field Strain Measurements

Prior to removal of the bridge from service, technicians from the University of Alberta placed electrical resistance strain gauges on one diagonal (Diagonal D1) and on one interior panel stringer in order to measure live load strains. Gauges were mounted on one

side of the web and on both flanges of the diagonal, as shown in Figure 3.4. The gauges were arranged in a Wheatstone bridge configuration, with two used to measure strain parallel to the length of the member and two used to measure strain transverse to the length of the member. This configuration made the circuit, which was intended to measure strains parallel to the length of the member, insensitive to transverse strains from Poisson effects.

A Validyne Carrier Demodulator provided excitation voltages to the gauges and also monitored and amplified the output signals. A data acquisition computer sampled the output voltage of each channel 10 times per second, and this voltage was stored for later conversion to strain. The accuracy of the strain measurement has been judged to be accurate to plus or minus five microstrains, based on experience using the same equipment in subsequent experimental research.

Live load strains in Diagonal D1 were measured under five freight trains and one passenger train that crossed the bridge. The speed limit at the bridge was 48 km/h (30 mph) for freight trains, and 56 km/h (35 mph) for passenger trains. In this report the six trains are designated T720, F100, F130, F430, F658, and F717, in reference to the day and time when they crossed the bridge. Unfortunately, not all of the strain gauges were functional for all trains, due to technical difficulties encountered in the field.

Additional information that was provided by CN Rail included the length, weight, and axle locations for each engine and each car for every train. However, the data obtained from CN Rail for two of the freight trains contained inaccuracies. For example, field observations and strain measurements indicate that Train F100 was powered by four engines, while the CN Rail records indicate that this train had only two engines. According to CN Rail officials, it is likely that additional engines were added to bring the train through the mountains, but the extra engines are not reflected in their records. Consequently, only the results of four trains for which accurate records exist will be discussed further in this chapter. Details of these four trains can be found in Appendix A.

3.4 Structural Models

Two linear elastic structural models have been developed so as to allow influence lines for the gauged diagonal to be obtained. The first model is a plane simple truss, and it is used to calculate the influence line for axial force in the diagonal. This model will be referred to as the *Simple Truss* model. The second model is a space frame, incorporating all of the major structural elements, with full continuity of all structural joints. This model is named the *Space Frame* model in this report. The *Space Frame* model is used to calculate influence lines for both axial force and bending moment in the diagonal.

3.4.1 Simple Truss Model

The *Simple Truss* model was developed in an attempt to achieve an upper bound solution for the axial force in Diagonal D1. The model consists of a single idealized truss, with no continuity or bending resistance between elements, that is, all connections are modelled as pins. The effects of continuity in the floor system are also neglected, so that maximum average axial forces in the truss are obtained. The *Simple Truss* model was used to obtain the influence line for axial force in the diagonal, in order to allow calculation of the average axial strain in the diagonal for a load placed anywhere along the track. Member properties for Diagonal D1 were calculated based on dimensions from the original construction drawings. The influence line was easily obtained by hand calculation, and it is shown in Figure 3.5.

3.4.2 Space Frame Model

Although the tension diagonals carried principally axial load, strain measurements of Diagonal D1 show that the north flange, located nearest to the track, was generally subjected to slightly greater strains than the south flange. This difference indicates the presence of flexure in the diagonal, likely caused by interaction of the diagonal with the floor beam at the bottom chord panel point. In order to replicate this behaviour, the *Space Frame* model was developed using the SAP90 series of structural analysis programs [Wilson and Habibullah, 1992]. All primary structural members of the bridge are included

in the model, and all connections are idealized as fully continuous. Minor elements are omitted, such as portal bracing and sway bracing, as their effect on results is assumed to be minimal. The *Space Frame* mesh shown with boundary conditions can be found in Figure 3.6. Appendix B contains the SAP90 input file, and all section properties in the input file were based on dimensions given in the original construction drawings.

The SAP90 post-processor SAPLOT was used to calculate two influence lines for Diagonal D1 in the *Space Frame* model. One influence line represents axial force in the diagonal, and one represents strong-axis bending moment (see Figures 3.5 and 3.7). Both influence lines show the effect of a unit load passing over one half of the bridge. It was only necessary to model one half of the bridge because both the structure and the loads were symmetrical about the longitudinal axis of the bridge.

3.5 Simulation of Trains

The influence lines obtained in Section 3.4 allow prediction of strains in the diagonal as simulated trains are moved across the bridge. These simulations are derived from the weight and configuration data for the trains that crossed the bridge when the field strain measurements were taken. Predicted strains for trains T720, F430, F658, and F717 are discussed in this section.

3.5.1 Train Simulation Algorithm

A computer program, known as the *Train Simulation Algorithm*, was written to analytically predict the strains at the gauged location of Diagonal D1 during passage of a simulated train. The input variables for the *Train Simulation Algorithm* include the influence lines for the diagonal obtained from the analysis described in Section 3.4, engine and car data for one of the trains, and train speed. A listing of this algorithm is presented in Appendix C.

In order to execute the *Train Simulation Algorithm*, the user must specify the structural model and train configuration data and must choose whether the output is to be for the

north flange strain, south flange strain, or web (average) strain. The program advances the train across the bridge in 0.1 second steps, and at each time step calculates the location of every axle. All of the axles that are on the bridge are used in conjunction with the influence line for the calculation of the total axial force and bending moment, if any, in the diagonal. The axial force and bending moment are then used in the calculation of the strain in the north flange, south flange, or web, as appropriate. The program then moves to the next time step, and the process is repeated until the entire train has crossed the bridge. The final output is a record of strain in the diagonal versus time.

3.6 Method of Comparison of Measured Strains with Simulated Strains

The simulated strain records calculated in Section 3.5 can be visually compared to their corresponding measured records, and can be seen as strain versus time plots in Figures 3.8 to 3.19. A slight difference in phase between the measured and predicted records can be seen in some of the plots. This is because simulated trains were modelled at constant speed, whereas the speed of actual trains undoubtedly varied slightly over time. A quantitative comparison of the strain records by visual inspection is not possible. This section develops a mathematical method to compare the predicted strains with the measured strains.

In order to compare a predicted strain record with a measured strain record, an effective strain range technique has been developed by Adamson [1995]. In a strain record, maxima and minima must first be identified, so as to allow rainflow counting of the number and magnitude of the strain ranges. These strain ranges are then used with a variation of Equation 2.3 to calculate an effective root-mean-cube strain range, which represents the entire strain record. Calculation of an effective strain range is practical because it is simple and allows an entire strain record having variable amplitude cycles to be represented by one number.

The function used to calculate the effective root-mean-cube strain range has the following form:

$$\Delta\varepsilon_e = \left[\sum_{i=1}^k \frac{\Delta\varepsilon_i^3 n_i}{N} \right]^{1/3} \quad (3.1)$$

where

$\Delta\varepsilon_e$ = effective strain range

$\Delta\varepsilon_i$ = strain range i

n_i = number of cycles at strain range i

N = total number of cycles in the strain record

k = number of different strain ranges

This function represents a weighted average, in which large strain ranges have the most significant influence on $\Delta\varepsilon_e$, while the effects of small strain ranges are diminished. This is desirable, because large strain ranges cause more fatigue damage than do small strain ranges. For the case of the strain records in this study, Equation 3.1 can be simplified. In general, there is only one strain range of a given magnitude in each strain record, so that n_i always equals one and the number of different strain ranges, k , equals the total number of cycles, N .

A simplified version of Equation 3.1 is thus used:

$$\Delta\varepsilon_e = \left[\frac{1}{N} \sum_{i=1}^N (\Delta\varepsilon_i)^3 \right]^{1/3} \quad (3.2)$$

where

$\Delta\varepsilon_e$ = effective strain range

$\Delta\varepsilon_i$ = strain range i

N = total number of cycles in the strain record

This method, which represents a strain record by an equivalent strain range, must be used with caution. As a real train passes over a bridge, there are undoubtedly many random and unpredictable small vibrations in the structure. Small strains due to these vibrations generally have no effect on fatigue life, but will invariably greatly increase the number of recorded cycles in the strain record. However, when a computer simulation of the same train passing over the bridge is performed, none of these small random vibrations are

present. Therefore, the total number of cycles in a measured strain record is generally considerably greater than the number of cycles in a calculated strain record. The importance of this difference can be seen when Equation 3.2 is used to compare $\Delta\epsilon_e$ of the predicted strain record to $\Delta\epsilon_e$ of the measured strain record. Because the equation for $\Delta\epsilon_e$ includes the number of cycles (N) in the calculation, it is imperative that the number of cycles for the predicted strain record and the measured strain record be identical, otherwise the results can not be compared. This fact will be illustrated later in this chapter with an example from the analysis of the Miette River Bridge.

It is possible to ensure that the number of cycles in the calculation of $\Delta\epsilon_e$ are the same for both measured and predicted strain records. To achieve this, all small strain ranges must be filtered from the record before an effective strain range is calculated. Small strain ranges may be filtered without adverse effects because small strain ranges do not contribute to fatigue damage and are thus negligible.

3.6.1 *Effective Strain Range Algorithm*

A second program written in Fortran 77, known as the *Effective Strain Range Algorithm*, was used to calculate the effective strain range and number of cycles for both predicted and measured strain records.

The first part of the *Effective Strain Range Algorithm* analyses a strain record, either a predicted record or a measured record, and identifies all of the maxima and minima. These values are stored for use in the second part of the program, which performs one-pass rainflow counting of strain ranges based on a method developed by Downing and Socie [1982]. The user is prompted to enter a filter value, so as to eliminate the effects of electronic noise and vibration from the measured strain records. A sensitivity analysis revealed that $10 \mu\epsilon$ was an appropriate filter value, in order to allow the measured and predicted strain records to have the same number of strain ranges. This filter value, which corresponds to stress ranges less than 2 MPa, is used for all calculations in this study.

The final portion of the algorithm uses Equation 3.2 and the list of filtered strain ranges in order to obtain a root-mean-cube effective strain range. The effective strain range allows entire strain records to be represented by a single number, so that each measured strain record can be compared to each associated calculated strain record. The *Effective Strain Range Algorithm* can be found in Appendix C.

3.7 Results of Comparison of Measured Strains with Simulated Strains

Effective strain ranges ($\Delta\epsilon_e$) and number of cycles greater than $10\ \mu\epsilon$ were calculated for strains recorded by all functional gauges for Trains T720, F430, F658, and F717. Effective strain ranges and number of cycles greater than $10\ \mu\epsilon$ were also calculated for simulations of Trains T720, F430, F658, and F717 for both the *Simple Truss* model and the *Space Frame* model. Table 3.1 shows the effective strain range results generated by the *Effective Strain Range Algorithm*, along with ratios of measured-to-predicted effective strain range.

3.7.1 Importance of Filtering

The following example illustrates the importance of filtering out the small strain cycles caused by electronic noise and vibration from the strain records. Consider the unfiltered strain records obtained by both prediction and measurement for the south flange of Diagonal D1 for Train T720. The *predicted* strain record for the passage of two engines and 30 cars has $N=32$ cycles of strain, with $\sum(\Delta\epsilon_i)^3 = 17.66 \times 10^6 \mu\epsilon^3$, and thus, from Equation 3.2, $\Delta\epsilon_e = 82.02 \mu\epsilon$. The *measured* strain record for the passage of the same number of cars has $N=96$ cycles of strain, with $\sum(\Delta\epsilon_i)^3 = 13.09 \times 10^6 \mu\epsilon^3$. It is apparent that $\sum(\Delta\epsilon_i)^3$ is reasonably similar in both cases, but the number of cycles (N) is substantially different. The reason that N is so different is because of the presence of very small strain cycles in the measured record resulting from vibrations and electronic noise that have almost no influence on $\sum(\Delta\epsilon_i)^3$.

When strain ranges below $10 \mu\epsilon$ are filtered from the *predicted* strain record, the effective strain range, $\Delta\epsilon_e$, remains at $82.02 \mu\epsilon$, since there are no cycles with a range of less than $10 \mu\epsilon$. However, when strain ranges below $10 \mu\epsilon$ are filtered from the *measured* record, the number of cycles drops substantially, from $N=96$ to $N=32$, but $\sum(\Delta\epsilon_i)^3$ remains unchanged at $13.09 \times 10^6 \mu\epsilon^3$, since only the smallest strain ranges have been deleted. Consequently, $\Delta\epsilon_e$ for the *measured* record changed from $51.48 \mu\epsilon$ in the unfiltered case to $74.25 \mu\epsilon$ in the filtered case. This makes a large difference in the ratio of $\Delta\epsilon_e$ (*measured*) to $\Delta\epsilon_e$ (*predicted*), a change from 0.63 for the unfiltered case to 0.91 for the filtered case. This example illustrates that when effective strain range is used to compare measured strain records to predicted strain records, the number of cycles must be the same for each of the calculations of effective strain range.

3.7.2 Comparison of Filtered Records

Table 3.1 indicates that when strain ranges less than $10 \mu\epsilon$ are filtered, all of the measured to predicted ratios correlate reasonably well for the *Simple Truss* model, with a range from 0.87 to 0.96. This shows that the *Simple Truss* model gives a conservative, but reasonably accurate, estimate of the average axial strains in the Diagonal D1.

The average axial strain predicted by the *Simple Truss* model is also compared to the north flange measured strains in Table 3.1. The strains measured in the north flange tend to be higher than average measured strains because of bending effects in the diagonal resulting from interaction with the floor system. Although the *Simple Truss* model does not model bending in Diagonal D1, it is sufficiently conservative so that it makes a good prediction of the maximum strain in the diagonal on the north flange. This is reflected in the measured-to-predicted ratios, which range from 0.92 to 1.01. In summary, the *Simple Truss* model is conservative in the prediction of *average* strain in the diagonal, to an extent that it can account for higher strains in the flanges due to bending effects.

The *Space Frame* model gives results that correlate well with measured strains at the north flange, south flange, and web. The measured-to-predicted ratios for the three

locations range from 0.91 to 1.02. This shows that the effect of bending in the diagonal is estimated accurately by the *Space Frame* model. However, for practical applications, the development of a space frame model is onerous, and is likely necessary only in situations where significant bending of the diagonal is probable.

In conclusion, the *Simple Truss* model is sufficiently conservative to account for the effect of bending in the diagonal. The use of a three-dimensional model led to better strain predictions, but may not be necessary in cases where a simple estimate of strain is all that is required. Since estimates of both past and future traffic are likely to be uncertain, the minor additional accuracy of the *Space Frame* model will not be warranted in most cases.

Table 3.1 Comparison of Measured Strains to Predicted Strains for Diagonal D1

Train	Cycles > 10 $\mu\epsilon$	MEASURED $\Delta\epsilon_c$ ($\mu\epsilon$)			PREDICTED $\Delta\epsilon_c$ ($\mu\epsilon$)			MEASURED/PREDICTED					
		South Flange (A)	Web (B)	North Flange (C)	SPACE FRAME			TRUSS		SPACE FRAME			
					Average Strain (D)	South Flange (E)	Web (F)	North Flange (G)	Web (B/D)	North Flange (C/D)	South Flange (A/E)	Web (B/F)	North Flange (C/G)
T720	32	74.25	NA*	NA	94.17	82.02	88.51	95.06	NA	NA	0.91	NA	NA
F430	14	58.48	NA	66.47	66.50	57.10	61.00	64.93	NA	1.00	1.02	NA	1.02
F658	70	NA	43.73	45.83	45.57	40.70	43.60	46.49	0.96	1.01	NA	1.00	0.99
F717	37	NA	53.95	56.38	61.96	52.92	56.23	59.55	0.87	0.91	NA	0.96	0.95

*Note: NA indicates that the measured strain record was unavailable.

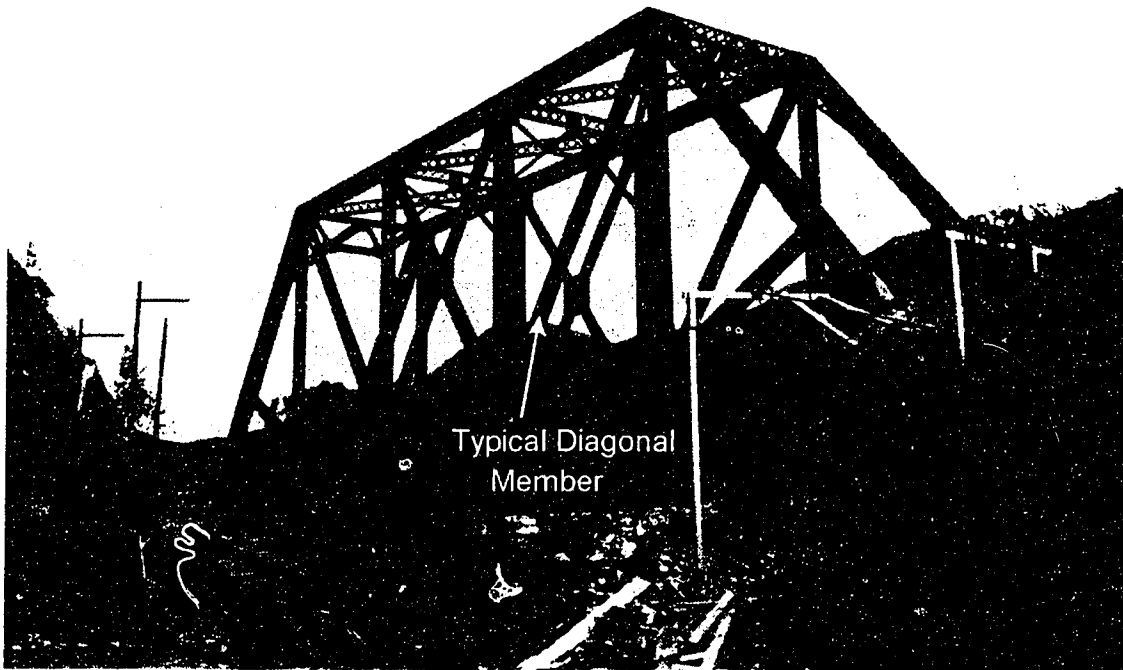


Figure 3.1 Bridge in Service

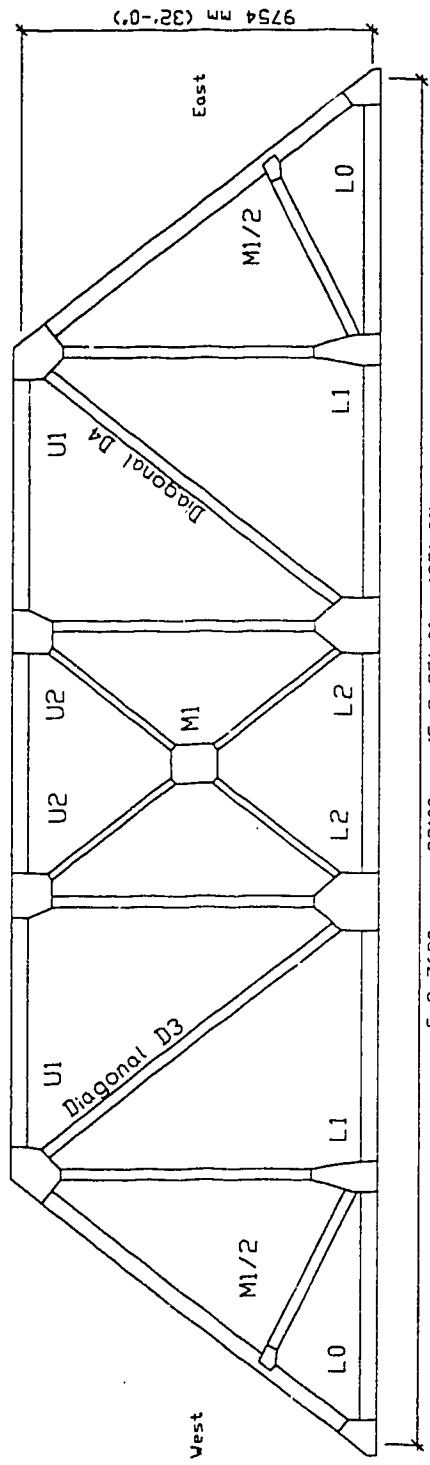
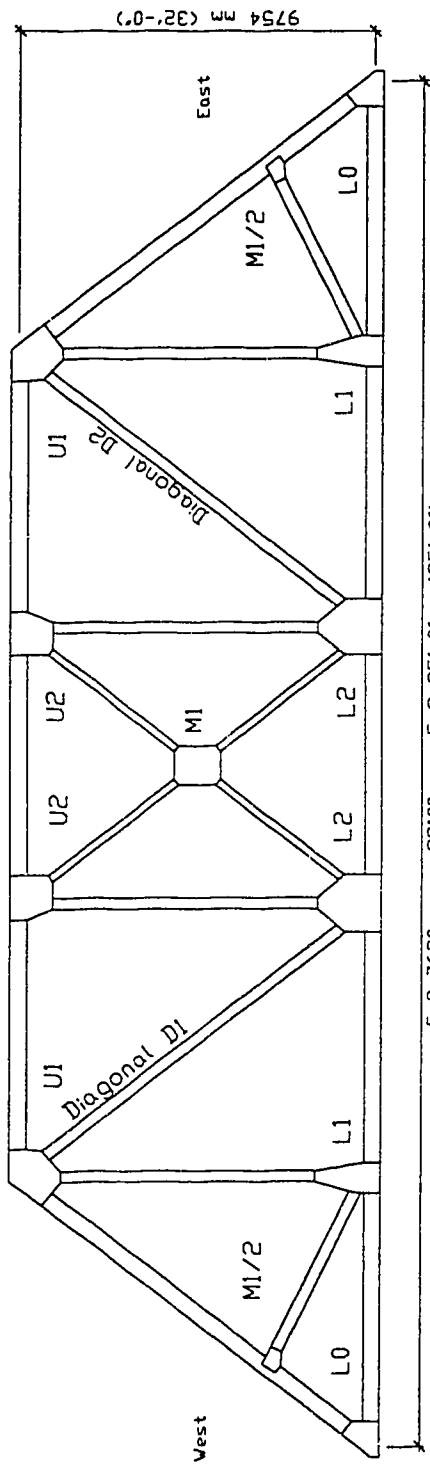


Figure 3.2 Elevations of Trusses

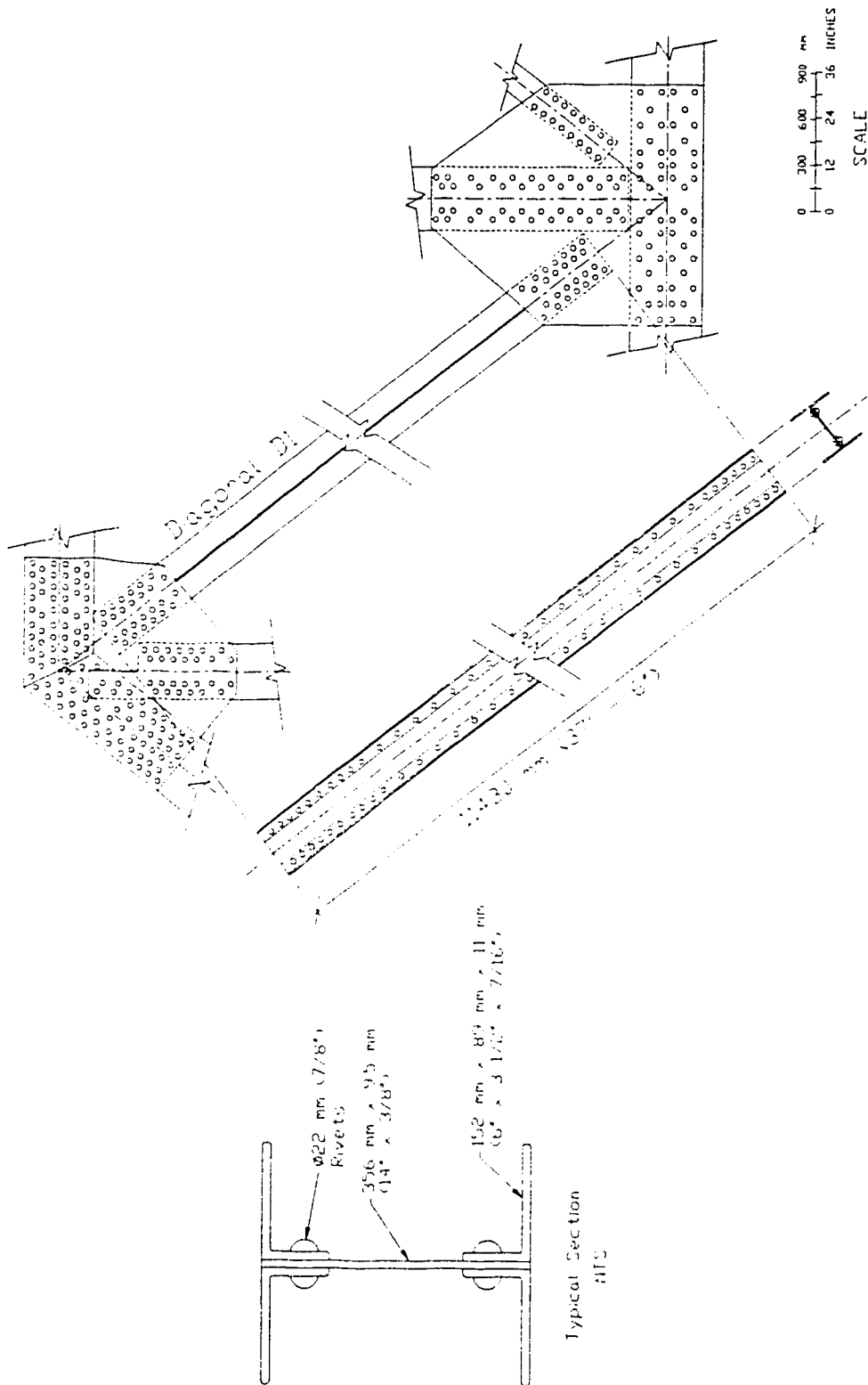


Figure 3.3 Views of Diagonal D1

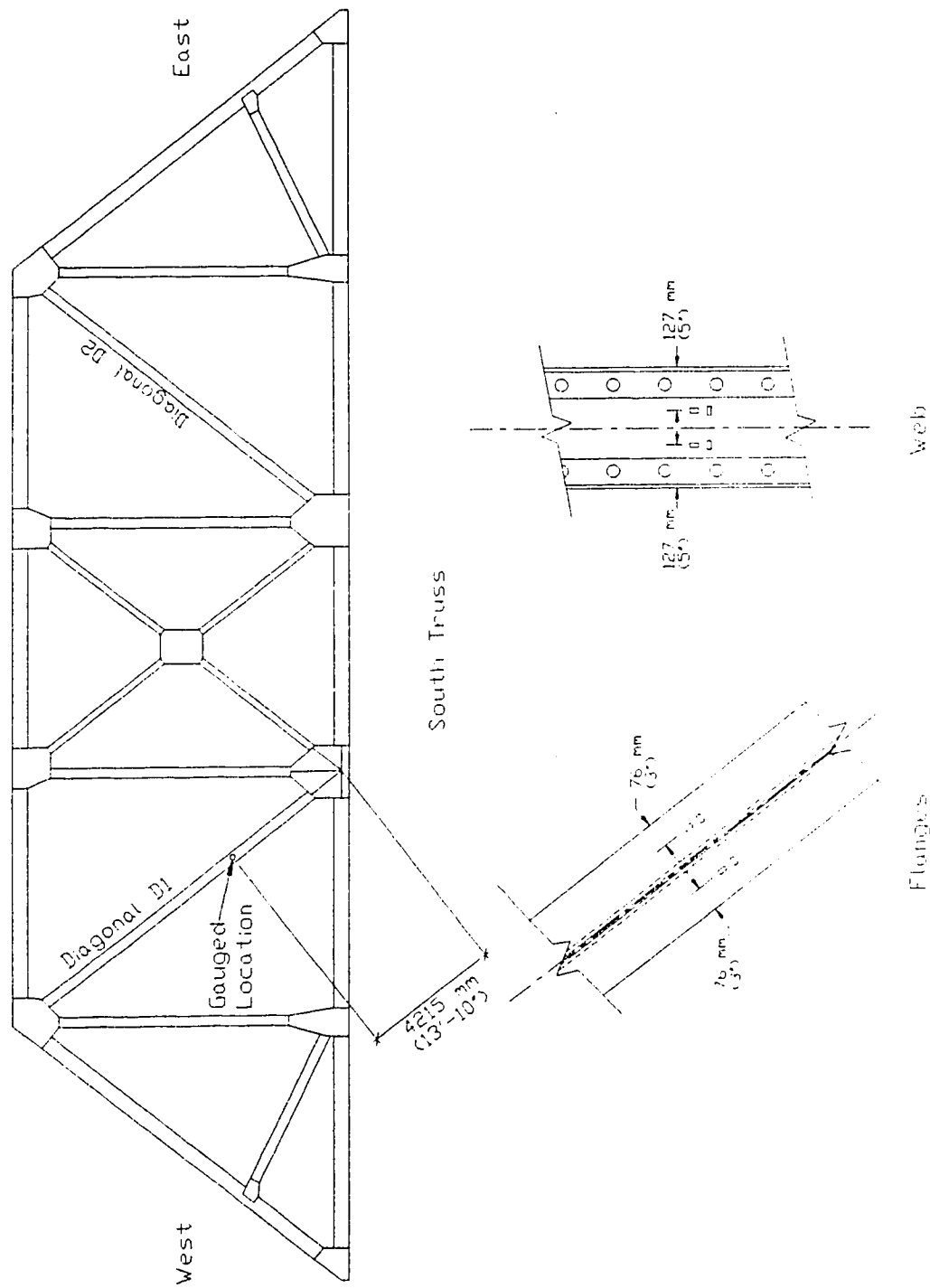


Figure 3.4 Locations of Strain Gauges

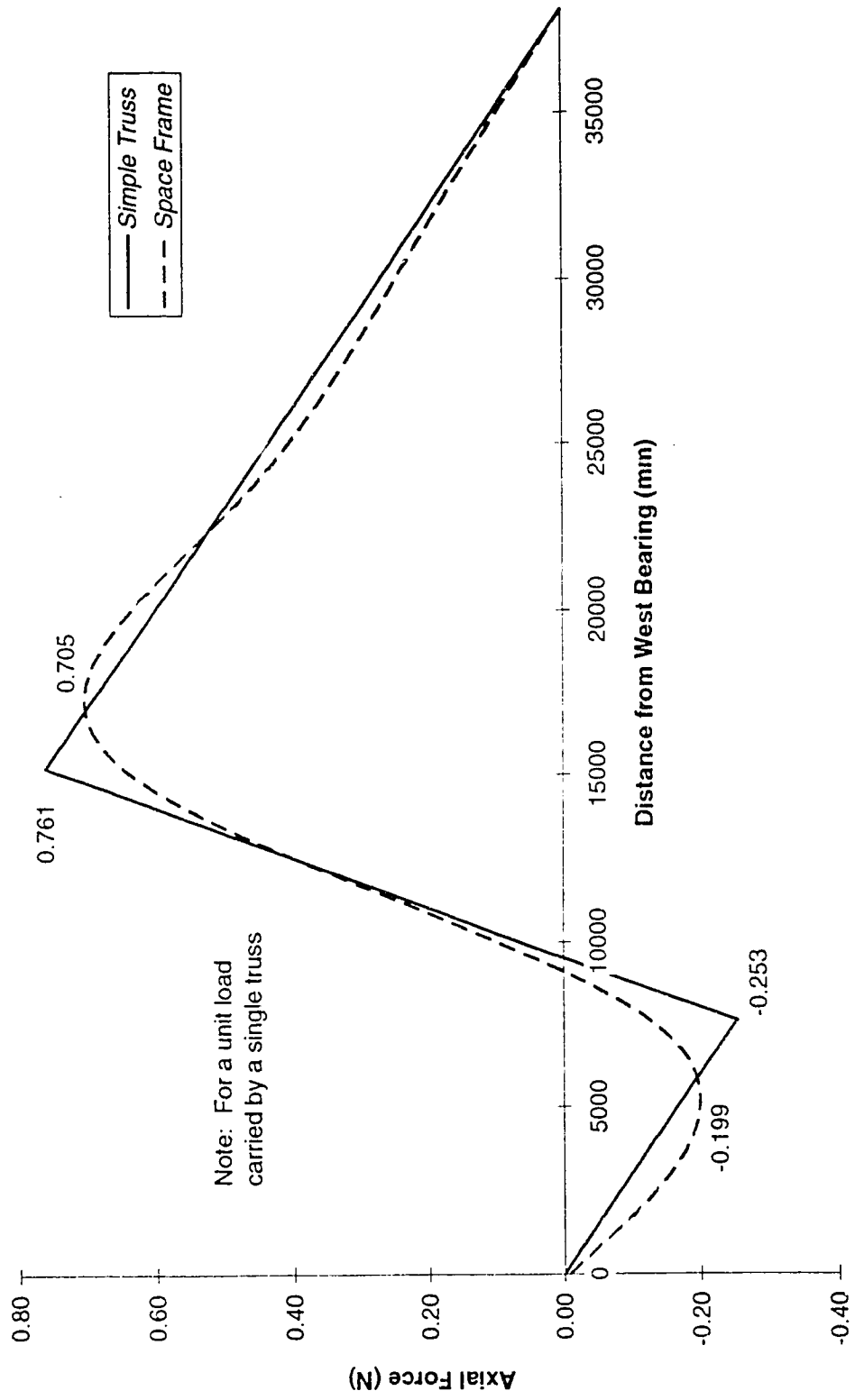


Figure 3.5 Influence Line for Axial Force in Diagonal D1 (Eastbound Unit Load)

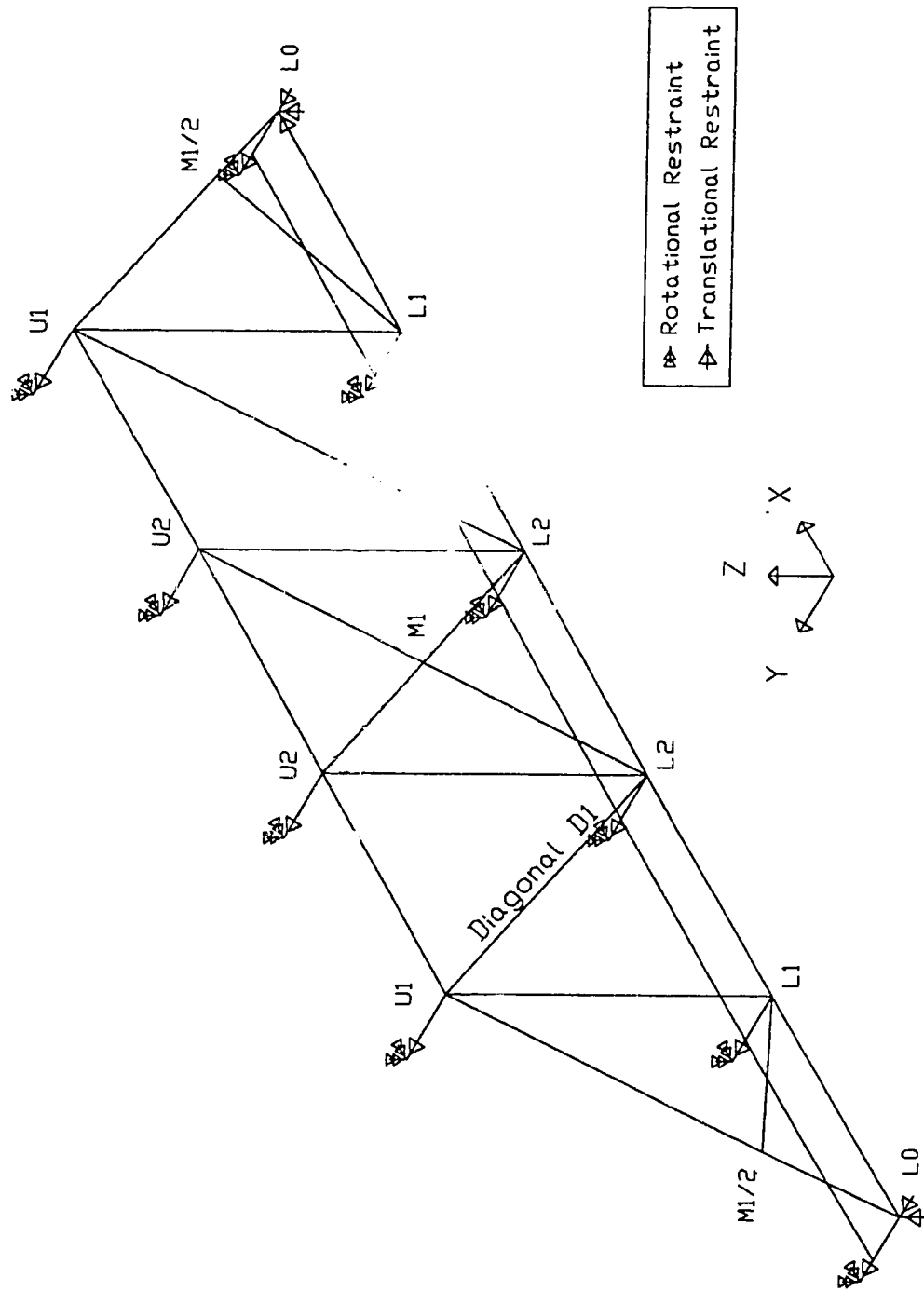


Figure 3.6 Space Frame Model

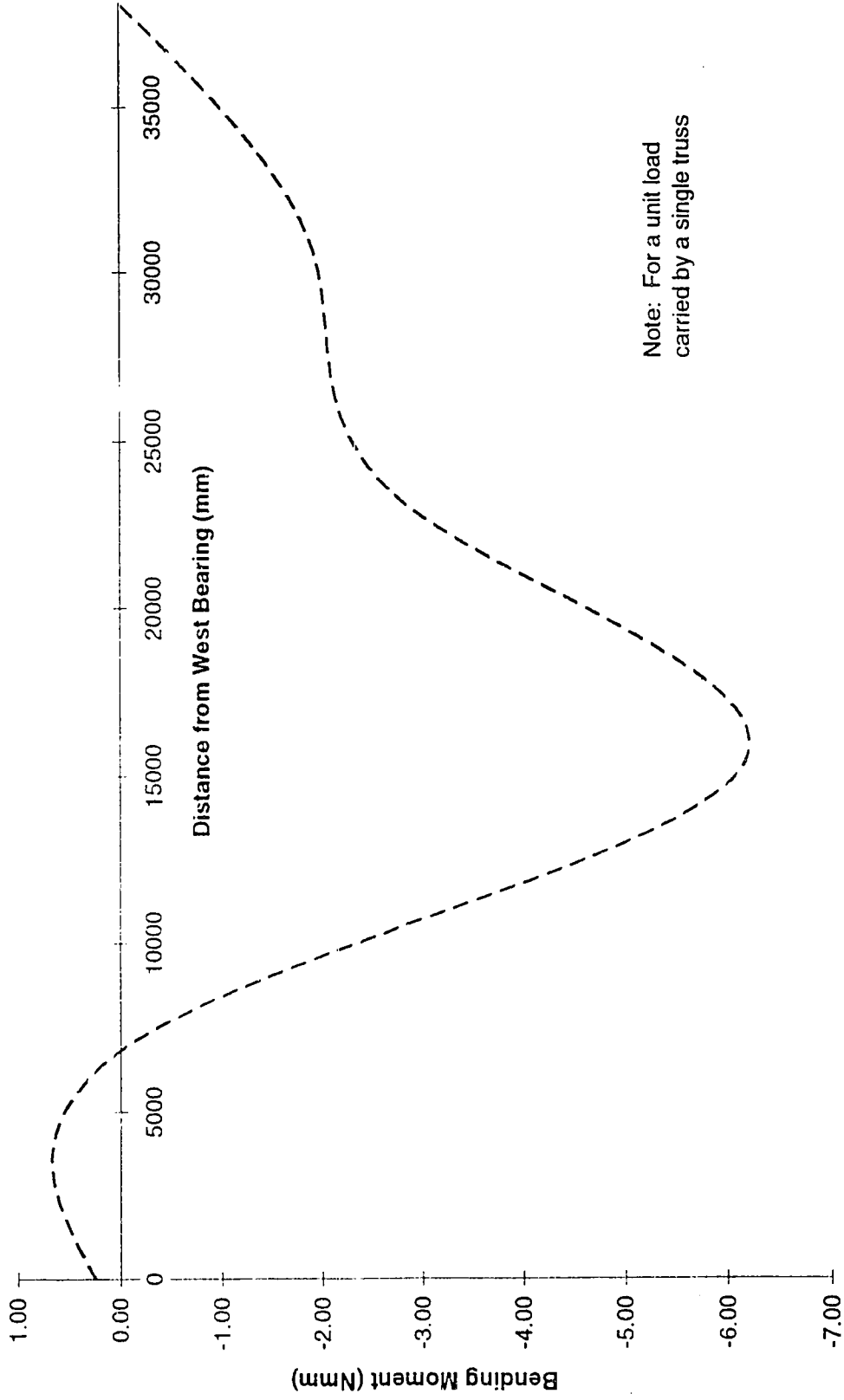


Figure 3.7 Influence Line for Bending Moment in Diagonal D1 (Eastbound Unit Load) Calculated Using the *Space Frame Model*

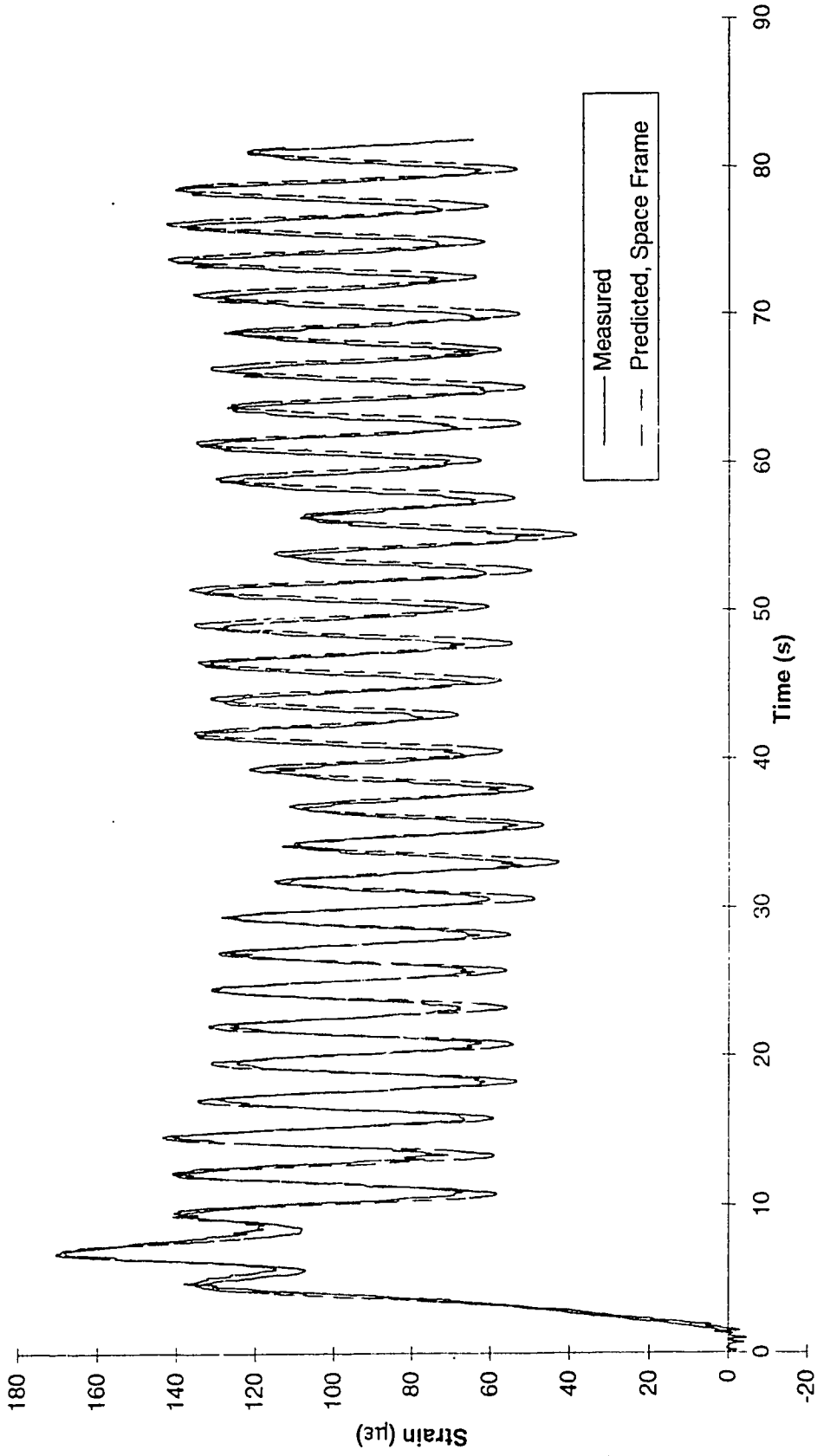


Figure 3.8 Measured and Predicted Strains in Diagonal D1, South Flange (Train T720)

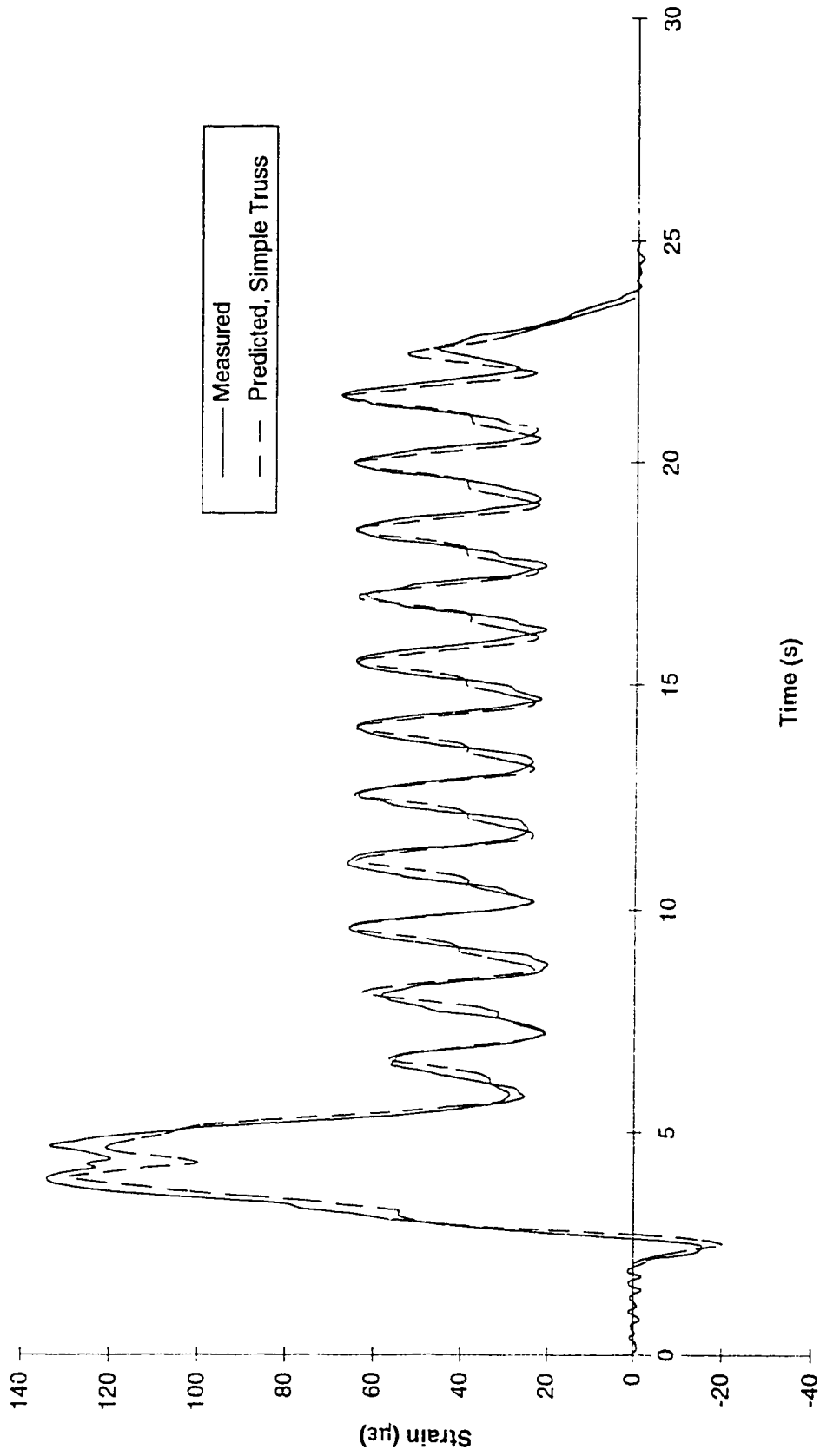


Figure 3.9 Measured and Predicted Strains in Diagonal D1, North Flange (Train F430)

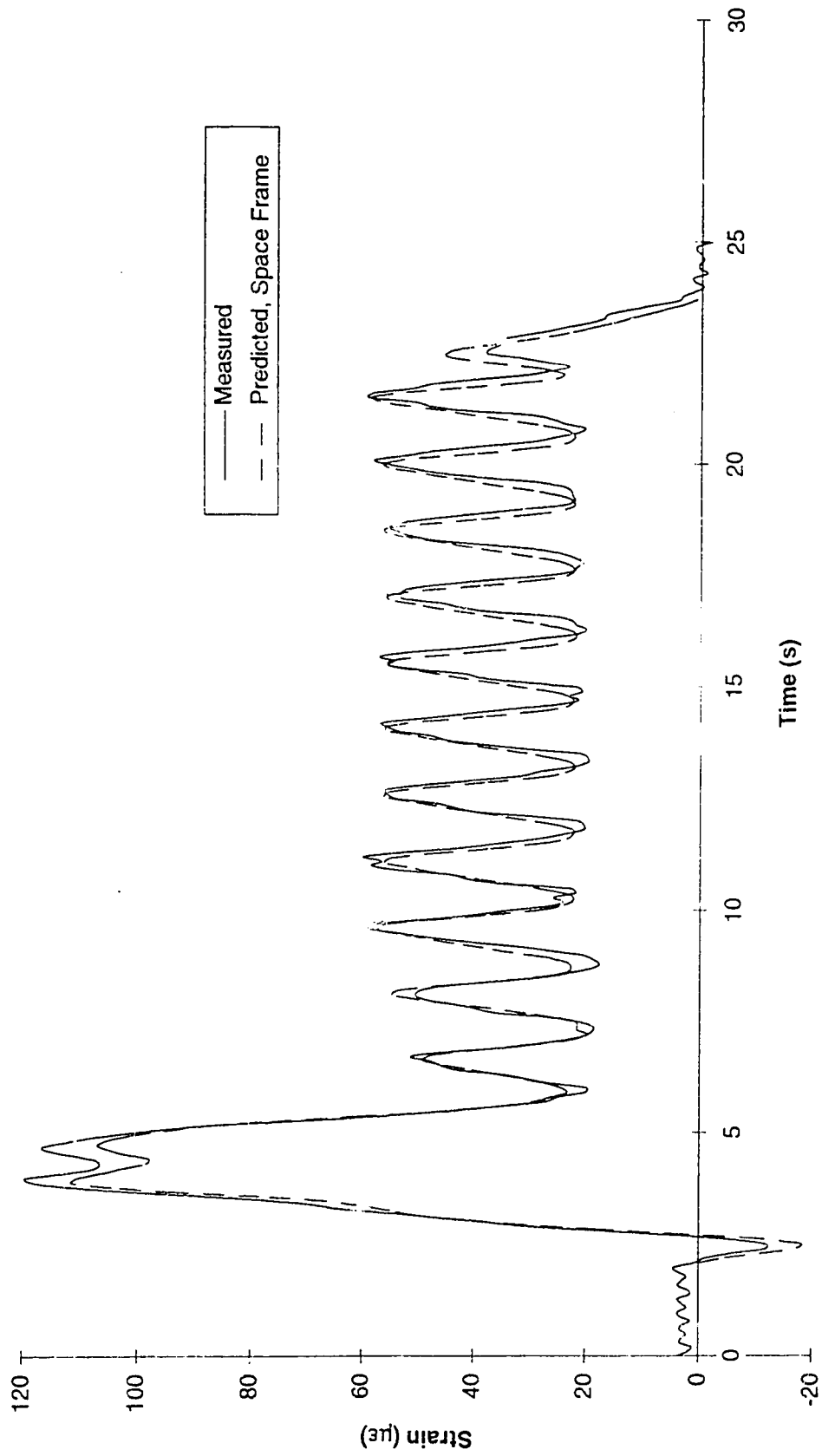


Figure 3.10 Measured and Predicted Strains in Diagonal D1, South Flange (Train F430)

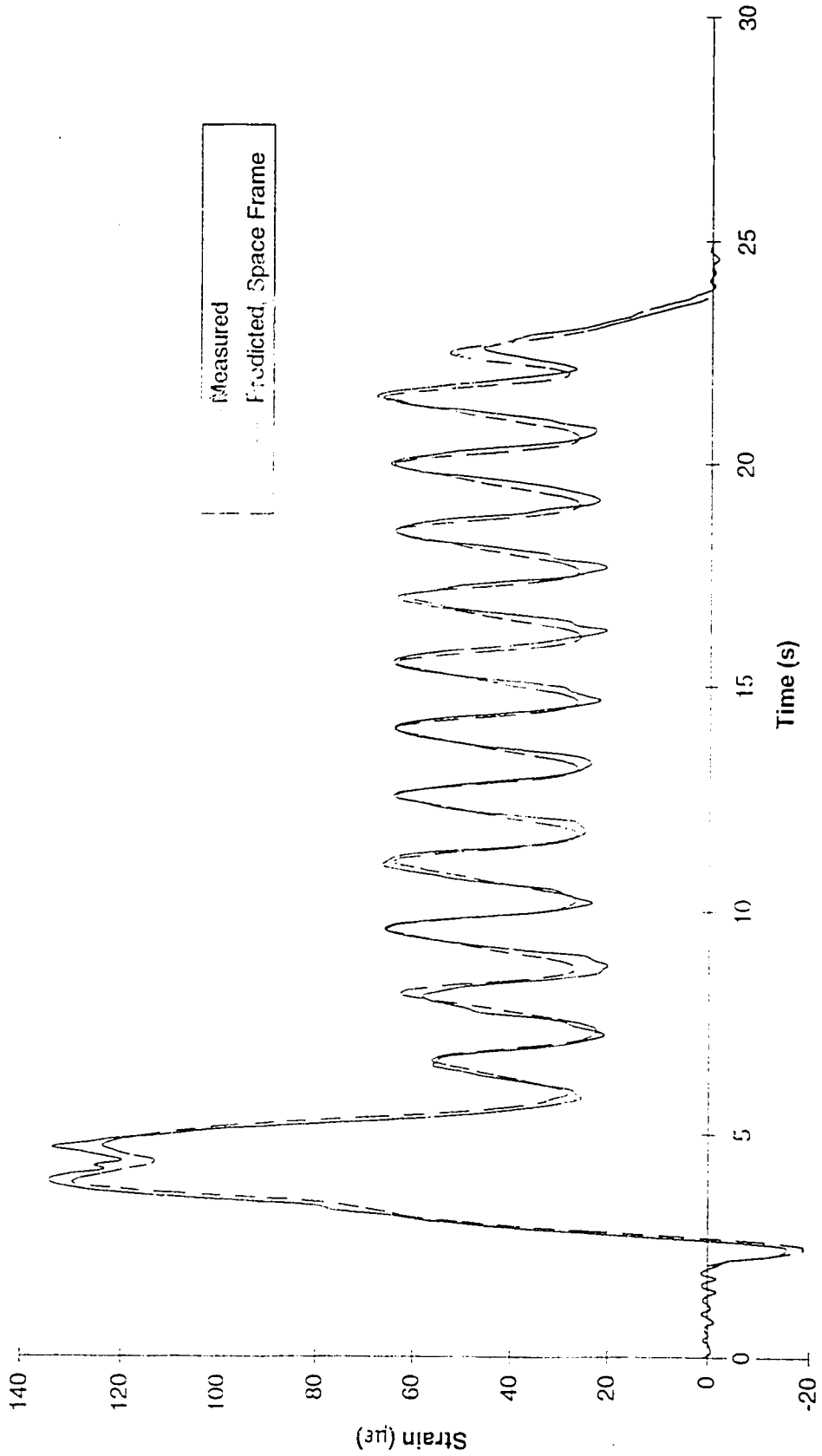


Figure 3.11 Measured and Predicted Strains in Diagonal D1, North Flange (Train F430)

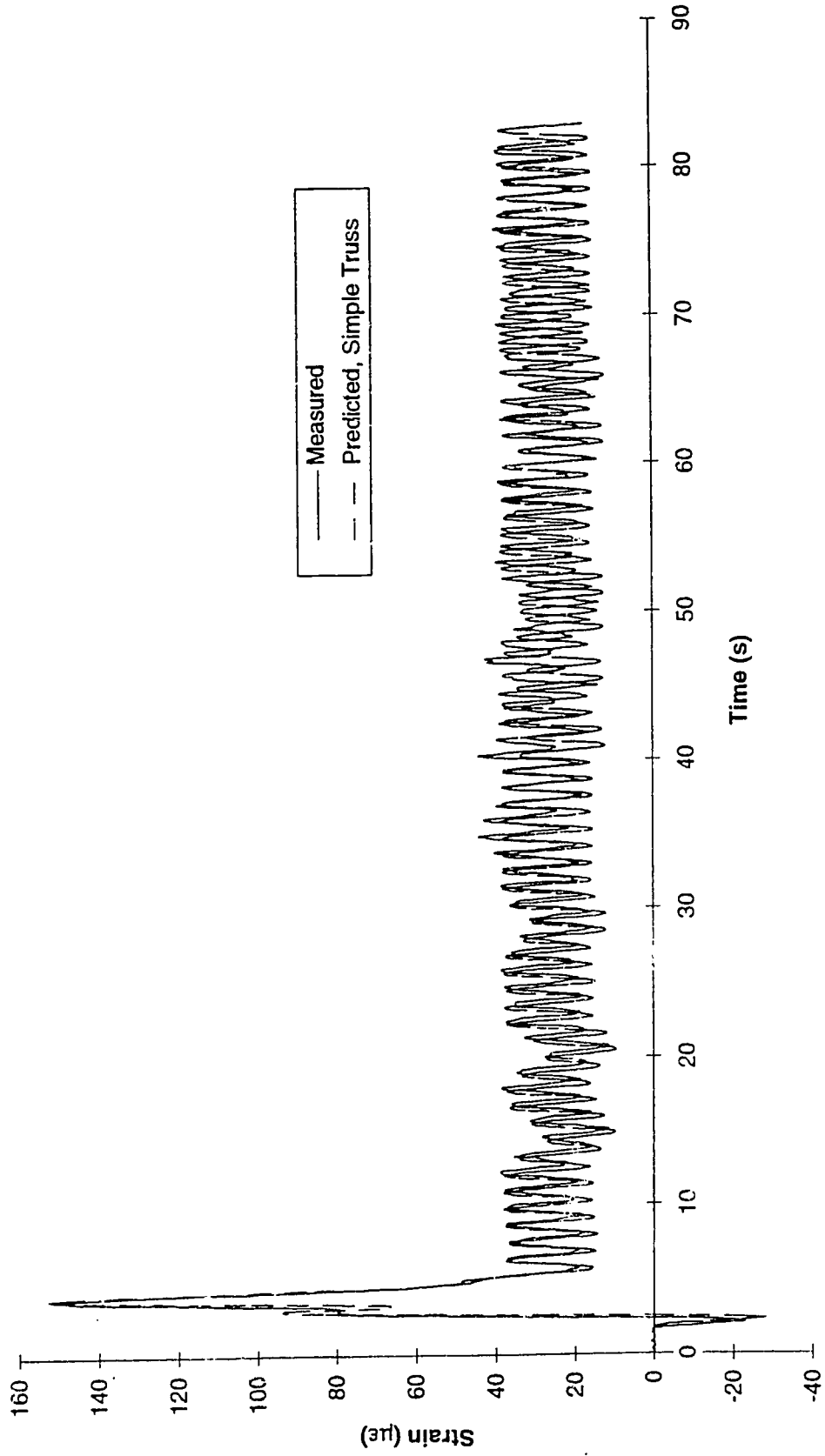


Figure 3.12 Measured and Predicted Strains in Diagonal D1, Web (Train F658)

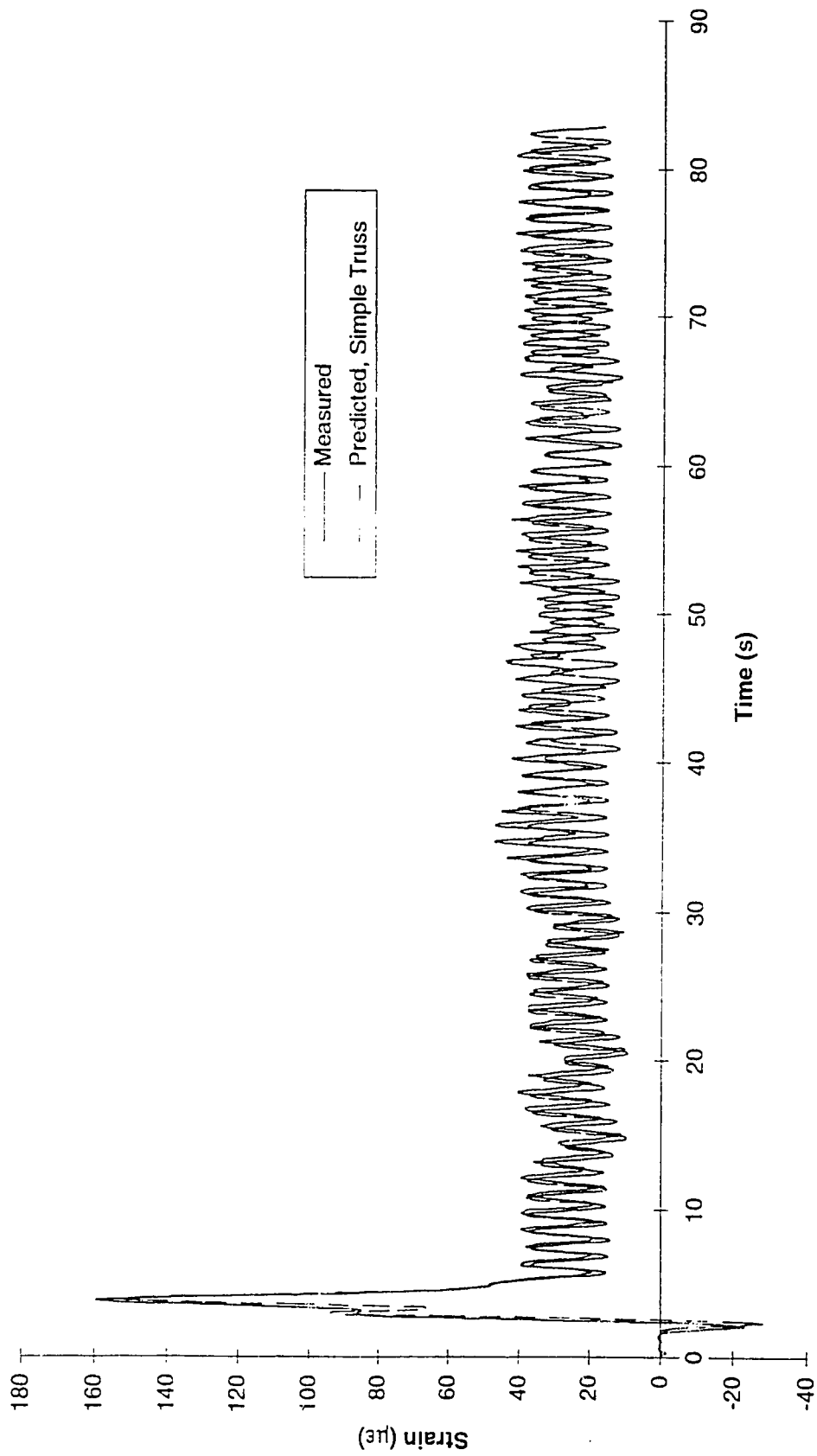


Figure 3.13 Measured and Predicted Strains in Diagonal D1, North Flange (Train F658)

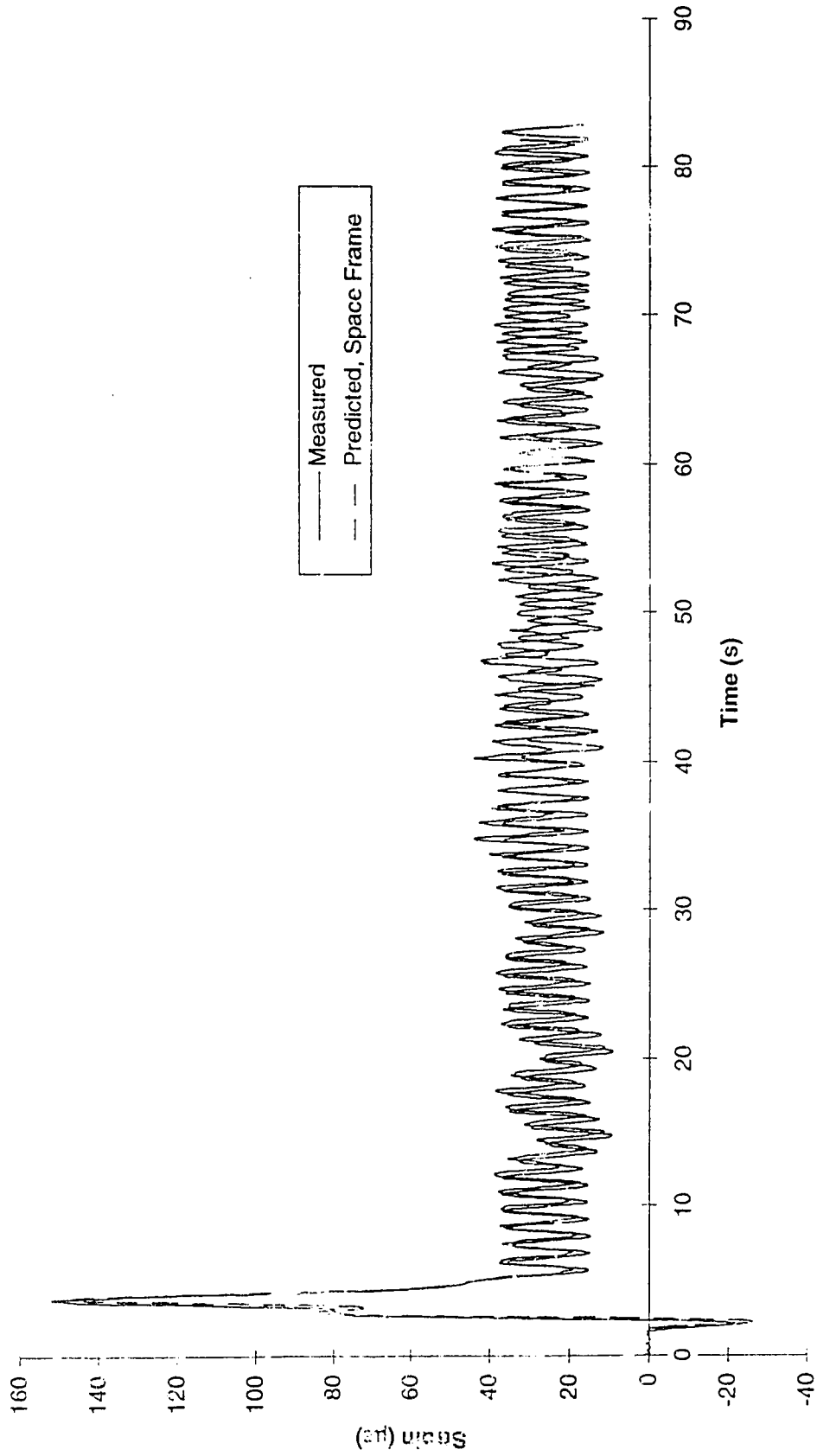


Figure 3.14 Measured and Predicted Strains in Diagonal D1, Web (Train F658)

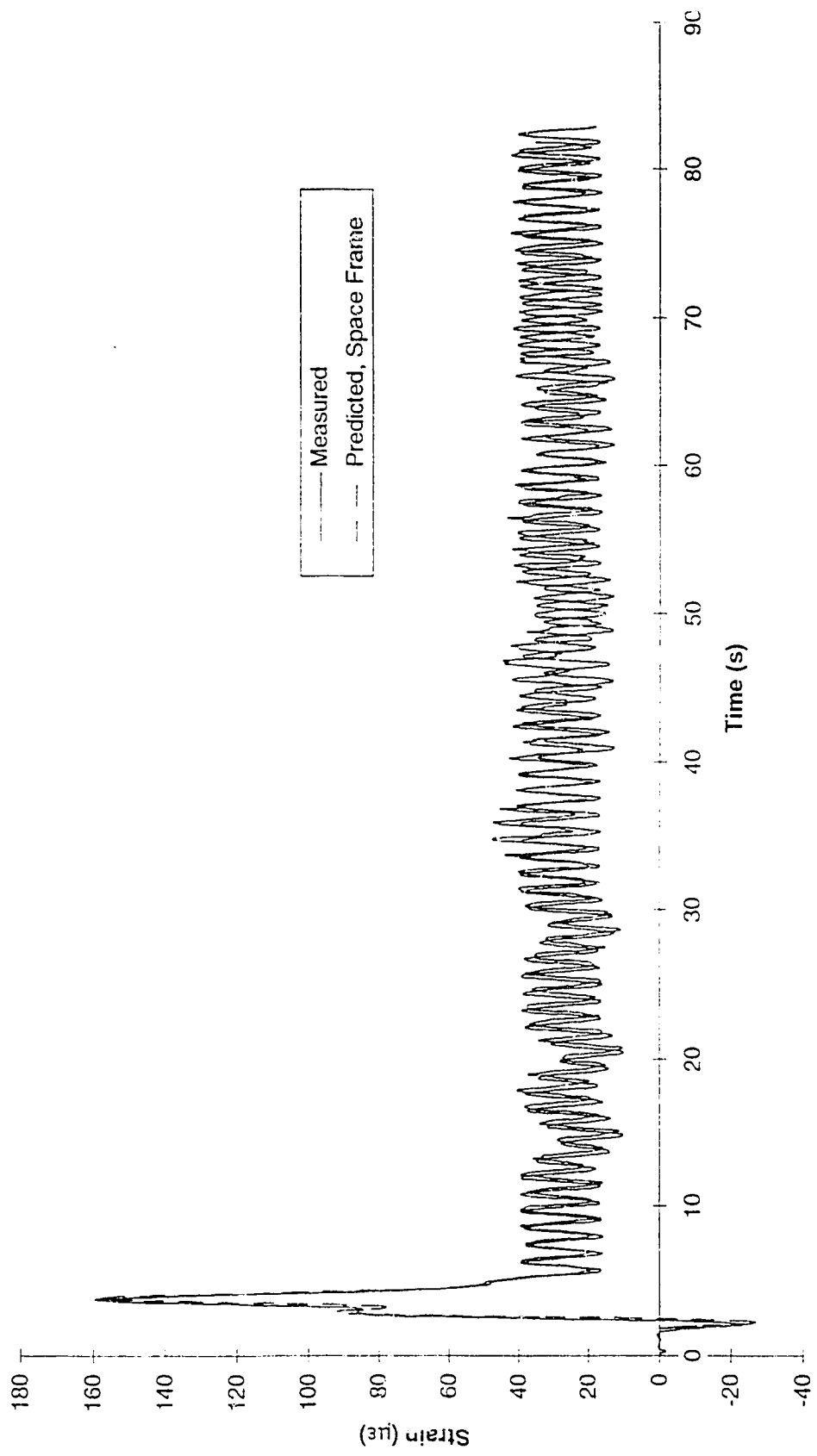


Figure 3.15 Measured and Predicted Strains in Diagonal D1, North Flange (Train F658)

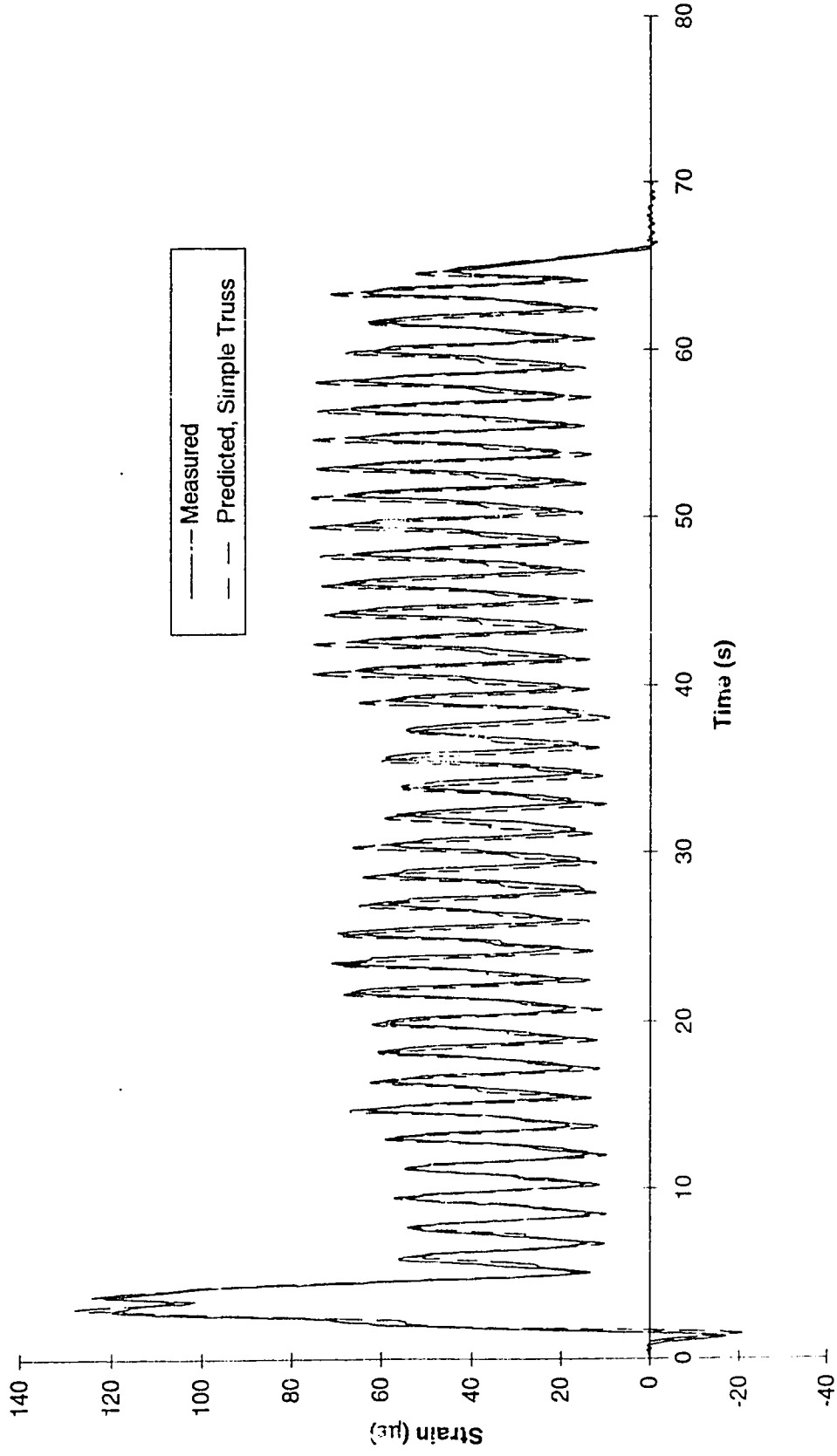


Figure 3.16 Measured and Predicted Strains in Diagonal D1, Web (Train F717)

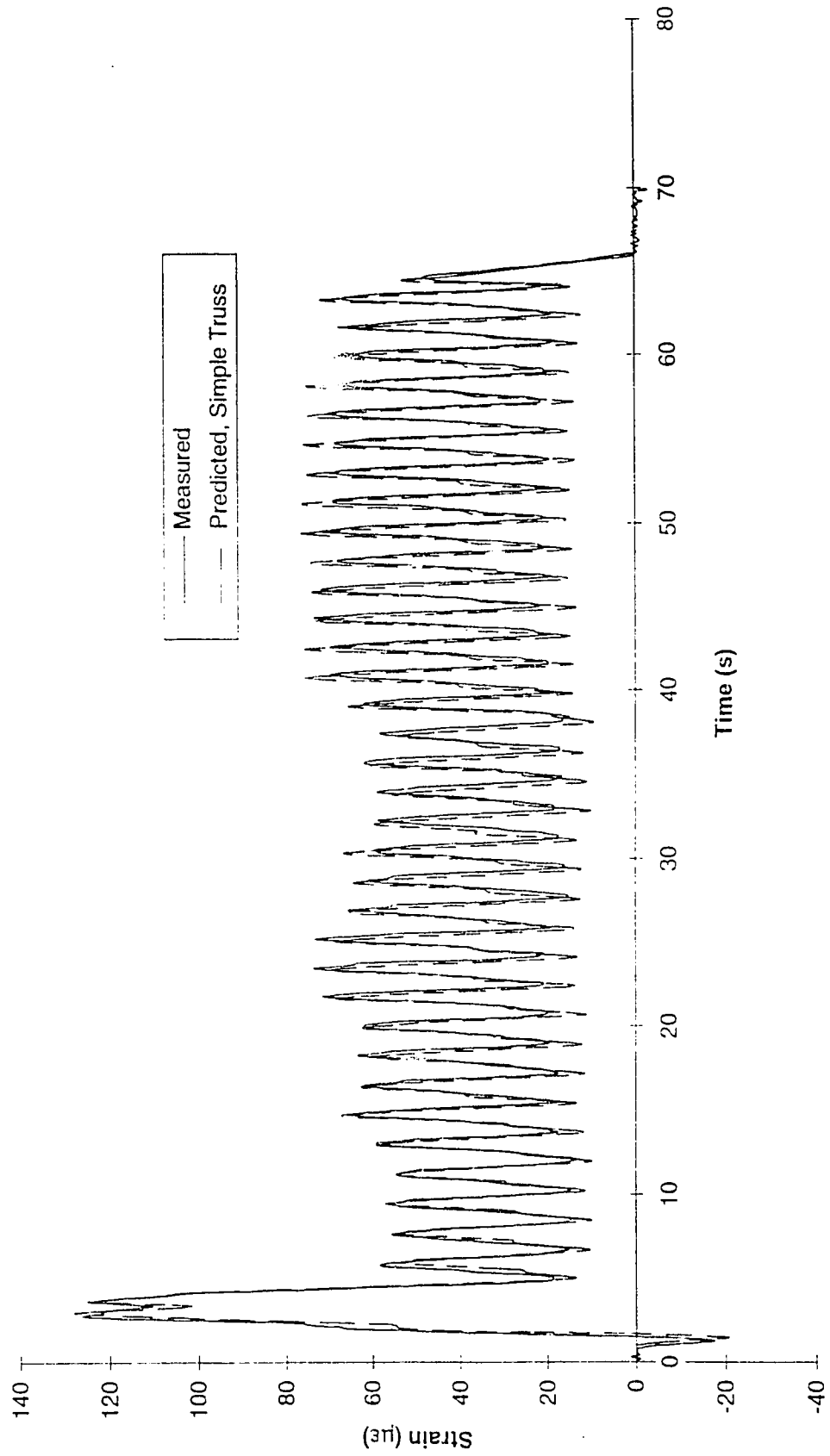


Figure 3.17 Measured and Predicted Strains in Diagonal D1, North Flange (Train F717)

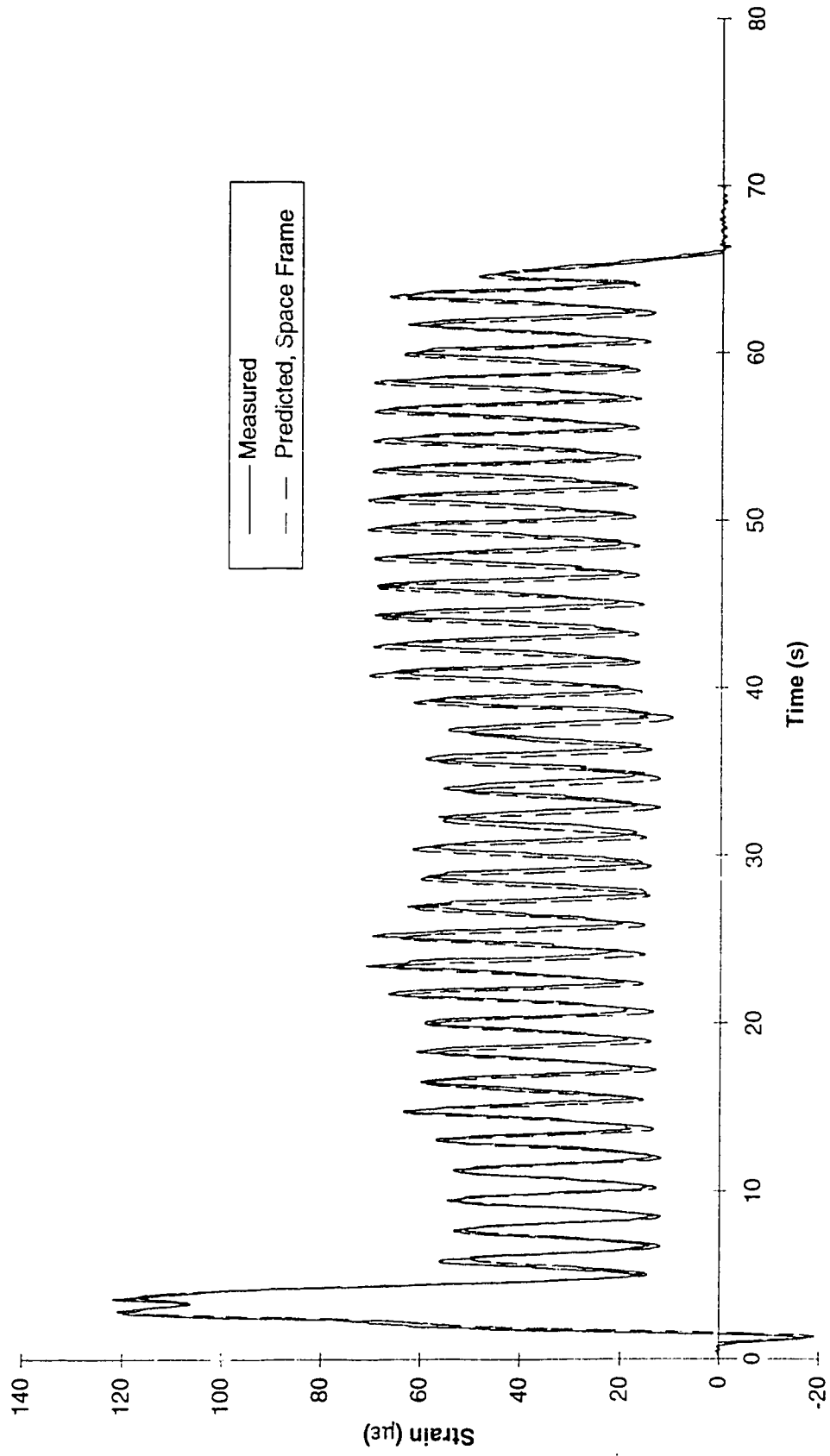


Figure 3.18 Measured and Predicted Strains in Diagonal D1, Web (Train F717)

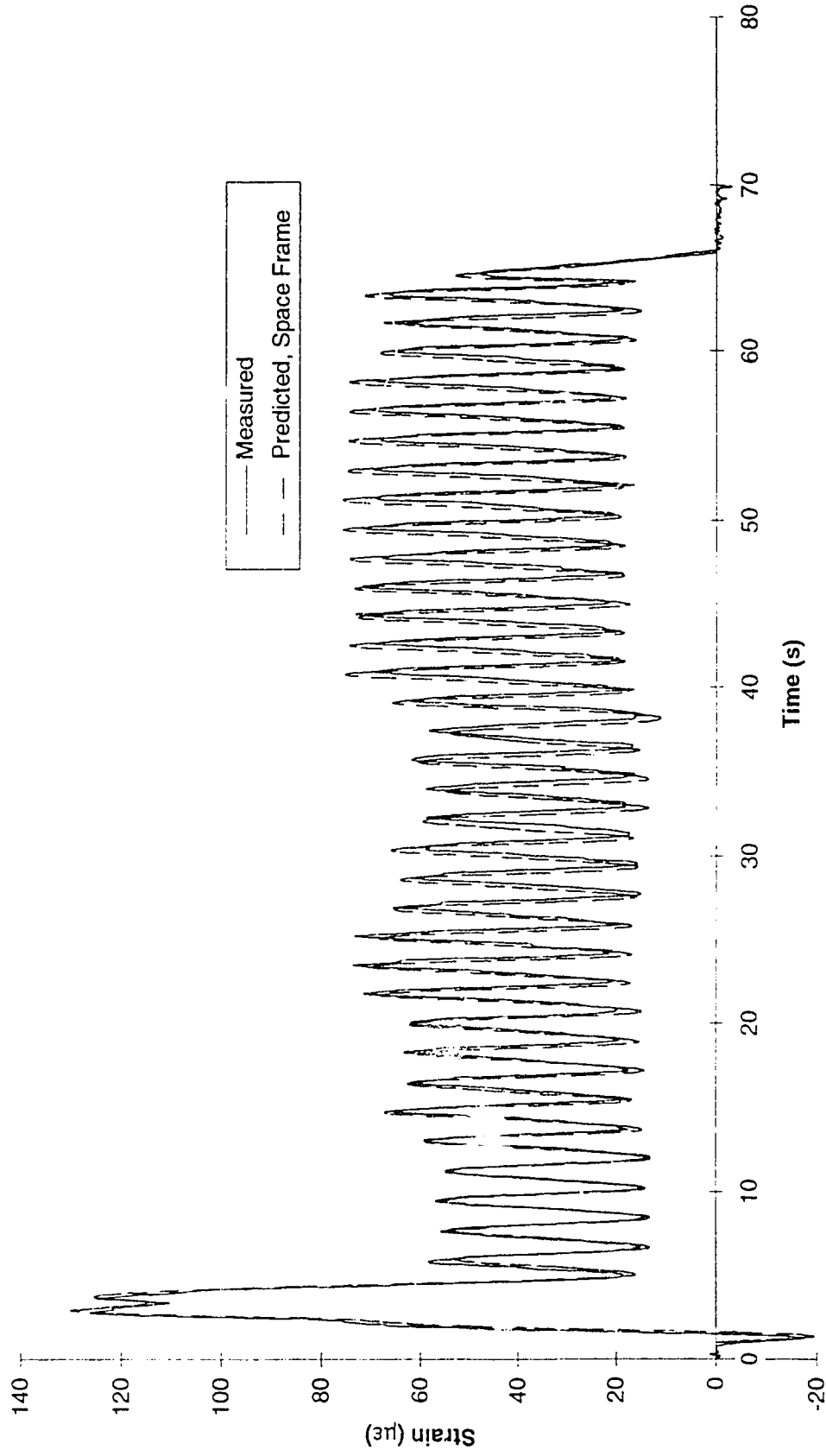


Figure 3.19 Measured and Predicted Strains in Diagonal D1, North Flange (Train F717)

4. Experimental Program

4.1 Goals of the Test Program

The literature review revealed that few fatigue tests of full-scale riveted members have been performed, and only one study has specifically investigated full-scale riveted shear splice connections. In addition, very few tests have been conducted at low stress ranges, that is, below about 75 MPa. Test results at low stress ranges are important in the prediction of remaining fatigue life because they help to define the location of the constant amplitude fatigue limit. The region near the constant amplitude fatigue limit is also the location of the Kunz transition region [Kunz, 1992]. In order to supplement the existing database of fatigue test results for riveted details, an experimental program was undertaken to study full-scale riveted shear splice connections subject to low stress range fatigue loads. Other issues have also been explored in this study, such as the fatigue strength of details where rivets are, theoretically, not in shear, the repair of fatigue cracks, and the condition of the fatigue crack surfaces.

The experimental program consisted of fatigue tests of full-scale gusset plate end connections from four riveted tension diagonals. The specimens were taken from the Miette River Bridge (described in Chapter 3), and all of the tests were conducted in uniaxial constant amplitude cyclic tension. Existing fatigue damage in the specimens was deemed negligible because strain measurements and historical records indicated that stresses on critical details in the diagonals likely never exceeded the Category D constant amplitude fatigue limit given in the AREA Manual [AREA, 1994].

4.2 Description of Test Specimens

The four primary tension diagonals of the Miette River Bridge were acquired by the University of Alberta in 1992, complete with the gusset plate end connections intact. Each diagonal was cut transversely in half during disassembly of the bridge in order to obtain manageable lengths, and this gave a total of eight specimens. Four of these had a length of

diagonal attached to a bottom chord panel point: these were designated BD1 through BD4. These specimens are numbered in accordance with their locations in the bridge as illustrated in Figure 3.2—specimen BD1 was taken from Diagonal D1, BD2 was taken from Diagonal D2, and so on. The four pieces that had a length of diagonal attached to a top chord panel point are hereafter referred to as specimens TD1 through TD4. The numbering of TD series specimens does not correspond to their locations in the bridge, because of an oversight that resulted in improper labelling of the specimens when the bridge was disassembled. Instead, specimens TD1 through TD3 are labelled in accordance with the chronological order in which they were tested. Because of time constraints, specimen TD4 was not tested as part of this study.

The original construction drawings show that all material was so-called *O.H. Steel*, indicative that the steel was produced using the open hearth process. Open hearth steel was commonly used early in this century, and it has properties similar to today's mild steel. The manufacturer's mark, *Carnegie*, was found on the web of the diagonal of all specimens, the mark *Carnegie C* was found on all flange angles, and the gusset plates had no distinguishing marks. It was noted that the angles that formed the flanges of the diagonal were rolled at slightly less than ninety degrees, and this was typical of all specimens. As a result, in some locations there was a significant gap, in the order of 3 mm, between the gusset plate and the outstanding leg of the angle. It is likely that minimal load was transferred by friction where the gap existed, although in some cases the gap was filled with rust and debris.

Corrosion of the diagonals was light, and they showed little evidence of loose or flaked paint. A series of small, circular indentations were noted in some of the diagonals. These were located in the flange angles near their connection to the gusset plate, and it is believed that they were formed in some way during the original fabrication process, possibly when the rivet holes were punched. In the final analysis, these indentations did not affect the fatigue life of any specimen.

4.3 Preparation of Test Specimens

The preparation of the specimens was done with the intent to model service conditions as accurately as possible. It is first necessary to consider the way that the specimens were loaded while in service and the locations of critical details. In general, a riveted gusset plate connection will have a critical net section area in one of two possible locations, as shown in Figure 4.1. One possible location of fatigue crack formation is in the member, at the line of rivets nearest the edge of the gusset plate. The other likely location is in the gusset plate, at the line of rivets nearest the end of the member [Kulak *et al.*, 1987]. The geometry of the diagonals taken from the Miette River Bridge was such that the critical detail was in the member, not in the gusset plate. Consequently, when the specimens were prepared, an adequate area of gusset plate was kept to ensure that the first crack would form in the diagonal, that is, the same failure mechanism that would have occurred in the original structure.

4.3.1 Locations of Critical Details

The gross cross-sectional area of each diagonal, calculated from the original construction drawings, is 13 620 mm². Measurements taken from several specimens verified that the fabrication was consistent with the drawings, and, as a result, all subsequent calculations were based on dimensions shown on the drawings. The net cross-sectional area for the BD series of specimens was calculated for a section through the diagonal at the first line of rivets nearest the edge of the gusset plates, as shown in Figure 4.2 (a). This section passed through holes for rivets that joined the angles to the gusset plates (hereafter called gusset-angle rivets) and through holes for rivets that joined the angles to the web of the diagonal (hereafter called web-angle rivets). There is no ambiguity in the selection of this cross-section. Specimens from the BD series have a critical net section area of 11 042 mm².

In the case of the TD series of specimens, there are no web-angle rivets in direct alignment with the first line of gusset-angle rivets. (See Figure 4.2 (b).) This means that the location of the critical net section area is not immediately apparent. However, a pair of web-angle rivets is in alignment with the second line of gusset-angle rivets. The net area of a section

taken at the first line of gusset-angle rivets is $12\,554\text{ mm}^2$, and the net area of a section taken at the second line of gusset-angle rivets is $11\,042\text{ mm}^2$. Although the second line of rivets has a smaller net area, it is subjected to less force because some load transfer out of the diagonal into the gusset has occurred at the first line of fasteners. The tests later revealed that the fatigue cracks for these members formed in the angles at the first line of gusset-angle rivets. Consequently, the net section area at the first line, $12\,554\text{ mm}^2$, was used to calculate stress ranges for all TD series specimens. The issue of net cross-sectional area for the TD series of specimens is discussed further in Chapter 5.

4.3.2 Preparation of Specimens

The specimens were cut to a length of 3 124 mm (123 in.) to prepare them for the tests, a length that was determined through consideration of several factors. A reduction of the length made construction of the loading system simpler. In addition, shorter specimens allowed increased cyclic load frequencies because the amount of deflection in the load system is reduced. Although it was desirable to minimize length, the behaviour of the specimen in the test still must match the expected behaviour of the diagonal in the bridge. The strain measurements taken while the bridge was in service showed that the strain distribution in the diagonal was relatively uniform away from the gusset connection. To replicate this behaviour, a sufficient length of diagonal was kept so that a reasonably uniform strain distribution could be maintained at mid-length of the specimen. This helped to ensure that the loads applied in the test would affect the connection in a manner similar to actual service loads.

When the diagonals were taken from the bridge, the gusset plates at the panel points and the diagonal were removed as a unit. In this arrangement, small stubs of the other members that framed into the panel points remained. Subsequently, all members that framed into the gusset plates at the panel points were removed, except for the diagonals. A pneumatic chisel was used to sever the rivet heads, and the rivets were then pushed out with a hydraulic punch to detach the unwanted members. This method proved to be effective, and it caused minimal damage to the gusset plates.

Each gusset plate was then trimmed to give manageable proportions and an approximately symmetrical shape. The shape of the gusset plates was also selected to avoid the presence of rivet holes near the free edges and, as already described, to maintain a sufficient cross-sectional area so as to prevent fatigue crack formation. This cross-sectional area was selected so that the net section stress range at the gusset plate was not more than 60 % of the stress range at the critical detail. Drawings of typical BD series and TD series specimens as prepared for testing are presented in Figure 4.3 and Figure 4.4, respectively.

4.3.3 Ancillary Tests

A total of six tension coupons were taken from excess material from one specimen, and these were tested prior to the fatigue study. Two coupons were taken from the web, two from the flange angles, and two from the gusset plate. The coupons from the web and flange angles were oriented parallel to the length of the member, and the coupons from the gusset plate were oriented perpendicular to each other. The tension coupon test results are assumed to be representative of all specimens.

The tension coupons were machined in accordance with the requirements of ASTM A 370-92 [1992], with a gauge length of 50 mm and a section width of 12 mm. An MTS 1000 universal testing machine was used to carry out the tests, which were conducted at a strain rate of approximately 10 $\mu\text{e/s}$ in the elastic range and 50 $\mu\text{e/s}$ in the plastic range. Strain in each coupon was measured using two electrical resistance strain gauges in the elastic range, and a clip-on extensometer in the inelastic range. Data was recorded both electronically and with an analogue plotter throughout the tests. Three static yield values, two in the initial yield stress plateau and one near the ultimate stress peak, were obtained for each coupon when the strain rate was reduced to zero for an interval of two minutes. The coupon tests showed that all of the components had an elastic modulus of approximately 208 000 MPa, a yield stress in the order of 230 MPa, and an ultimate strength of about 380 MPa. Specific results from the tension coupon tests can be found in Appendix D.

• Load System

Each specimen was loaded in tension using a single Pegasus hydraulic linear actuator (hereafter referred to as a jack) that has a maximum dynamic capacity of approximately 500 kN. In the experiment, the jack was always loaded in compression and the specimen was always loaded in tension. Because of the large cross-sectional area of the full-scale specimen, forces larger than 500 kN were required to achieve the desired stress range at the critical detail. In order to exert these forces on the specimen, a lever system having a mechanical advantage of 2.5:1 was incorporated into the load frame, as shown schematically in Figure 4.5.

A spherical roller bearing was used to attach each end of the specimen to the load frame. This ensured that only uniaxial force was applied, because the bearings did not allow moment resistance to be developed at the end connections. The bearings were self-aligning spherical roller bearings, and they held solid 130 mm diameter pins made of heat-treated AISI 4140 steel. The pins penetrated steel plates, known as load transfer plates, in order to transfer force to the specimen. Two similar bearings were also used at the fulcrum, so as to allow rotation to occur with minimal friction and to provide torsional stiffness to the lever system. A design drawing and a photograph of the loading system are presented in Figures 4.6 and 4.7, respectively.

4.4.1 End Connections

A slip-critical bolted connection was used to transfer load into the ends of each specimen. At the end of the specimen with the existing riveted connection, the gusset plates were fastened to the load transfer plates with 7/8 in. diameter A325 bolts. Several new holes were drilled in the gusset plates for installation of these bolts, and all existing holes in the gusset plate that had been left open by the removal of rivets were also filled. All holes in the gusset plate left open by the removal of rivets that were not part of the connection to the load transfer plate were also filled with pretensioned 7/8 in. diameter A325 bolts in order to reduce their influence as stress raisers.

At the end of the specimen away from the existing gusset plates, it was necessary to develop an entirely new connection that would exceed the fatigue strength of the critical detail. A slip-critical bolted connection was designed, incorporating ten 7/8 in. diameter pretensioned A490 bolts, so as to join each flange of the specimen to a load transfer plate. In order to avoid crack formation at the riveted connection of the flange angles to the web in each specimen, the six rivets that connected the flange angles to the web near the connection were removed and replaced with pretensioned 7/8 in. diameter A490 bolts (see Figure 4.8).

4.4.2 Control and Data Acquisition

Cyclic loads were provided by an electronically-controlled servovalve that regulated the hydraulic jack to provide the desired force. The system was capable of producing a maximum tensile force in the specimen of approximately 1000 kN, limited by the shear capacity of the spherical roller bearings. The cyclic load followed a sine wave function, and frequencies in the range 2.5 Hz to 3 Hz were used.

The stress range in each specimen was monitored using two separate systems. The primary system consisted of six electrical resistance strain gauges placed at mid-length of the specimen and monitored by a computer data acquisition unit. One gauge was affixed to the outstanding leg of each of the four angles, and two gauges were mounted on the web. When the test was in operation, each strain gauge was read dynamically by the computer approximately 75 times per second. From these strains, the maxima and minima were displayed on the computer screen, and data from all gauges was stored once every three hours.

In order to set any desired net section stress range, the modulus of elasticity obtained from the tension coupon tests was used in conjunction with the net section area to determine the required net section strain range. However, the strain gauges had to be located away from riveted details, and thus they measured the strain in the gross section area of the member. In order to obtain the net section strain at the critical detail, the average of the measured gross section strains was multiplied by a conversion factor. This factor was

simply the ratio of the gross cross-sectional area to the critical net cross-sectional area. This ratio is 1.23 for the BD series of specimens and 1.08 for the TD series of specimens.

The critical net section stress range was also monitored by a secondary system that measured the compressive force exerted by the hydraulic jack. Based on the mechanical advantage ratio of the lever, it was possible to calculate the axial force in the specimen, and, therefore, the critical net section stress range. Load cell measurements were not recorded, but were monitored throughout each test to ensure that load levels were within allowable tolerances as compared to the strain gauge measurements.

4.5 Test Procedure

The literature review indicated that very few tests have been conducted at stress ranges below 75 MPa, and no tests of full-scale riveted shear splices have been conducted below 125 MPa. The tests reported herein were carried out at comparatively low critical net-section stress ranges—two specimens at 73.0 MPa and one each at 69 MPa, 66 MPa, 64 MPa, 62 MPa, and 58 MPa. In order to avoid instability in the load frame, the minimum net section applied stress for all specimens was approximately 10 MPa of tension.

The failure criterion used in this study was defined as the complete severing of one element of the built-up cross section of the diagonal and the first detection of a crack in a second element. This definition of failure was used to maintain consistency with similar tests of flexural members performed by others [Adamson, 1995]. This failure criterion was used for all specimens except for BD3, which was repaired immediately after the first element had severed.

In general, after one element of the built-up cross-section had severed and a crack had been detected in a second element, the test was stopped in order to avoid damage to the load system. Only one test, that of BD4, was allowed to continue until it was no longer able to carry the applied load. This was done in order to determine how closely the failure

criterion as defined in the study approximated actual failure, that is, the inability of the specimen to carry the applied load.

4.5.1 Inspection for Cracks

All specimens were completely sandblasted prior to testing in order to permit improved crack detection, which was done at intervals that varied with the number of stress cycles applied. Inspection was usually performed at least once daily (approximately once every 250 000 cycles) until first crack detection, and at least twice daily thereafter. Inspection for cracks was done visually, generally with the naked eye, but sometimes aided with a magnifying glass. When possible, the locations of the crack tip were recorded as the test progressed.

4.5.2 Repair of Cracks

With the test set-up described, it was also possible to obtain fatigue life data for the locations where the rivets simply fasten one part of the cross-section to the other, namely those rivets that join the angles to the web of the diagonal. At these locations the rivet is, theoretically, not loaded at all and the detail is simply one of a hole filled by a rivet. For specimen BD3, after a crack had severed one angle at the member-to-gusset plate connection, splice plates were introduced that took the force in the member around the location of the crack. The splice plates allowed the test to continue so that additional data on the fatigue strength of rivets theoretically not in shear could be obtained. The stress range for the critical detail, that is, the web-angle riveted detail, after repair in specimen BD3 was 66.6 MPa. At the same time, these splice plates are in themselves a repair technique that may have applications in the field, so it was useful to determine the effectiveness of this type of repair.

The splice plates used in this repair had dimensions of 25 mm x 330 mm x 1120 mm (1 in. x 13 in. x 44 in.). The plates were designed so that the net section stress range in the plates would not exceed the AREA Category D constant amplitude fatigue limit, based on the conservative assumption that the uncracked portion of the specimen carried no load. A

spacer plate was used to allow the repair plate to have clearance over the tops of the existing rivet heads. Each plate was fastened to the specimen using six pretensioned 7/8 in. diameter A325 bolts at each end. The repair plates are shown in Figure 4.9.

4.6 Post Test Examination

4.6.1 Examination of Fatigue Crack Surfaces

After completion of a test, the region containing the fatigue crack was cut from the specimen with an oxygen-acetylene torch. A sufficient area of material was removed so that the crack surfaces would not be affected by heat. The pieces were then sawed to manageable dimensions, and then the crack surfaces were exposed. The cracks were first inspected visually, with the naked eye and an optical microscope. From the initial inspection, several specimens were selected for further investigation using a scanning electron microscope. The goals of this inspection were to determine whether the details had any abnormalities that may have affected the fatigue test results, and to attempt to establish whether any fatigue cracks existed before the tests began. Abnormalities in the steel that might be expected are voids, inclusions, or damage to the rivet holes produced during fabrication or during assembly. Evidence that may support the presence of prior fatigue cracks is the presence of rust in the crack near its nucleus. If rust exists near the nucleus but not elsewhere, it is likely that the crack surfaces rusted while the bridge was still in service, an indication that an existing fatigue crack was present.

4.6.2 Examination of Rivets

A portion of the riveted gusset plate connection was also flame-cut from two BD and from two TD series specimens. The joint was then sawed down the centre of a line of rivets, parallel to the longitudinal axis of the diagonal, revealing the riveted connection in cross-section. The sections were then smoothed with a rotary grinder and finally polished with a belt sander. The sections allow examination of how well the rivets fill the holes, and also reveal shear deformation of the rivets.

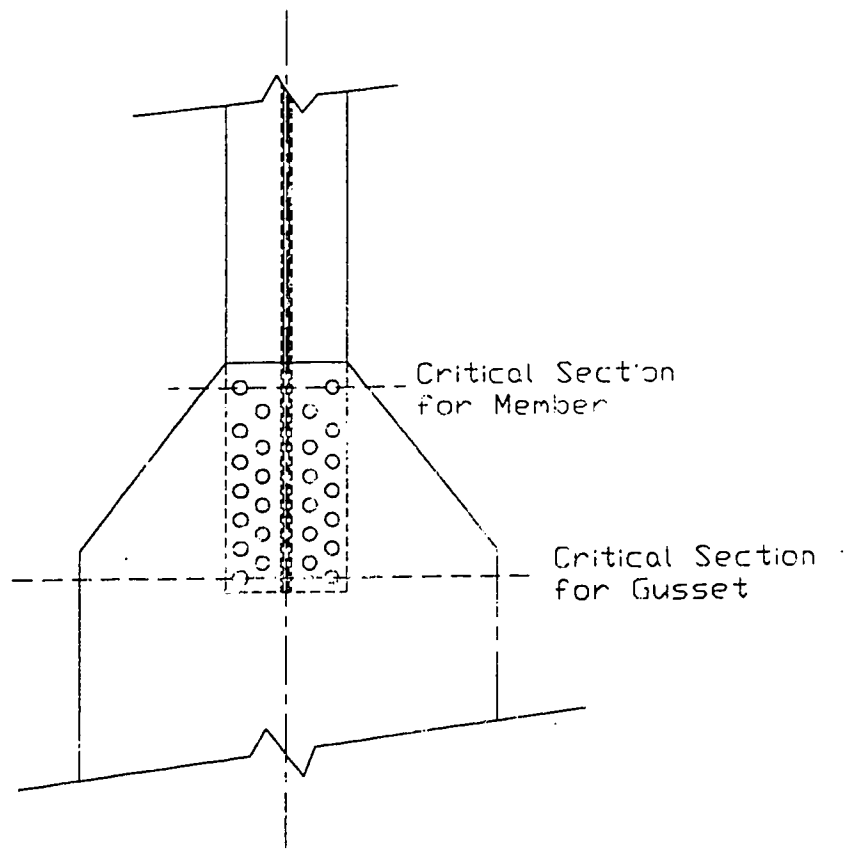


Figure 4.1 Potential Locations of Fatigue Cracking

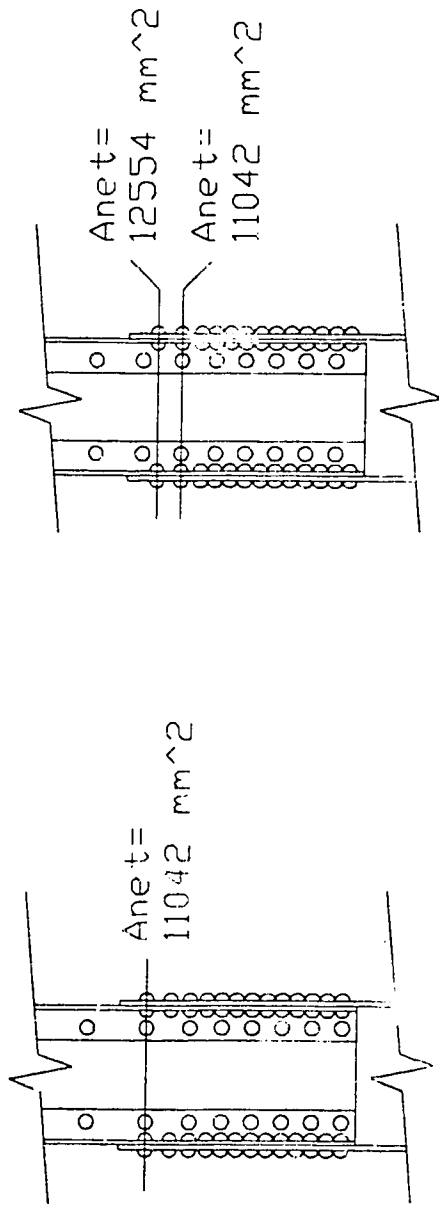


Figure 4.2 Critical Net Cross-Sectional Areas

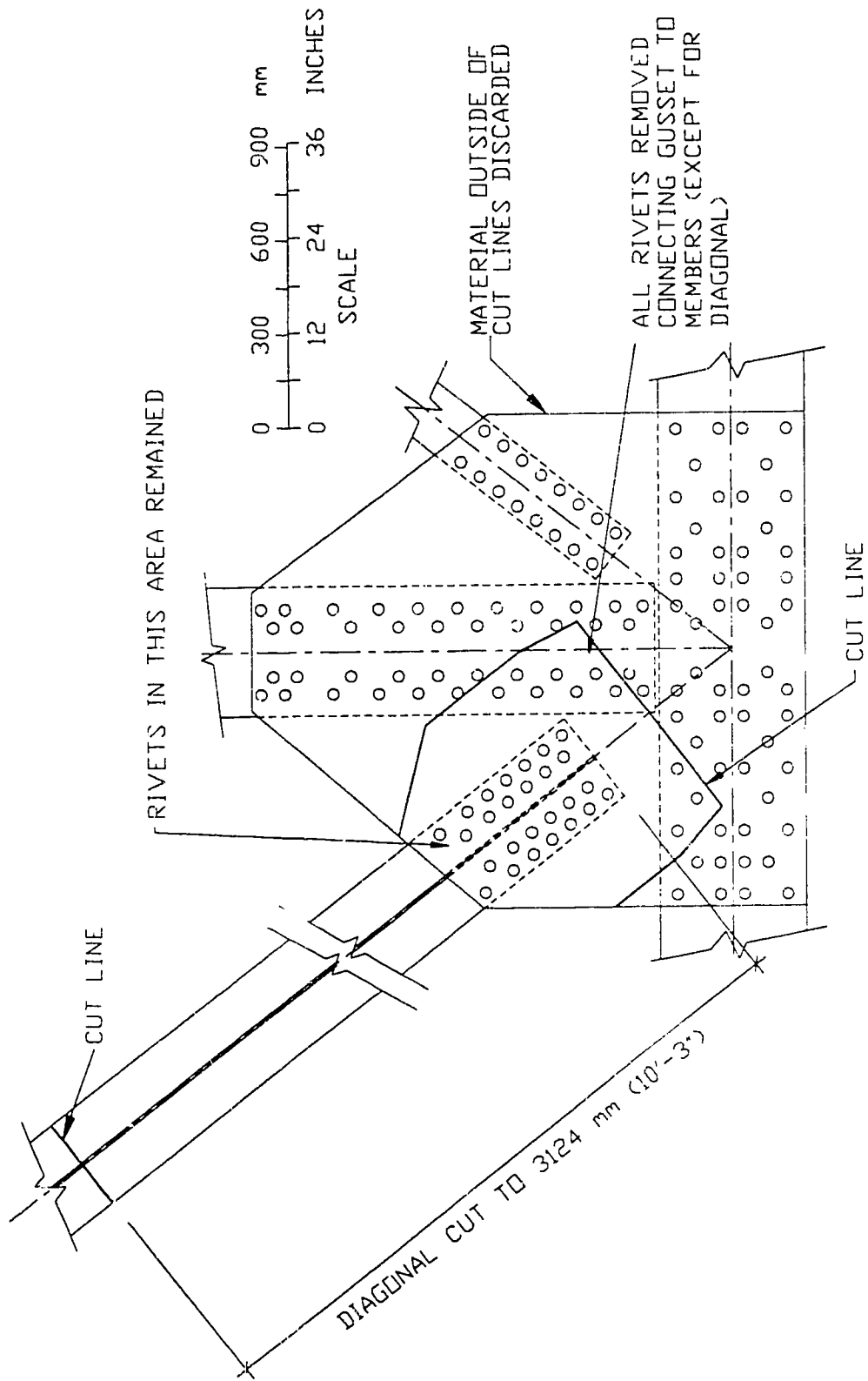


Figure 4.3 Typical Fabrication Details, BD Series

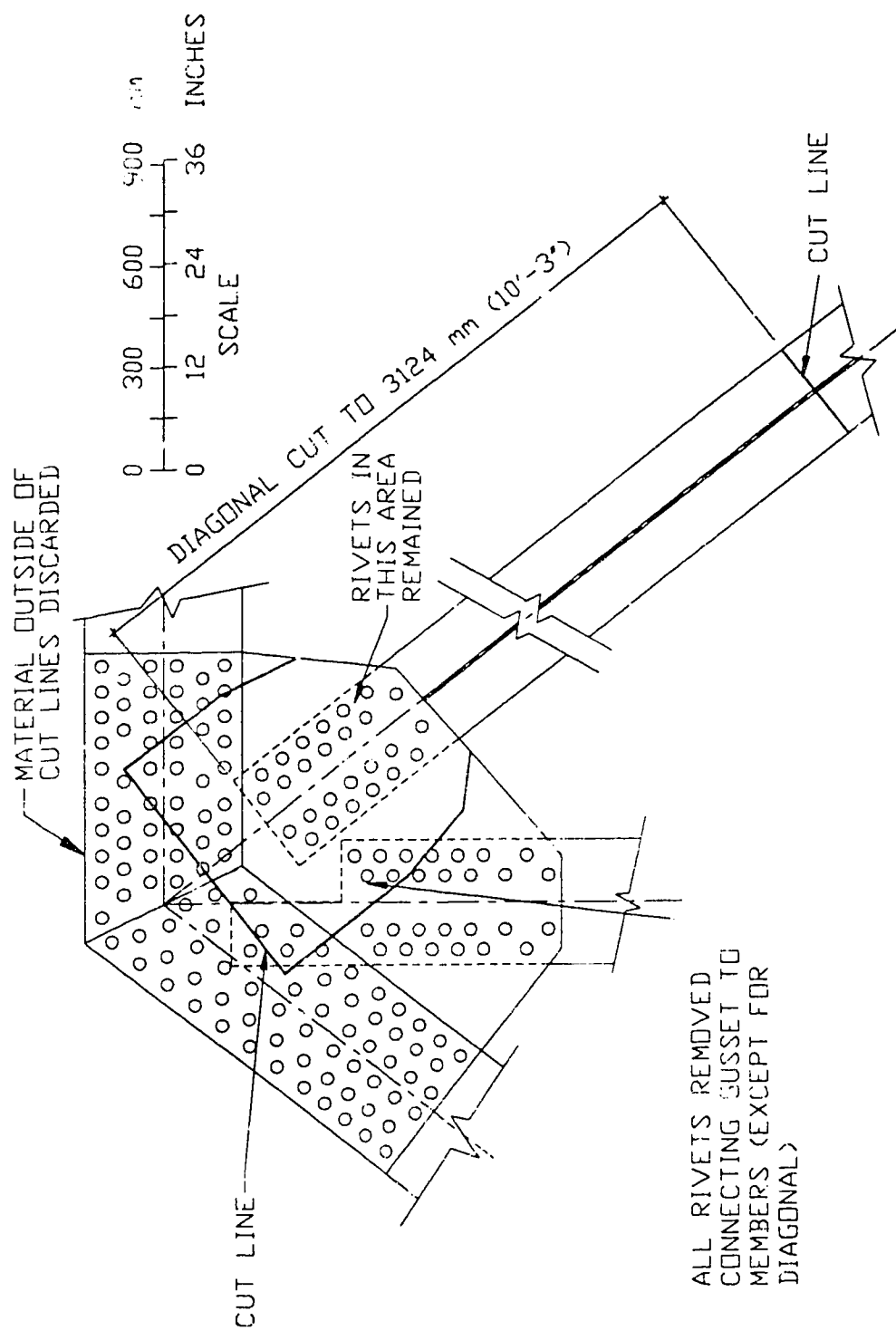


Figure 4.4 Typical Fabrication Details, TD Series

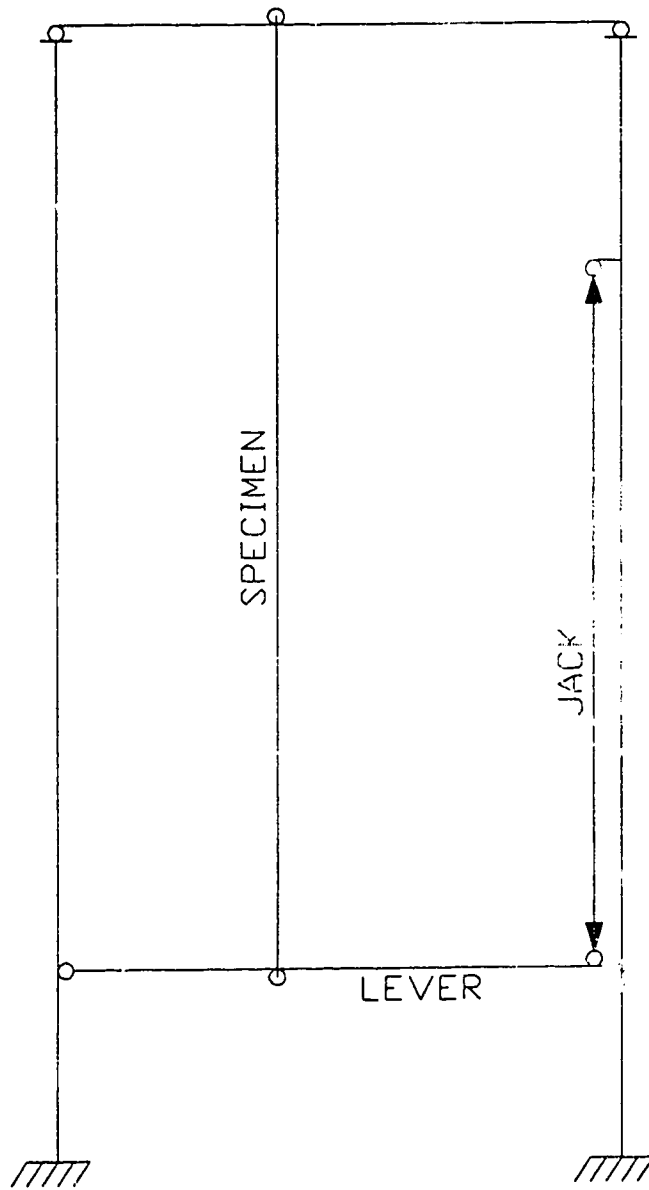


Figure 4.5 Schematic of Load Frame

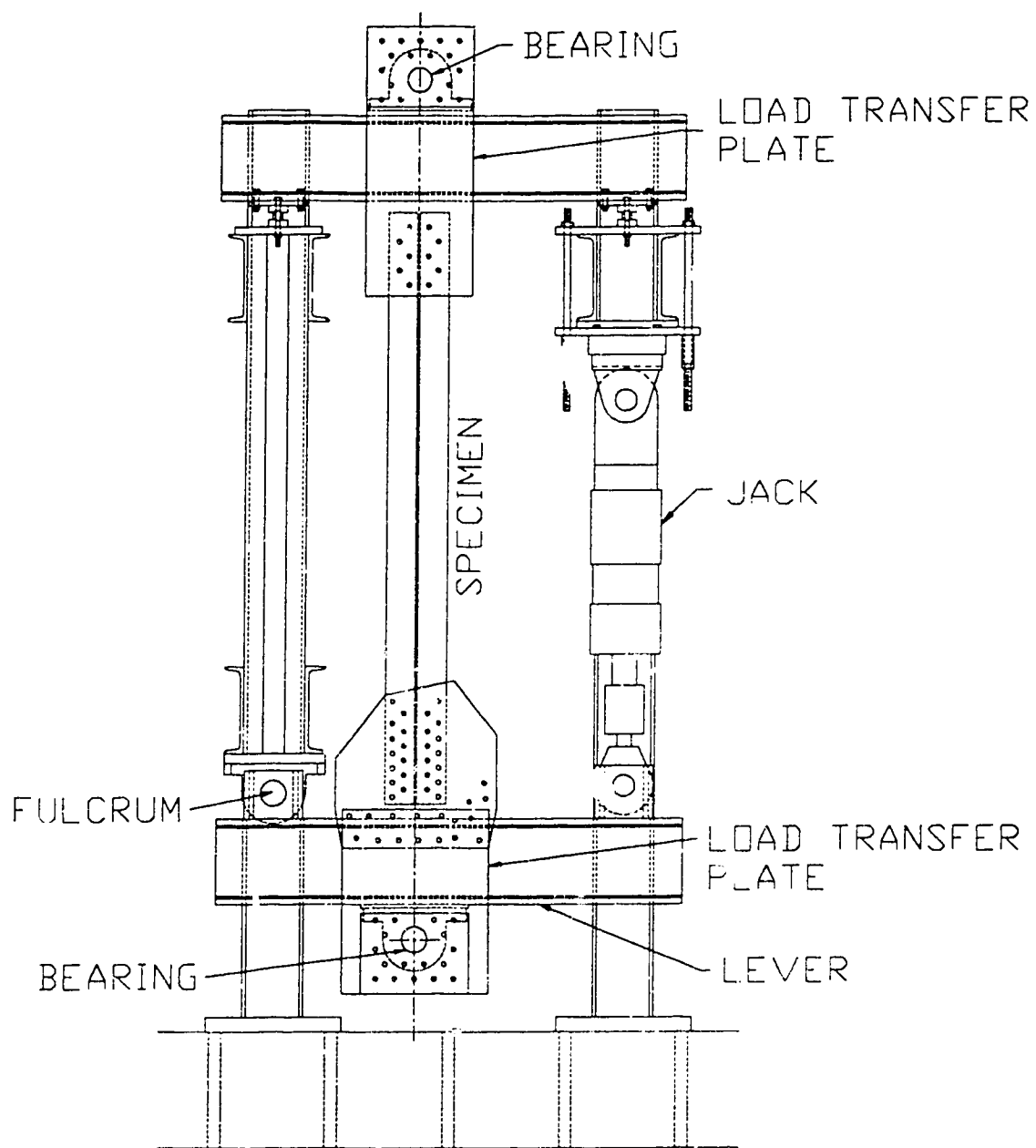


Figure 4.6 Details of Load Frame



Figure 4.7 Overall Test Setup

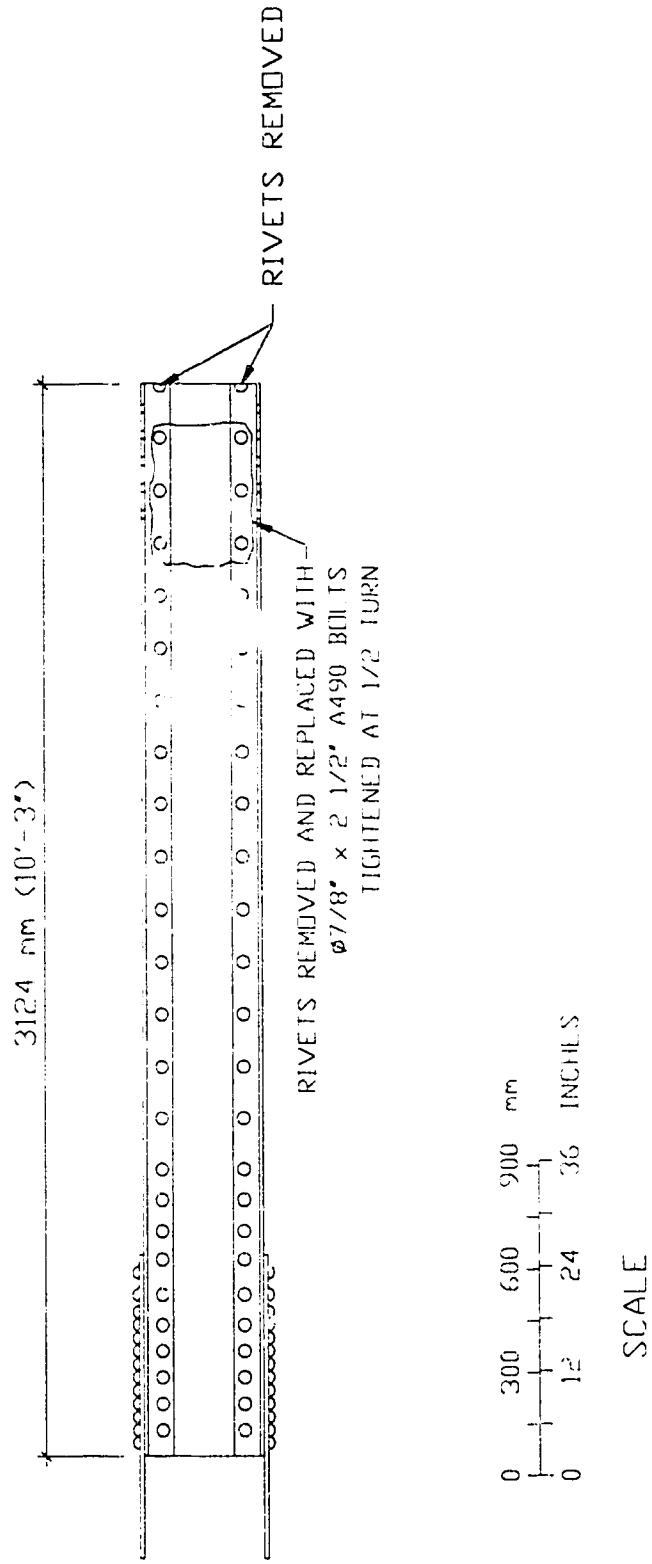


Figure 4.8 Rivets Replaced with Bolts to Prevent Cracking at Connection to Load Frame

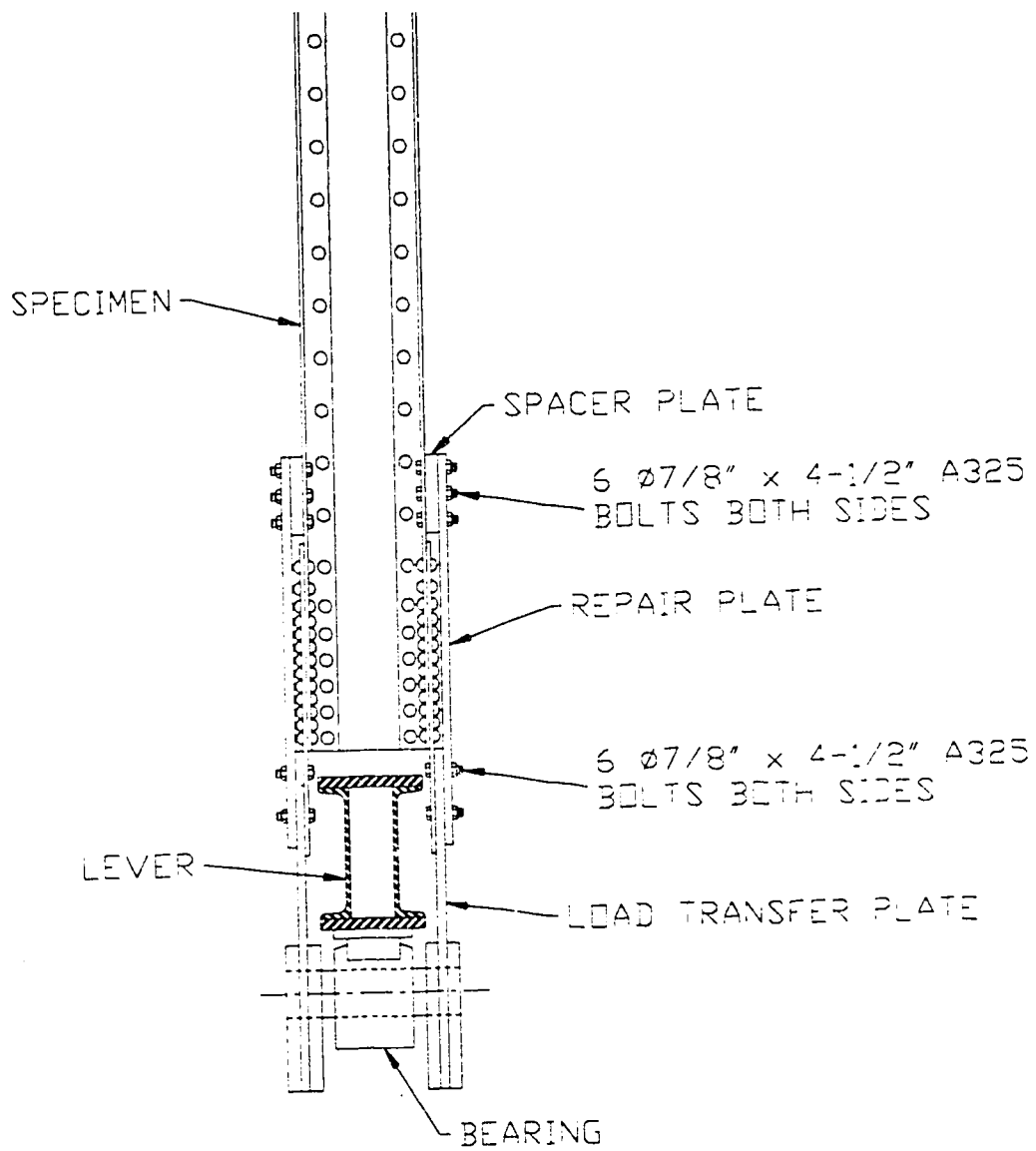


Figure 4.9 Repair of Specimen BD3

5. Experimental Results

5.1 General Observations from Fatigue Tests

Constant amplitude uniaxial tension fatigue tests were performed on a total of seven specimens taken from the tension diagonals of the Miette River Bridge. In this chapter, observations that were made during the tests are explained, and the results from the tests are described and discussed.

It can be difficult to provide the large axial forces that are required for full-scale fatigue tests of tension members. However, the loading system developed for this test program and described in Chapter 4 functioned well, and there were only minor difficulties. One of the spherical roller bearings was badly damaged early in the test program when its cast-iron pillow block housing developed fatigue cracks. The bearing was replaced, and the hollow underside of the pillow block housing was filled with concrete in order to improve its rigidity. One of the pins that joined the specimen to the load frame also developed a fatigue crack, and it was replaced by a shot-peened pin made of heat-treated AISI 4340 steel. These modifications were successful, and no further problems were experienced with the load frame. A total of about 21 million cycles of fatigue loading was applied to the various components of the loading frame during this test program.

The specimens were tested as intended, that is, in axial tension. Flexure of the specimen, which was possible if there was uneven bearing of the load transfer plates or friction in the bearings, was not significant. The strain gauges that were mounted at mid-length of the specimen all gave similar values, within a reasonable tolerance, for strain over the gross cross-sectional area. In addition, measured strain ranges and mean strains in the specimen did not vary significantly over the course of a typical test. Because the strain gauges were located far enough away from the critical detail, they were not influenced by shear lag, and the strains did not vary even after a crack had developed. The force in the hydraulic jack also did not vary appreciably over the course of a test. The net section stress range in the

specimen was first calculated from the measured strains and was then verified by the force in the jack. These values were usually within 3 % of one another.

The detection of cracks was performed with the naked eye, although in a few cases a magnifying glass was used. The detection of cracks was best performed visually because the specimens had been sandblasted so as to be free of paint. Fretting dust, a red-brown powder of oxidized metal that is formed when two steel surfaces rub against one another repeatedly, was commonly found at or near all cracked locations. It appears that the majority of the iron oxide was formed when a cracked portion of an angle rubbed against the underside of a rivet head. The use of powerful magnifying devices or other methods of crack detection, such as dye penetrant, was unnecessary.

5.2 Fatigue Test Results

Results from the fatigue tests of the diagonals are presented in Table 5.1 and in Figure 5.1. The results for the TD series shown in Figure 5.1 are presented in two different ways, for reasons that will be explained later. The results labelled Option 1 are consistent with the values presented in Chapter 4 and in Table 5.1. Except for specimen BD3, the number of cycles reported in Figure 5.1 corresponds to a condition in which one element of the built-up cross-section had severed and a crack was detected in another element. The point that represents specimen BD3 in this figure corresponds to a condition in which only one component of the cross-section had severed. Category C and Category D fatigue resistance curves are also shown in Figure 5.1.

The general fatigue crack growth process was similar for all of the tests, and the behaviour of each specimen is described below. In all cases, cracks initiated at a rivet hole at the critical detail, that is, in the diagonal at the line of gusset-angle rivets nearest to the edge of the gusset plate. For clarity in these descriptions, various components of the built-up cross-section are referred to by their orientation in the load frame. The flanges are referenced as either east or west, and each angle as north-east, south-west, and so on. The legs of the angles are referred to as the short leg (attached to the web), and the long leg

(attached to the gusset plate). A typical cross-section of the diagonal is shown in Figure 3.3.

5.2.1 Behaviour of BD Series Specimens

Figure 5.2 is illustrative of a typical fatigue crack for the BD series of tests, in this case specimen BD2. The photograph shows the specimen after failure, that is, the angle had severed and a crack had been detected in the web. The crack in the web is too small to be seen in the photograph, but the location of its tip is indicated by the arrow. Note the presence of fretting dust and the small circular indentations that were described in Section 4.2. (All photographs of cracks presented in this chapter were taken with a tensile load of approximately 750 kN applied to the specimen.)

In all tests for the BD series, the element that severed was an angle and the crack in a second element, if any, was in the web. The detection of a crack in the web was only possible when the crack had grown to an appreciable length and its tip had emerged between the short legs of the angles. Crack detection at the edge of the web was not possible because it was concealed by the gusset plate. Diagrams that illustrate the stages of fatigue crack propagation in each BD series specimen are found in Appendix E (Figures E.1 to E.4).

Specimen BD1 was tested at a net section stress range of 73 MPa. A crack in the north-east angle was discovered at 1 509 710 cycles. This corresponds to the locations marked #1 in Figure E.1. At the time of detection, the crack had reached the edge of the long leg of the angle from under the gusset-angle rivet and had begun to propagate toward the heel. The crack reached the underside of the web-angle rivet at 1 707 040 cycles (location #6) and fully severed the angle at 1 903 220 cycles (location #7). The test continued until a crack was discovered at 2 401 580 cycles, at the rivet hole on the east side of the web (location #8). (The crack tip location system in Appendix E is similar for all of the other specimens.)

Specimen BD2 was tested at a stress range of 69 MPa, and a crack was discovered first in the north-east angle at 2 655 330 cycles. The crack had reached the edge of the long leg of the angle from the top extremity of the gusset-angle rivet hole, and it had not begun to propagate toward the heel. The crack emerged from under the gusset-angle rivet head at 3 090 890 cycles and reached the underside of the web-angle rivet at 3 332 190 cycles. By 3 563 000 cycles, the angle had completely severed. The test was stopped at 3 958 270 cycles when a crack was detected that originated at the rivet hole on the east side of the web.

Specimen BD3 was tested at a stress range of 73 MPa. The crack had reached the edge of the long leg of the north-east angle from the gusset-angle rivet and was also progressing toward the heel when it was first detected at 2 273 500 cycles. It reached the underside of the web-angle rivet at 2 461 040 cycles, and the severed angle was discovered at 2 849 000 cycles.

In order to demonstrate the effectiveness of a bolted splice plate repair, two plates were fastened to the specimen in order to transfer some of the load around the cracked detail. This repair was described in Section 4.5.2. After the repair had strengthened the original critical detail, the new critical detail became a cross-section through the web-angle rivets, taken anywhere along the free length of the member. The test was restarted using the same amount of force in the specimen, and this resulted in a new critical net section stress range of 66.6 MPa. After total of 7 895 130 cycles were applied, a serious failure of the hydraulic system required that the test be discontinued. No new cracks were discovered along the length of the diagonal and there had been no further propagation of the existing crack.

Specimen BD4 was tested at 66 MPa, the lowest net section stress range in the BD series. At 3 722 300 cycles, a crack was discovered that had propagated from under the south-west gusset-angle rivet head to the edge of the long leg of the angle. The crack emerged from under the other side of the rivet head at 3 995 710 cycles and it continued to propagate toward the heel of the angle. The crack in the angle reached the underside of

the web-angle rivet at 4 192 350 cycles, and the angle severed at 4 619 780 cycles. The test continued until a crack was discovered in the web at 5 250 610 cycles, originating at the rivet hole on the west side. Detection of the crack in the web occurred somewhat belatedly because the crack formed and grew substantially during an overnight period. As a result, this crack was much longer when it was detected than those in the other specimens.

This particular test had now reached completion according to the failure criterion already established. However, the test was restarted in order to determine how closely the failure criterion as defined in the study approximated actual failure, that is, the inability of the specimen to carry the applied load. Because the first detection of a crack in the web had been late, only 1 830 cycles were required from the time the crack in the web was first discovered to the time that the specimen was no longer able to carry the applied load. However, when the specimen was checked at 5 154 710 cycles, there was no crack detected in the web. The specimen was no longer able to carry the applied load at 5 252 440 cycles. Therefore, it required less than 99 730 cycles from the time the crack could have been detected visually in the second element to the time that the specimen could no longer carry the applied load. Figure 5.3 shows the cracks on one side of specimen BD4 after it was no longer able to carry the applied load.

5.2.2 Behaviour of TD Series Specimens

Figure 5.4 shows specimen TD1 at the end of the test, and its appearance is typical of the TD series. Note the presence of a fatigue crack that caused the separation of a piece of the gusset-angle rivet head. This occurred as a result of fretting and/or prying as the underside of the rivet head contacted the angle. This behaviour was seen in several specimens of both the BD and TD series, but it does not appear to have affected the results. For all tests in the TD series, the element that severed was an angle, and the second element in which a crack was detected was the other angle of the same flange. The crack in the second element of Specimen TD1 is shown in Figure 5.5. Crack tip locations for the TD series are found in Appendix E (Figures E.5 to E.7).

Specimen TD1 was tested at a net section stress range of 64 MPa, and a crack was first detected at 1 735 140 cycles in the south-west angle. The angle had severed by the time the first crack was detected, but a crack had not yet started in a second element. It is assumed that the first crack originated at the gusset-angle rivet of the south-west flange. The test continued until a crack was detected in north-west angle, at 1 944 670 cycles.

Specimen TD2 was tested at a stress range of 62 MPa. Cracks were detected at 2 248 060 cycles in both angles of the east flange. Both cracks originated from under the gusset-angle rivet heads and both cracks had propagated only toward the heel of each angle. At 2 263 100 cycles, a crack was found that had progressed toward the edge of the long leg of the north-east angle. By 2 272 210 cycles, the south-east angle also had a crack that was propagating toward the edge of the long leg. The crack in the north-east angle reached the edge of the long leg at 2 395 900 cycles. The south-east angle also cracked through to the edge of the long leg shortly thereafter, at 2 406 850 cycles. The north-east angle severed at 2 415 840 cycles, and the failure criterion was satisfied. Because the south-east angle contained a large crack, the test was allowed to continue briefly and the angle severed 380 cycles later.

Specimen TD3 was tested at a stress range of 58 MPa, the least value used throughout the program. A small amount of fretting dust was noted on the top of the south-east gusset-angle rivet at 1 717 170 cycles, and a crack was detected in this angle at 2 062 400 cycles. This crack had begun to propagate from under the rivet head, both toward the long leg and toward the heel of the angle. A second crack, propagating toward the heel, was discovered in the north-east angle at 2 314 250 cycles. The first crack severed the south-east angle at 2 415 140 cycles, and the test was stopped. It was observed that the size of the gap between the angles and the gusset plate at the critical detail was greater than the gap at the same location in other specimens. The gap was in the order of 5 mm, and the rivet shanks were clearly visible in the space between the angle and the gusset plate (see Figure 5.6).

5.3 Discussion of Results

All of the BD series test results exceeded the fatigue strength predicted by Category D, and they were very close to the strength described by Category C. This is consistent with fatigue test results of riveted connections reported by others, as described in Chapter 2. However, all of the test results for the TD series fell below the strength predicted by the Category D curve. Two contributing factors have been identified that may explain why the TD series exhibited a lower strength than the BD series. These factors are (1) the presence of web-angle rivet holes close to the critical detail and (2) the amount of clamping force present in the rivets. These points are discussed in greater detail below.

5.3.1 BD Series

In the BD series tests, the first crack always began in an angle at a rivet that joined the angle to the gusset plate. Typically, the crack propagated from under this rivet head to the edge of the long leg of the angle (which was the leg connected to the gusset plate). In some cases, up to approximately 500 000 cycles were required before the crack began to progress toward the heel of the angle. Upon reaching the heel, the crack usually then progressed rapidly to the underside of the head of the web-angle rivet. Between 200 000 and 400 000 cycles were typically required for the crack to emerge from under the web-angle rivet, and the angle severed soon after the appearance of this crack.

Specimen BD4, which was tested until it was no longer able to carry the applied load, showed that fewer than 97 730 cycles were applied between the time the second element cracked and the time that complete failure occurred. This indicates that the failure criterion defined in this study was appropriate because it closely approximated the condition where the specimen was no longer able to carry the applied load. The failure criterion used in this study should, therefore, accurately represent the strength of comparable members in real structures.

The results from specimen BD3 show that the repair technique was a success. No new cracks were discovered after the repair and the existing crack did not propagate further,

even though many additional cycles of stress were applied. After the repair, the rivets at the critical detail (those that simply fastened the components of the diagonal together) were not subjected to substantial bearing. This gives a data point (66.6 MPa at 7 895 130 cycles) that represents the strength of details where the rivets are not in bearing. It may be concluded that a repair of this nature could be used as either a temporary or permanent solution in actual applications, although more tests should be conducted to validate the result from this one test. Other factors, such as the geometry of a tension connection that is still intact in a bridge, may require that a slightly different repair technique be used in actual applications.

5.3.2 TD Series

The TD series test results, plotted in accordance with the net cross-sectional area that is defined in Chapter 4, are shown in Figure 5.1. These points are shown as solid triangles, and they are designated as Option 1 (explained below). These results fall below the Category D fatigue strength curve. Several factors may have contributed to this behaviour, including the effect of rivet holes close to the critical section and the clamping force in the rivets.

5.3.2.1 Effect of Web-Angle Rivet Holes

The net cross-sectional area at the critical detail of the BD series was clearly defined, and it is explained in Section 4.3.1. In that series, the web-angle rivets are in the same plane as the adjacent gusset-angle rivets at a section taken through the diagonal at the rivets nearest to the edge of the gusset plate. This is shown in Figure 4.2(a). There is no ambiguity about the definition of the critical net cross-sectional area for the BD series. However, in the TD series, the web-angle rivets were not located within the same plane as the gusset-angle rivets. The pitch, or distance between these rivets measured along the length of the member from the centre of the web-angle rivet to the centre of the gusset-angle rivet, is only 38.1 mm (1.5 in.). If the diameter of the holes is also considered, it is apparent that there is only 14.3 mm (9/16 in.) of longitudinal distance between the bottom extremity of the web-angle rivet hole and the top extremity of the gusset-angle rivet hole.

The close spacing of these sets of holes obscures the definition of the critical net cross-sectional area. Review of the literature (Chapter 2) did not reveal any circumstances where this issue has arisen in other fatigue studies.

In order to account for the effect of the presence of the nearby web-angle rivet holes, it is logical to consider three different options for the calculation of the net cross-sectional area of the TD series members. These are:

- Use a plane that passes through only the gusset-angle rivet holes. This says that the net cross-sectional area is obtained by deducting only the holes in the flange angle-to-gusset plate connections. The effect of the web-angle rivet hole is thereby ignored.
- Calculate the net area by deducting both the gusset-angle holes and the web-angle holes. This gives the smallest possible net cross-sectional area and is an upper bound for the net section stress range. Obviously, this is correct only when the holes are physically in the same plane.
- Use a staggered cross-section that passes through both the gusset-angle holes and the web-angle holes.

The first option is consistent with how the fatigue cracks grew, that is, they started at a gusset-angle rivet hole and then moved horizontally (in the orientation of these tests). However, it is recognized that the actual stress on this plane might be greater than the calculated value because of the close proximity of the holes in the flange angle-to-gusset plate connection. In Figure 5.1, the solid triangles show the data plotted when this option is used.

The second option results in the calculation of a higher stress range than the first because both the gusset-angle rivet holes and the web-angle rivets holes are deducted from the gross cross-sectional area of the diagonal. This possibility was explored because of the close proximity of the web-angle holes to the plane of the gusset-angle holes in the test members. For a given force in the specimen, the use of this definition of net cross-sectional area results in the largest possible values of net section stress. This calculation has the effect of moving all of the data points for the TD series upward on the graph in

Figure 5.1, as shown by the points that correspond to Option 2 (small diamonds). This upward shift thereby indicates a greater stress range for a given number of cycles when the net cross-sectional area is calculated by taking into consideration both the gusset-angle and web-angle rivet holes.

The third option, that is, calculation of the net section according to a section that passes through both sets of holes, is done in North American practice according to the so-called $s^2/4g$ rule [Cochrane, 1922]. This is a calculation that is founded on the maximum stress theory, and it attempts to predict the failure condition corresponding to plastic flow. Over and above the limitations of the procedure itself [McGuire, 1968], there is the question as to whether its use is appropriate for fatigue, that is, at stress levels that might be considerably less than the yield strength of the material. Obviously, the calculation of the net area according to this option gives a result that lies between the other two options.

Option 1 is the way that the stress range for the TD series generally has been calculated throughout this report. To reiterate, the net cross-sectional area was calculated for a planar section, taken through the diagonal at the line of gusset-angle rivets nearest the edge of the gusset plate. The use of this section to calculate the stress range is supported by the geometry of the cracks in the specimens. However, Option 1 ignores the presence of the nearby web-angle rivets, and, as a result, the calculated net cross-sectional area is large and the reported stresses are at a minimum. It should be appreciated that the "true" value of net cross-sectional area, and thus net section stress, is not known because the magnitude of the effect of the web-angle rivet hole is unclear—it is likely that the true stress range is higher than that obtained with Option 1. Conversely, Option 2 gives a minimum net cross-sectional area, and it is thus an upper bound for the net cross-sectional stress. It should be appreciated that the true net section stress range lies somewhere between the Option 1 and Option 2 points that are shown in Figure 5.1.

As already indicated, the stress range for the TD series must lie within the limits defined by Option 1 and Option 2. However, it is important to point out that it does not matter which net cross-sectional area is chosen if a fatigue evaluation is conducted for a member

that has a cross-sectional geometry that is identical to the TD series specimens. In this case, in the process of calculating a permissible number of cycles corresponding to a given load range (or, *vice versa*), the load and stress range are uniquely related by the net area. However, the definition of net cross-sectional area becomes important when the results of the TD series are compared to results from other fatigue studies or to design standards. This issue is discussed in further detail in Chapter 7.

5.3.2.2 Effect of Clamping Force

As discussed in Chapter 2, it is known that greater clamping forces produce higher fatigue strengths. This is believed to occur because local compressive stresses discourage crack growth and more force can be transferred by friction rather than by bearing. Although it was not possible to measure the clamping force for any rivets in this study, it did appear that the clamping force in the BD series was greater than that in the TD series. This is suspected because of the large size of the gap between the flange angle and the gusset plate near the critical detail. The angles that made up the flanges of the diagonal were rolled such that the angle between the legs was less than 90 degrees, and this caused a natural gap between the angle and the gusset plate. In general, the rivets had sufficient clamping force in the BD series to pull the elements together and substantially reduce, or even close, the gap. In the case of the TD series, however, the size of this gap was generally greater. This indicates that it is likely that the rivets in the TD series had less clamping force than did the rivets in the BD series. In the most extreme case, specimen TD3, the gap was in the order of 5 mm, and the rivet shanks near the critical detail could be seen between the gusset plate and the angle (see Figure 5.6). This indicated that there was little clamping force present, and local compressive stresses in the angle directly under the rivet head were probably small.

5.4 Examination of Crack Surfaces

After completion of a test, cracked portions of the specimen were removed by flame-cutting. The region containing the crack was then opened up and the surfaces were cleaned gently with compressed air to remove fretting dust and other contaminants. These

pieces were then examined in an optical microscope in order to determine whether any unusual surface characteristics existed. Following this preliminary inspection, four specimens were selected for additional examination using a scanning electron microscope. Specimen BD2 was chosen for examination because the crack had started at the extreme top edge of the gusset-angle rivet hole and it was suspected that this unusual location of crack initiation was caused by fretting. Specimen TD3 exhibited a lower than average fatigue strength, so it also was chosen for additional analysis. Two other specimens were selected for examination in the scanning electron microscope simply because they appeared to be typical of their respective series. (The use of the optical microscope did not reveal any unusual characteristics of specimens BD3 or TD1.) The procedure used for the scanning electron microscope inspection was described in Section 4.6.1.

The scanning electron microscope images of these four samples did not reveal any indication of existing fatigue damage, inclusions, or irregularities that may have affected the fatigue test results. In general, the surfaces do not have the well-defined fatigue striations that are often typical of mild steel of the type used in the diagonals. This lack of clearly defined striations make it difficult to identify the location of crack nuclei. However, investigation of specimen BD2 supports the supposition that the crack was initiated by fretting of the rivet head on the angle. Some striations were noted on this sample that indicate that the crack began where the angle contacted the underside of the rivet head. Figure 5.7 is a photomicrograph of the fatigue striations in specimen BD2 (the striations are generally oriented vertically in the figure).

5.5 Examination of Riveted Joints

Portions of the riveted gusset plate connections were taken from two BD and two TD series specimens. Each piece was cut down the centre of a line of rivets so as to reveal the line of rivets in cross-section, as described in Section 4.6.2. The diagonals were loaded principally in tension in the bridge, and this is illustrated in the measured strain records in Figures 3.8 to 3.19. Shear deformation consistent with the direction of the tensile load in the diagonal was found in most of the samples (see Figure 5.8). However, it was not

possible to determine conclusively if the deformation occurred as a result of service loads, or whether the holes were simply slightly misaligned when the rivets were hot-driven into their holes during erection of the structure. One of the sections showed slight shear deformation in the direction opposite to the tensile load in the diagonal. This tends to support the theory that the shear deformation occurred when the rivets were hot-driven into slightly misaligned holes. In general, the sections showed that the rivets substantially filled the holes, indicating that they transferred load reasonably evenly onto the sides of their holes.

Table 5.1 Experimental Results

Specimen	Stress Range (MPa)	Initial Crack Detection (cycles)	Severing of First Element (cycles)	Crack Detection in Second Element (cycles)	Failure Criterion Reached (cycles)
BD1	73	1 509 710	1 903 220	2 401 580	2 401 580
BD2	69	2 655 330	3 563 000	3 958 270	3 958 270
BD3	73	2 273 500	2 849 000	NA*	NA
BD4	66	3 722 300	4 619 780	5 250 610	5 250 610
TD1	64	1 735 140	1 735 140	1 944 670	1 944 670
TD2	62	2 248 060	2 415 840	2 248 060	2 415 840
TD3	58	2 062 400	2 415 140	2 314 250	2 415 140

*NA indicates that the test was stopped

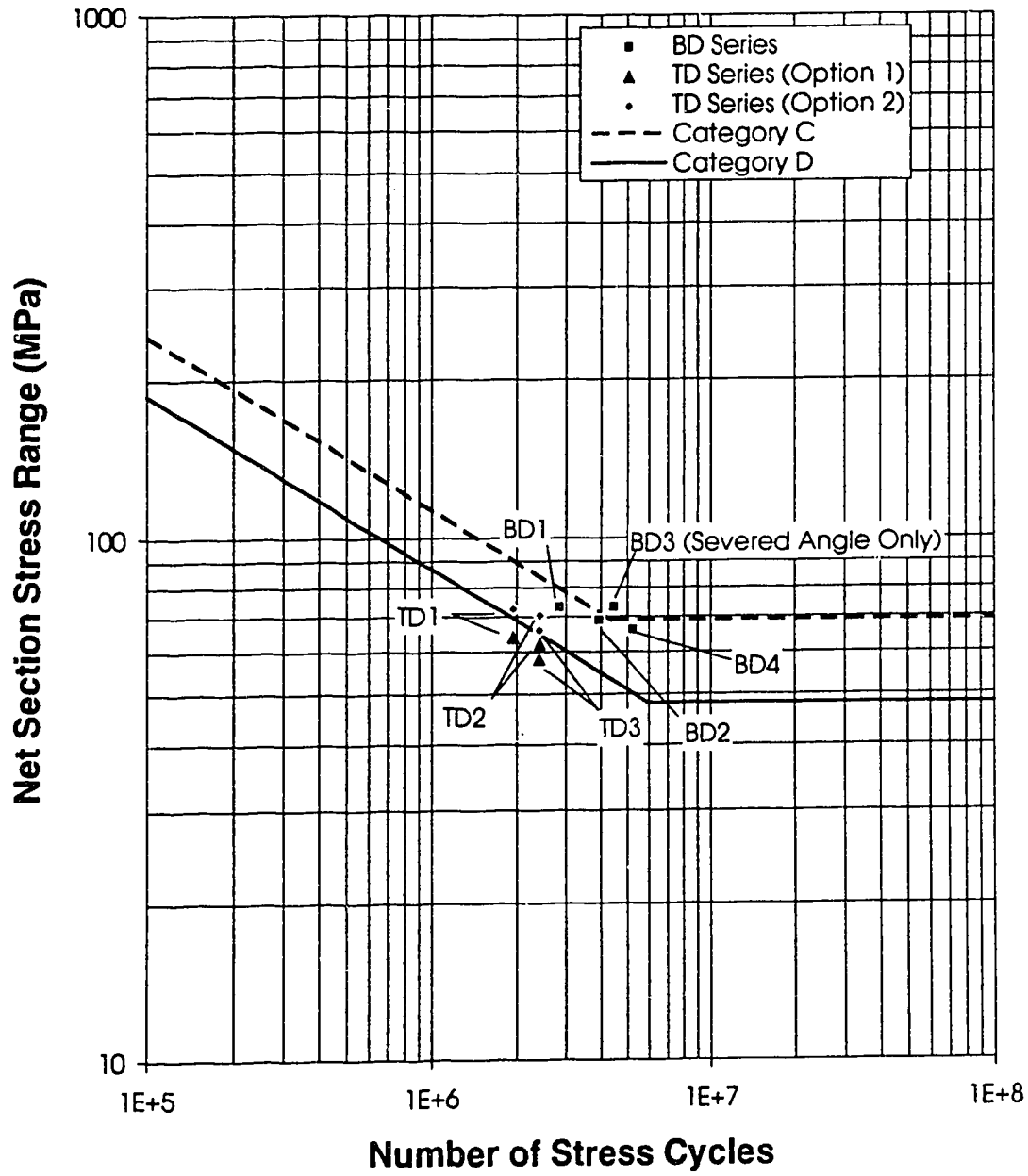


Figure 5.1 Results of Experimental Program

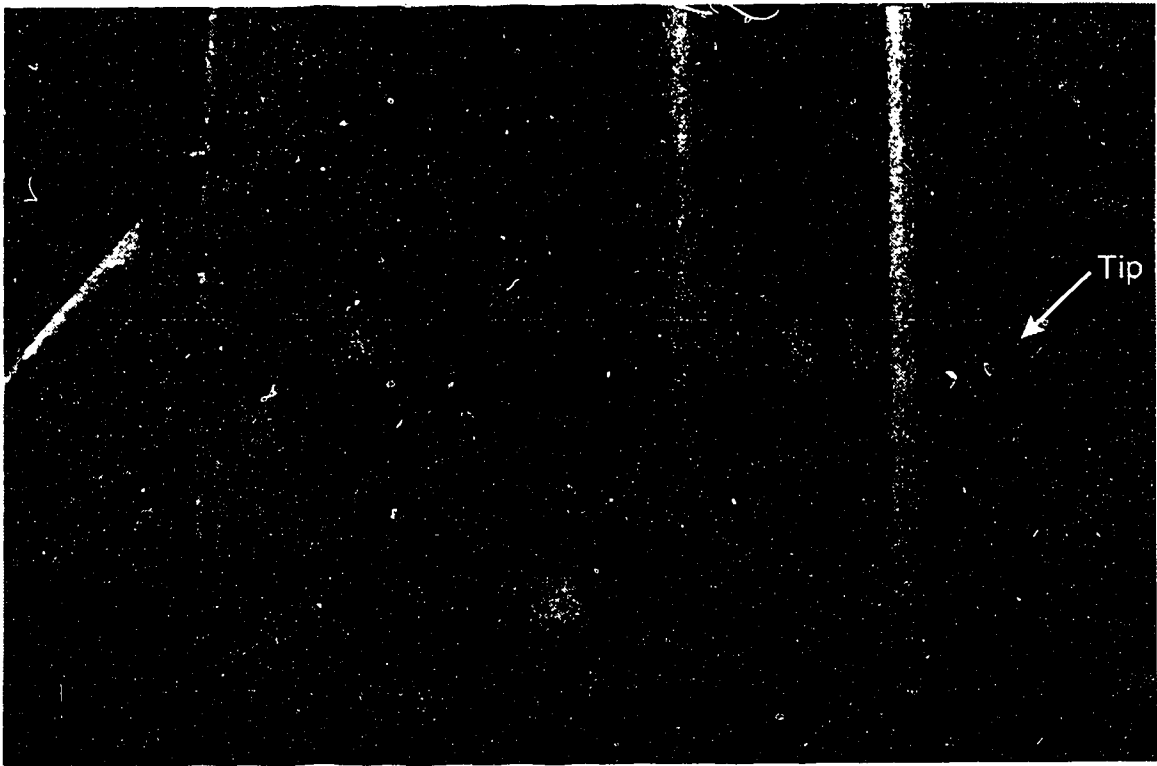


Figure 5.2 Specimen BD2, Typical Severed Element at Failure, BD series

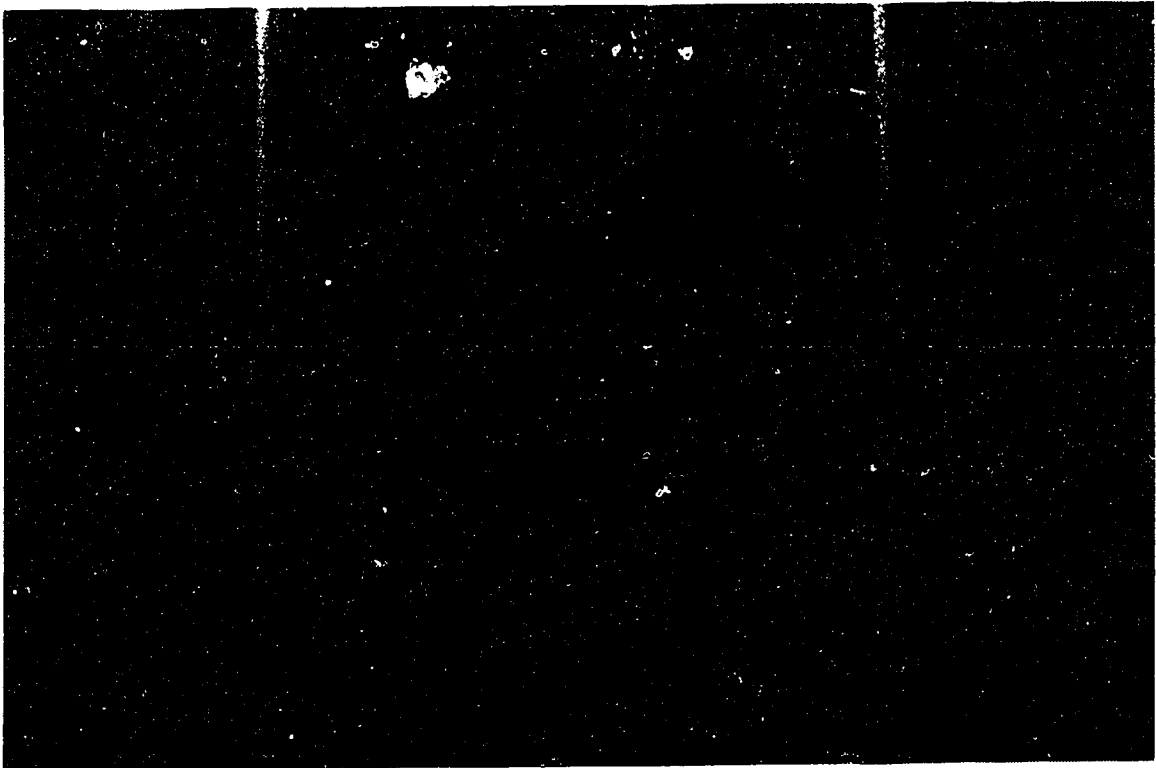


Figure 5.4 Specimen TD1, Typical Severed Element at Failure, TD series

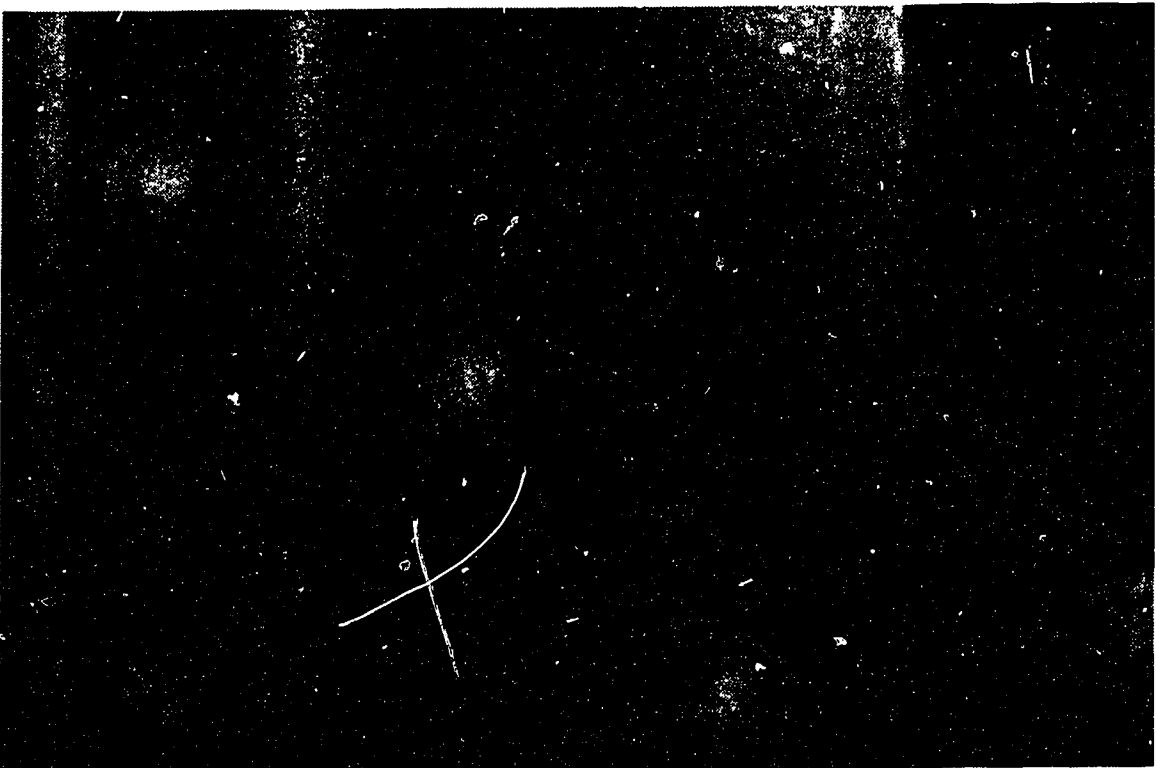


Figure 5.5 Specimen TD1, Crack in Second Element



Figure 5.6 Gap Between Angle and Gusset Plate, Specimen TD3

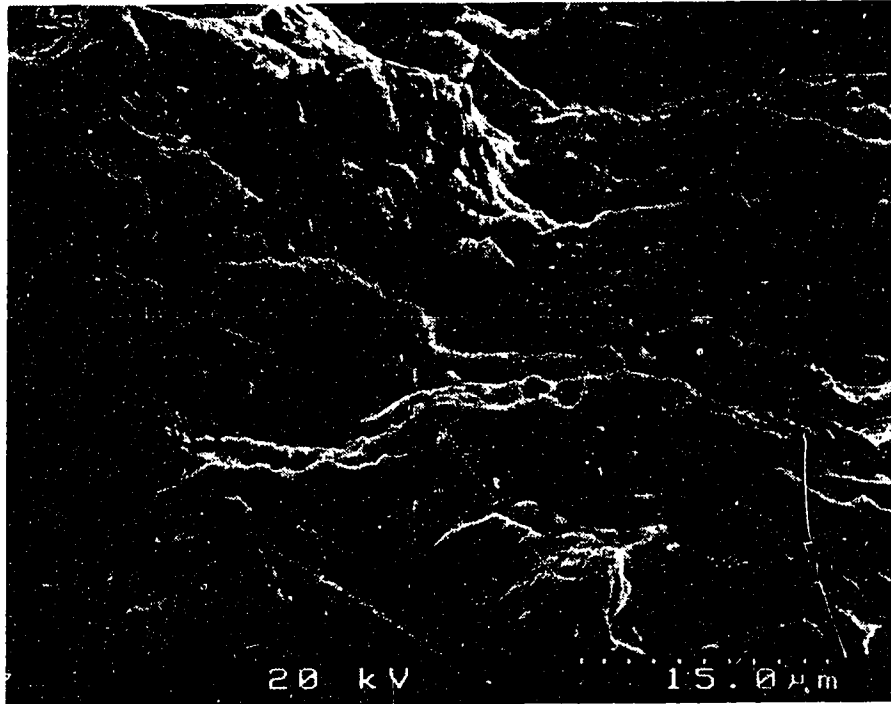


Figure 5.7 Photomicrograph Showing Striations on Fracture Surface, Specimen BD2

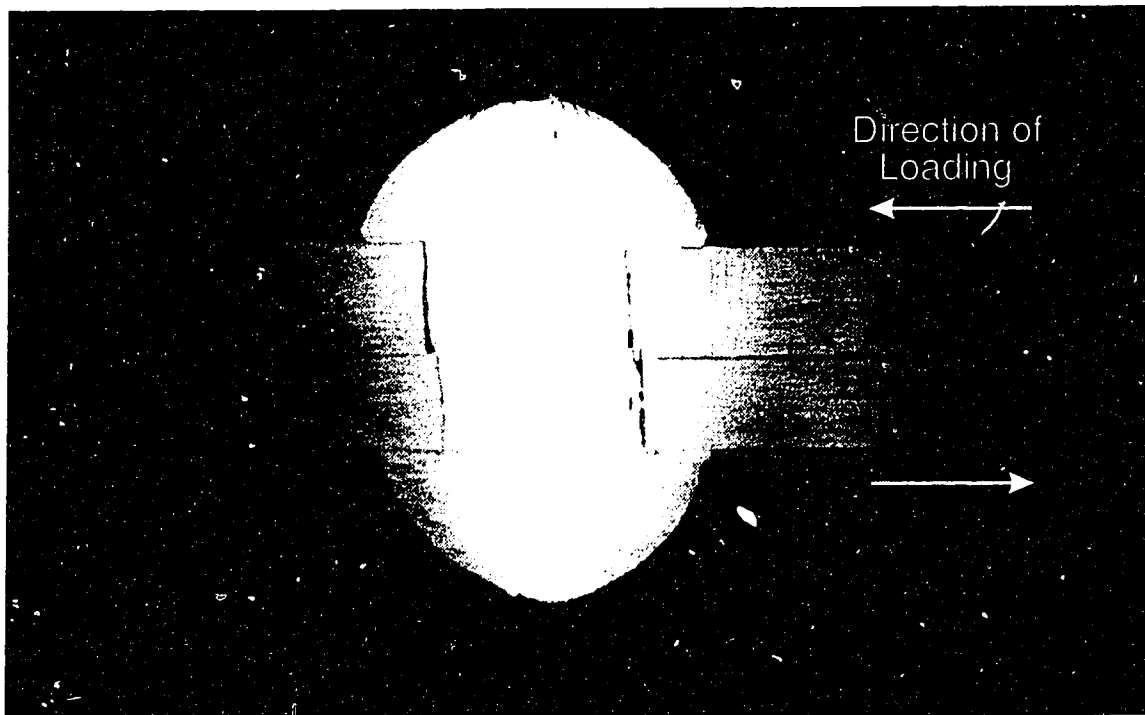


Figure 5.8 Cross-section of Gusset-Angle Rivet

6. Prediction of Remaining Fatigue Life

6.1 Scope

In this chapter, a fatigue evaluation of the diagonals of the Miette River Bridge is made in order to determine the life remaining at the time the structure was taken out of service. The calculations will serve to illustrate the differences between various methods of fatigue life prediction, and to help to establish whether fatigue damage existed prior to the tests described in Chapter 4. If an estimate of the fatigue life of the structure as a whole were required, all other members in the bridge that have fatigue-critical details would also have to be considered.

The fatigue evaluation is made specifically for the detail where the diagonal is connected to the bottom chord panel point of the bridge. This location corresponds to the critical detail in the BD series of tests, and it was chosen because it has a smaller net cross-sectional area than the critical detail of the TD series. In addition, the bending moment in the diagonal at the lower panel point is greater than that at the upper panel point, although the axial force is the same at both locations. Thus it is logical to conclude that, for these remaining fatigue life calculations, the BD critical detail will yield the lowest fatigue life. Stress ranges at the critical detail are calculated for both the *Simple Truss* and *Space Frame* models (see Chapter 3), and the loads on the structure are taken from the work of Adamson [1995].

The intention of this exercise is to predict the remaining fatigue life as accurately as possible, but errors may arise from several sources. The traffic models, developed by Adamson, are conservative estimates of the actual traffic based on load information provided by CN Rail. The bridge was about eighty years old at the time it was disassembled, and it is also possible that the records for its use may not be accurate for the early years of its life. The accuracy of the calculations is also compromised by changes in traffic patterns that may arise in the future, because these changes usually can not be estimated accurately.

6.2 Methods used to Evaluate Remaining Fatigue Life

The AREA, Eurocode 3, and Kunz evaluation techniques discussed in Chapter 2 are used in conjunction with the *Simple Truss* and *Space Frame* models to predict the remaining fatigue life of the diagonals. The AREA and Eurocode 3 standards use an equivalent stress range formulation to accumulate damage. The Kunz method has a more elaborate method of damage accumulation, which will be explained later. The AASHTO standard is not used because it applies specifically to highway bridges and loads.

The AREA standard can be used on the basis that the rivets have either "normal" clamping force or lower than normal clamping force. There was no physical evidence obtained in the experimental program of this study to indicate that the rivets were not tight at the critical detail in the BD series. However, to be conservative, the fatigue evaluation herein is also performed with the assumption that the rivets had a lower than normal clamping force. If it is assumed that the rivets are not tight, the AREA Manual requires that the fatigue resistance of the detail be considered as Category D. If the rivets are assumed to have normal clamping force, Category C is used to evaluate the fatigue resistance of the detail, but the constant amplitude fatigue limit is still that of Category D, namely 48 MPa (7 ksi). When variable amplitude stress ranges are applied, the constant amplitude fatigue limit is discarded as soon as it is exceeded by any one stress cycle. Thereafter, all stress ranges are considered to cause damage, that is, the fatigue resistance curve simply has a slope of 3. A root-mean-cube equivalent stress range is then calculated for all stress cycles, so as to allow evaluation of remaining fatigue life of the detail.

The Eurocode 3 standard gives three variations of fatigue resistance curves for the strength of a detail, as described in Chapter 2. Although the Eurocode 3 standard does not recommend a Detail Category for riveted connections, the value 69 has been judged to be appropriate for this work. This Detail Category is equivalent to AREA Category D, that is, the primary slope of the curve is 3 and it has a value of 69 MPa at 2 million cycles. In this chapter, each of the three possible variations for evaluation of fatigue life are used: (a) a curve with a single slope of 3; (b) a curve with a slope that changes from 3 to 5 at

5 million cycles and a constant amplitude fatigue limit at 5 million cycles; and (c) a curve with a slope that changes from 3 to 5 at 5 million cycles and a constant amplitude fatigue limit at 5 million cycles and a cut-off limit at 100 million cycles. The dual slope technique attempts to account for the situation in which only few cycles exceed the constant amplitude fatigue limit. Whereas AREA simply discards the constant amplitude fatigue limit, and thus gives very conservative solutions in most cases, Eurocode 3 allows the slope to be changed from 3 to 5 in an attempt to make a more realistic evaluation.

The Kunz method presented in Chapter 2 is also used to estimate remaining fatigue life. There are two features of the Kunz method that distinguish it from AREA and Eurocode 3: Kunz proposes a different method of damage accumulation and uses a modified form of the fatigue resistance curve. When this method is applied, the damage limit is initially set equal to the constant amplitude fatigue limit. Each time the damage limit is exceeded by a stress cycle, its value is decreased. This is done because the crack has grown and the detail has therefore become more susceptible to damage. The damage limit is recalculated after each cycle, and it is based on a Miner summation of the total damage at that time. When the value of the Miner summation reaches unity, the failure criterion is met, and the remaining fatigue life is obtained.

In the Kunz method, a modified form of the fatigue strength curve may also be used. The distinguishing feature of this modified curve is that it has a smooth transition region between the linear fatigue resistance line and the damage limit. Such a transition region is observed in experimental fracture mechanics data and has been explained in Chapter 2. The Kunz method is used herein both with and without the transition region. The fatigue curves used are those of the AREA Manual, that is, the detail is either Category C or D, but the initial value of the damage limit is that of Category D in both cases.

6.3 Method of Calculation

In order to calculate the remaining fatigue life of the diagonals with any of the above methods, a computer program called **Remaining Fatigue Life (RFL)** has been used [Kunz, 1994]. The program determines the remaining fatigue life of a detail based on input

parameters specified by the user. There are five types of input information required: the configuration and weights of railcars and locomotives, typical trains made up from the defined rolling stock, the traffic patterns of typical trains, the method of fatigue evaluation, and the influence line for the structural detail. The program is written in Fortran and can be run on an IBM-compatible personal computer.

Input details for rolling stock include the weight, number of axles, and axle locations relative to each car coupler. Typical trains are then assembled using cars and locomotives from the defined rolling stock. The trains are identified as either freight or passenger, since annual traffic records kept by railway companies generally distinguish between the two types. Various arrangements of cars in the trains enable a reasonably realistic set of loading sequences to be reproduced.

After typical trains have been defined, traffic models must be developed to estimate the yearly frequency and the order of typical trains. In order to define a traffic model, the total number of trains that cross the bridge annually is specified, along with a percentage value that indicates the relative frequency of each type of train. Generally, the first year for which traffic is defined is the year the bridge was built, but the user may elect to include or exclude traffic in any year. A reference year is also chosen, and the prediction of remaining fatigue life is calculated relative to the reference year. The speed of each typical train is also an input parameter so that impact can be evaluated, if desired.

The influence line for the critical detail is defined at a series of locations along the length of the bridge. The multiplication factor necessary to convert the influence line to stress must be developed by the user and entered into the program. When the program is executed, the train is moved across the bridge, and the influence line is used to calculate stress at the critical detail for various positions of the train on the bridge.

The fatigue evaluation methods available in the program are very general, and can be applied to a wide variety of fatigue strength curves. Eight general options are available to define the fatigue strength curve. The curves may have either a single slope, such as those given in the AREA standard, or a dual slope, such as those specified in the Eurocode 3

standard. Each curve may be taken alone, but it may also have a cut-off limit, or a cut-off limit and a constant amplitude fatigue limit, and this gives a total of six options. Input parameters vary with the type of curve selected, and may include the slope of the primary curve, the slope of the secondary curve, the number of cycles at which the transition of slope occurs, the value of the fatigue strength at 2 million cycles (detail category), and the values of the cut-off limit and constant amplitude fatigue limit.

The other two options incorporate the Kunz damage accumulation method, that is, a fatigue limit that decreases as damage increases. The fatigue resistance curve in this case has only a single slope, and it can be used with or without the transition region. Parameters that must be defined for the fatigue strength curve include the slope of the primary curve, the value of the fatigue strength curve at 2 million cycles, and the initial value of the damage limit.

RFL applies the traffic models to the influence lines in a manner similar to that used in the *Train Simulation Algorithm* of Chapter 3. The program then performs a rainflow counting technique to determine stress ranges at the detail, and damage is accumulated with the Miner summation. When the total damage reaches unity, the failure criterion has been met and the process ceases. Output for the detail is then generated, including the amount of damage at the reference year and the remaining fatigue life in years, measured from the reference year. The program terminates automatically if the remaining fatigue life exceeds 1000 years.

6.4 Calculation of Remaining Fatigue Life for Diagonals

The program RFL was used for the prediction of the remaining fatigue life for the diagonals of the Miette River Bridge. The input for this analysis includes the influence lines shown in Figure 6.1. These represent the stress at the critical detail and they differ in several ways from the influence lines developed in Chapter 3. The influence lines in Chapter 3 represented the behaviour at the location of the strain gauges, which were some distance away from the critical detail. The influence lines shown in Figure 6.1 are for stress at the critical detail of the diagonal, predicted from both the *Simple Truss* and *Space*

Frame models. The influence line for the *Space Frame* model includes both the effects of axial stress and bending at the critical detail, and it therefore gives slightly greater values than does the *Simple Truss* model. The fatigue resistance curves from the AREA and Eurocode 3 standards, and traffic information from work done by Adamson [1995] are also part of the input to the program. The strains measured while the bridge was in service include the effects of impact. Since there was a very good correlation between the structural models developed in Chapter 3 and the strains measured while the bridge was in service, an impact factor of unity is used in the remaining fatigue life calculations.

6.4.1 Traffic Model

A traffic model was developed that was based on information obtained from CN Rail. This model, used for all remaining fatigue life calculations, was obtained from work reported by Adamson [1995]. Details of the types of locomotives, cars, and traffic patterns will be described herein, but not the CN Rail information from which it was derived.

The traffic model includes three types of trains, namely two freight and one passenger. All trains use two locomotives, each with four axles and a total weight of 1 157 kN. Freight train railcars have four axles, a length of 18.3 m between the couplers, and range in weight from 267 kN to 1 263 kN. Passenger railcars have four axles, a length of 25.9 m between the couplers, and a weight of 623 kN. These cars were judged by Adamson to be a conservative estimate of typical traffic for the Miette River Bridge. Adamson constructed typical trains made up of these cars, and then developed traffic patterns in order to represent each type of train on an annual basis. Traffic prior to 1971 was taken by Adamson to be negligible. (This decision was based on advice from CN Rail.) A second, parallel, bridge was built at this site in 1982, and therefore the traffic for the period 1971 to 1981 was estimated to be double that of 1982–1992. (It was assumed that the two bridges carried equal numbers of trains.) It was also assumed by Adamson that traffic patterns after 1992 would have continued indefinitely at the same levels as those in the period from 1982 to 1992. Details of the three types of trains are shown in Table 6.1, and yearly traffic patterns can be found in Table 6.2.

6.5 Results of Evaluation of Remaining Fatigue Life

The combinations of parameters for the AREA, Eurocode 3, and Kunz methods used to calculate remaining fatigue life are shown in Table 6.3. In general, the results indicated that it is unlikely that fatigue of the diagonals would have occurred if the bridge had remained in service.

The AREA Category D and the Eurocode 3, Detail Category 69, with a single slope of three and no constant amplitude fatigue limit and no cut-off limit, both yielded the lowest predicted remaining fatigue life. It is expected that these techniques will give nearly identical solutions, because both have the same principal fatigue strength curve. Both methods predicted a remaining life in the order of 245 years with the *Space Frame* model, and 275 years with the *Simple Truss* model, referenced from the time the bridge was disassembled in 1992. All of the other methods predicted remaining lives longer than these, and several of the least conservative were greater than 1000 years. From these results it is clear that fatigue cracking is highly unlikely at this critical detail in the diagonal, and that other issues, such as corrosion, would likely take precedence. It is therefore not logical to attempt to compare, or even to report, the results, because the estimates of remaining fatigue life are so great that they are no longer realistic. For example, the assumption that future traffic patterns will remain at the same level as those in 1992 is sufficient for a short duration, but extension of this assumption into the distant future is not satisfactory.

It can be noted, however, that the remaining fatigue lives predicted by the *Space Frame* and *Simple Truss* models were similar in all cases, as expected because of the similarity of their results in Chapter 3. In general, the *Space Frame* model did predict marginally shorter remaining fatigue lives, consistent with the slightly higher stress values shown in the influence lines in Figure 6.1.

In summary, both the *Space Frame* and *Simple Truss* models, used in conjunction with any fatigue evaluation method, predict remaining fatigue lives in the order of 250 years or

longer. It can, therefore, be concluded that the amount of fatigue damage in the diagonals of the Miette River Bridge was negligible at the time it was disassembled.

Table 6.1 Composition of Typical Trains

	Weight (kN)	Number of Cars		
		Freight Train #1	Freight Train #2	Passenger Train #1
Locomotive	1 157	2	2	2
Freight Car #1	267	26	26	0
Freight Car #2	534	4	4	0
Freight Car #3	961	6	6	0
Freight Car #4	1 023	3	3	0
Freight Car #5	1 103	2	2	0
Freight Car #6	1 157	15	15	0
Freight Car #7	1 263	0	1	0
Passenger Car #1	623	0	0	7

Table 6.2 Typical Traffic Patterns in Trains per Year

Train Type	Period	
	1971-1981	1982 onward
Freight Train #1	6671	3336
Freight Train #2	437	218
Passenger Train #1	362	181

Table 6.3 Summary of Remaining Fatigue Life Calculation Parameters

Method	Parameters
AREA	Category D CAFL = 48MPa
	Category C CAFL = 48MPa
Eurocode 3	DC 69, $m = 3$
	DC 69, dual slope $m = 3$, $m = 5$ CAFL at 5 million cycles
	DC 69, dual slope $m = 3$, $m = 5$ CAFL at 5 million cycles Cut-off limit 100 million cycles
Kunz	Detail AREA Category D Initial damage limit 48 MPa
	Detail AREA Category D Transition region Initial damage limit 48 MPa
	Detail AREA Category C Initial damage limit 48 MPa
	Detail AREA Category C Transition region Initial damage limit 48 MPa

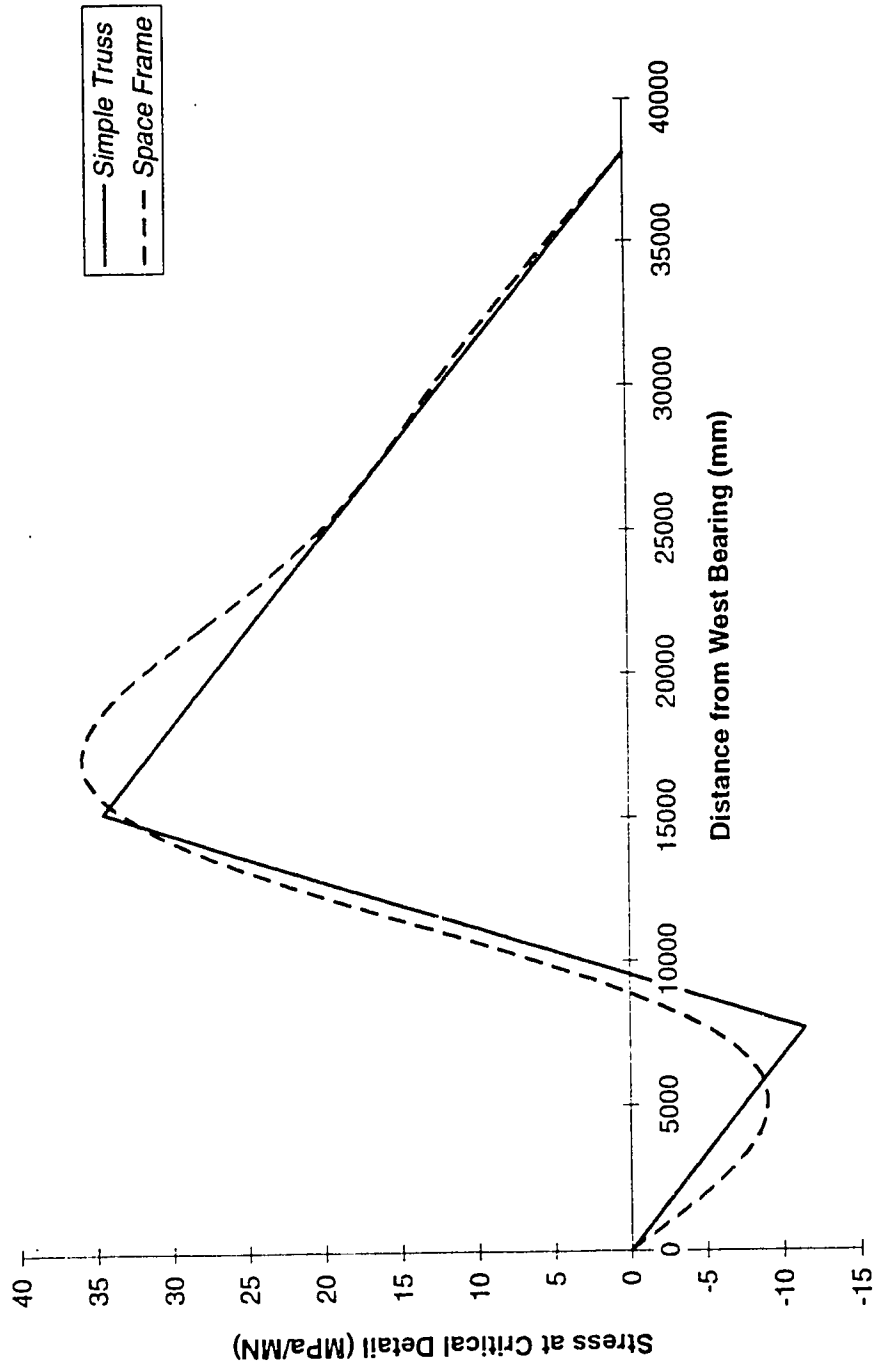


Figure 6.1 Influence Lines for Remaining Fatigue Life Calculations

7. Discussion

7.1 Literature and Current Standards

7.1.1 Experimental Studies of Full-Scale Riveted Specimens

The literature review identified that most full-scale fatigue tests of riveted members have been flexural tests of built-up girders, and that the critical detail for the majority of these tests was within a region of constant moment. Elementary mechanics of materials can be used to show that the rivets that join the elements of a prismatic girder are not subject to shear, and, hence, bearing, within the constant moment region. However, moving loads must be carried in most real structures, and, as a result, the rivets generally do act in bearing. The difference in fatigue life between cases where rivets act in bearing and where they do not can be significant [Parola *et al.*, 1963]. The results from tests in which the rivets were not in bearing may, therefore, give unconservative results if these results are used to predict the life of riveted details that are in bearing. It is difficult in any test program to establish the degree to which bearing may be present, of course.

7.2 Interpretation of Experimental Results

The literature review shows that two types of results are available from fatigue tests of riveted members. In some tests, fundamentally identical riveted details are subjected to identical stress ranges and then failed in fatigue. The way these tests are conducted (e.g., Baker and Kulak [1982]), the elements in a given member fail in succession: the first detail to fail is the weakest and the last one to fail is the strongest. This process can be likened to testing the links in a given chain. After each link fails, the test is continued (after the necessary repairs) until the next link fails. In this type of testing, the results are biased because the sample is constantly changing (getting stronger).

In contrast to this, many fatigue test results are the result of testing a number of members, each containing a number of fundamentally identical riveted details. When the critical detail in one member has failed, (e.g., Adamson [1995]), the testing of that member is

discontinued and the next member is tested likewise. Continuing with the analogy, this can be compared to the testing of a number of chains in which each individual test is ended when the first element within that chain fails. As each test result is obtained, it can be said to come from an unbiased sample, that is, the result of any given test does not depend upon the result of any other (previous) test.

These two types of testing regimes will not produce the same result, but how significant the difference might be can be only be a matter of conjecture.

At the present time, codes that regulate the evaluation of riveted members, including AREA, do not require that consideration be given to the number of riveted details in the member under consideration, nor do they consider how the fatigue life data for the details were obtained. Considering all of the other unknowns in the determination of the fatigue life of a given member, this is not unreasonable. However, as more and more fatigue life data is obtained, consideration should be given to how the data were obtained in order that design rules can be established that are sufficiently conservative.

7.3 Performance of Structural Models

7.3.1 *Simple Truss and Space Frame Models*

Strains were measured in a diagonal of the Miette River Bridge under the action of several trains, and information on the configurations and weights of these trains was obtained from the operator, CN Rail. Two structural models were developed to obtain influence lines for the gauged location in the diagonal. The first was a plane truss model, in which all connections modelled as pinned, and this was designated as the *Simple Truss* model. The second was a three-dimensional model, in which all connections were modelled as continuous. This was designated as the *Space Frame* model. The *Simple Truss* model accounts only for axial force in the diagonal, whereas the *Space Frame* model accounts for both axial force and strong-axis bending moment in the diagonal.

The structural models were used in conjunction with information of the train configuration and loading to generate a record of predicted strains. In order to evaluate the results of the models, an effective strain range was calculated for both the measured strain records and the predicted strain records. In this process, small strain ranges (caused by vibration of the bridge and electronic noise) were filtered from the records since they do not affect fatigue life. For reasons described in Section 3.7.1, these small strain ranges must be removed in order to enable the calculation of the effective strain range. The ratios of measured-to-predicted effective strain range were then determined so as to allow evaluation of the structural models.

The *Simple Truss* model gave results that are conservative when comparing calculated strain in the diagonal to measured average axial strain in the diagonal. Bending effects from interaction of the truss with the floor system are also present in the diagonal, however. Although the *Simple Truss* model itself does not include flexure of the diagonal, in the work reported herein it was sufficiently conservative such that it still encompassed the higher strains that are actually present as a result of bending of the diagonal.

The *Space Frame* model gave results that are generally slightly less conservative than the *Simple Truss* model, and it more accurately predicted the behaviour of the diagonal at the gauged location. The *Simple Truss* model gave more conservative results because it does not include the beneficial effects of continuity.

It can be concluded that either method gives a reasonable approximation of the true behaviour of the diagonal. However, the *Simple Truss* model is substantially faster and less complex to set up and use than the *Space Frame* model. The *Simple Truss* model is also sufficiently conservative to account for the effect of bending in the diagonal. Although a three-dimensional model gives better strain predictions, it may not be necessary in cases where a simple estimate of strain is all that is required. Since it is likely that estimates of both past and future traffic are uncertain, the minor additional accuracy of the *Space Frame* model will not be warranted in most cases.

7.3.2 Comparison with Results of Others

Adamson [1995] also developed models to predict the behaviour of a diagonal and a stringer of the Miette River Bridge. He developed two models for prediction of strains in the diagonal: a so-called *Pinned* model, which was a plane truss that had all joints modelled as pins; and a so-called *Continuous* model, which was three-dimensional and had full continuity of all joints.

In effect, the Adamson *Pinned* model is identical to the *Simple Truss* developed herein. Therefore, it was to be expected that the predictions of strains in the diagonals made by Adamson for the same trains and the results obtained in this report should be identical. In some cases this held true. For example, Train F658, where Adamson's results indicate that the measured-to-predicted ratio is 1.01 for the north flange strain and 0.98 for the web strain, correspond exactly to the results reported in Table 3.1 of this report. However, some of the results reported by Adamson differed slightly, but not significantly, from those in this report. Adamson does not indicate whether the strain records were filtered in order to remove small cycles caused by electronic noise and vibration, and this may account for the differences.

Adamson's *Continuous* model did not include the effects of bending in the diagonal, and therefore it differed from the *Space Frame* model presented herein. The results of the Adamson *Continuous* model gave measured-to-predicted ratios that ranged from 0.86 to 1.11 for trains T730, F430, F658, and F717. The results reported herein for the same trains and using the *Space Frame* model ranged from 0.95 to 1.02. The improvement in prediction is attributed to the incorporation of the effects of bending of the diagonal and to the use of a filter to remove the effects of electronic noise and vibration from the strain records.

In results reported by Fisher and Daniels [1976], measured-to-predicted axial stresses in the hangers of a riveted truss bridge ranged from 0.96 to 1.02 when a three-dimensional model was used. Thus, the quality of these predictions is about the same as those attained with the *Space Frame* model presented in this report. The similarity of results suggests

that the behaviour of tension members of truss bridges can be modelled effectively, with or without accounting for bending of the members due to interaction with the floor system.

7.4 Fatigue Tests of Full-Scale Riveted Members

7.4.1 Experimental Results

During the service life of the Miette River Bridge it is unlikely that any significant fatigue damage occurred to the diagonals. This conclusion is supported by three facts: (1) measured strains in the diagonal for several trains indicated that the stress range at the critical detail did not exceed 40 MPa, well below the constant amplitude fatigue limit of 48 MPa for riveted details given in the AREA Manual [1994]; (2) examination of the surfaces of cracks created during the experimental program gave no indication that crack initiation had started prior to the fatigue study; (3) estimates of remaining fatigue life, conservatively assuming heavy traffic, predict a remaining life of at least 250 years. As a result, it can be taken that the fatigue strength information obtained from the experimental program is unaffected by prior fatigue damage.

All of the test results from the BD series exceeded the fatigue strength predicted by Category D and were very close to the strength described by Category C. This is consistent with results of riveted connection tests reported by others, as described in Chapter 2. However, the test results for the TD series are somewhat more difficult to evaluate. In Section 5.3.2.1 the issue of the definition of net cross-sectional area for the TD series was raised. The stress range, as reflected by the net cross-sectional area, is ambiguous in the case of the TD members. Although the crack grew at right angles to the longitudinal axis of the member, it is reasonable to think that the actual stress that was driving the crack growth is affected by the close proximity of nearby holes.

The options that were explored for the definition of net cross-sectional area for the TD series included (1) a plane that passes through only the gusset-angle rivet holes, (2) deduction of both the gusset-angle and web-angle rivet holes from the gross area, and

(3) the use of a staggered cross-section that passes through both the gusset-angle and the web-angle holes, as calculated by the $s^2/4g$ (Cochrane) rule.

The net section stress range calculated by these three options will, of course, produce different results for a given load range. For the geometry of the TD members, Option 1 will give the lowest stress range, Option 2 will give the highest stress range, and Option 3 will give an intermediate value. Option 1 has generally been used in this report for the purposes of calculating the net cross-sectional area of the TD series members. This was done in order to be consistent throughout the report and also so that the location of the net cross-sectional area is in agreement with the location of the fatigue cracks in the members.

When the data from the TD series tests are compared to the results from other tests, the definition of the net cross-sectional area is significant because a consistent method must be used in all cases. However, the appropriate value of the net cross-sectional area for the TD series is not known—it will lie in the range between the limits described by Option 1 and Option 2. In this report Option 1 has been used, and it is the most conservative method of presentation of the results, that is, the plotted points appear at the lowest possible value of net section stress on the fatigue strength curve. Of course, it must be appreciated that the "true" location of the TD series results will likely lie higher than those points shown by Option 1 in Figure 5.1.

Regardless of the way the net cross-sectional area is calculated herein, a designer will generally use the $s^2/4g$ rule (Option 3) to calculate the net cross-sectional area of a member that is to be evaluated. Despite the limitations of the method (discussed in Chapter 5), the rule does serve to account for the effect of staggered hole patterns. With this method, the designer will obtain a smaller net area and, as a result, a larger stress range, for a given load range than would be obtained with Option 1. If the $s^2/4g$ rule were to be used to present the TD series results from this study, a net cross-sectional area of 11 223mm² is obtained and the data points would lie between the Option 1 and

Option 2 locations, slightly above the Category D line. This implies, for the specific geometry of the TD series tests, that Category D is an appropriate description of the fatigue strength of the members when the $s^2/4g$ rule is used. However, it is important to note that the rule has not been shown to be appropriate in a general way for fatigue life evaluation for any cross-sectional geometry.

The clamping force at the critical detail may also have affected the fatigue strength of the TD series, as discussed in Section 5.3.2.2. The amount of clamping force present in the rivets of the TD series appears to be lower than that in the BD series. The literature survey reported in Chapter 2 indicates that lower clamping force generally results in lower fatigue strength. The results of the TD series are consistent with this expectation. It can be seen in Figure 5.1 that the fatigue strength of the TD series is distinctly lower than that of the BD series, regardless of method used for the calculation of net cross-sectional area.

Table 7.1 contains a comparison of the fatigue strengths obtained in the experimental program with the fatigue strengths predicted by AREA Category D and by the Kunz method. For the results reported in the table, the transition region and damage limit of the Kunz method are based on the Category D fatigue strength curve. The Kunz predictions were calculated using the program *Remaining Fatigue Life* (RFL). In order to predict the test results using RFL, the influence line for the member consisted of a constant axial force of value unity for every position of a unit load on a bridge. A train was defined that consisted of only a single axle, and this axle load was taken as the magnitude of the stress range used in the test. This allowed the constant amplitude fatigue stress range of each test to be simulated so as to obtain the Kunz prediction of total fatigue life.

The table shows that the Kunz method produces a slightly better prediction than that provided directly by Category D for the BD series and that both methods were conservative. For the TD series, the Kunz method produces less accurate predictions if Option 1 is used to obtain the net section stress range. However, the Kunz method is slightly more accurate than AREA if Option 2 is used in the calculation of net section stress range. Overall, the Kunz method appears to yield slightly better predictions than a

simple fatigue evaluation for the results obtained in this study. However, the number of tests and their scope are not sufficient to say whether it is, in general, a more effective way of predicting fatigue life.

The rivets at the critical detail after the repair of specimen BD3, those that simply fastened the components of the diagonal together, are not subjected to bearing. This gives a result that represents the strength of details where the rivets are not in bearing (66.6 MPa at 7 895 130 cycles).

7.4.2 Suitability of Failure Criterion

The failure criterion used for all of the tests, except for specimen BD3, corresponded a condition in which one element of the built up cross-section had severed and a crack was detected in another element. In order to determine the suitability of this failure criterion, one specimen, BD4, was tested until it was no longer able to carry the applied load. The results show that less than 97 730 cycles (approximately 2 % of the total fatigue life) were applied between the time the second element cracked and the time that complete failure occurred. This indicates that the failure criterion defined in this study was appropriate because it closely approximated the condition where the specimen was no longer able to carry the applied load. The results of these tests should therefore accurately represent the strength of comparable members in real structures.

7.4.3 Effectiveness of Repair

The results from specimen BD3 show that the repair technique was a success, as discussed in Section 5.3.1. The repair appears to have prevented the initiation of new cracks, and the existing crack did not propagate even after many additional cycles of stress. It may be concluded that a repair of this nature could be used either temporarily or permanently in actual applications, although more tests should be conducted to validate the result from this one test.

7.4.4 Comparison of Results with the Work of Others

In general, the results reported herein fall below the strengths of specimens reported in the literature. Because most of the other tests were conducted where the rivets were not in bearing, at least nominally, this may support the position that connections where the rivets carry shear load have a lower fatigue strength. The results from this report along with all of the applicable results from the tests described in Chapter 2 are shown in Figure 7.1. The TD series test results are plotted in accordance with Option 1, which is the most conservative representation of these results. The result for specimen $\Delta D3$ after its repair is shown with an arrow to indicate a run-out condition, that is, the test was stopped before the specimen cracked. (In this case the actual fatigue strength of the specimen will lie somewhere to the right of the plotted point.)

Reemsnyder [1975] tested truss connections in which load was considered to be transferred primarily by bearing of the rivets, although some transfer by friction undoubtedly was also present. These tests were conducted at stress ranges that are much higher than can be expected in most bridges. The results generally lie between the Category C and Category D curves, as shown in Figure 7.1.

Baker and Kulak [1982] tested riveted built-up bridge hangers, and the tests were done at stress ranges well over 150 MPa. The critical detail for these tests was a rivet that was not in bearing. All of these results lie substantially to the right of the Category D line, and many lie well to the right of the Category C line. As has already been noted, many of the data do not represent the strength of the weakest detail in the specimen.

Out *et al.* [1984] tested riveted built-up girders that were severely corroded. The critical detail was the flange-to-web connection, and the rivets in this connection were, theoretically, not in shear. Results from the three tests where cracking occurred at a riveted detail (rather than at a corroded location) are plotted in Figure 7.1. The choice of failure criterion was not consistent for all of the tests, but the data indicate fatigue life well in excess of the Category D fatigue strength curve.

Fisher *et al.* [1987] tested girders with cover plates riveted to the tension flange. Coverplate terminations were created within the region of constant moment at a few locations, so that any rivets in the region where the change of geometry occurred were subjected to bearing stresses. Some cracks also started at riveted details in the shear spans, and these rivets also acted in bearing. These results are shown in Figure 7.1.

Brühwiler *et al.* [1990] tested rolled girders with riveted coverplates, built-up riveted plate girders, and riveted lattice girders. Results from the rolled girders and plate girders are shown in Figure 7.1. The rivets in the coverplate were not subjected to bearing stresses within the constant moment region, nor were the rivets that joined the angles to the web of the plate girders acting in bearing. The results lie near the Category C fatigue strength curve in Figure 7.1.

Tests were conducted on twenty girders at Lehigh University [ATLSS, 1993], using both constant and variable amplitude cyclic loads. The results shown in Figure 7.1 are for the constant amplitude tests, and represent only those tests in which failure occurred at a riveted detail. Failure was defined as a condition in which one component of the built-up cross-section severed, and most of these failures occurred within a region of constant moment. Some of the results represent the severing of an angle at a second location in the same member, and are thus biased because they do not represent the fatigue strength of the weakest detail in the member. One result represents a crack in a shear span, and in this case it is expected that the rivet was in bearing. All of the points that represent cases in which there was no bearing lie above or on the Category D fatigue resistance curve, and the result of the rivet in bearing lies below the Category D curve.

Adamson [1995] tested riveted girders in which there was a riveted gusset plate detail on the tension flange, and the rivets that joined this plate to the flange were, theoretically, loaded in bearing. One specimen was tested in the inverted position where no gusset plate was present, so the critical detail was the continuous flange-to-web connection. In this case the rivets were not in bearing. In Figure 7.1 four of the results plot near the Category D line, and two, results from specimens that never cracked, plot well to the right

of the Category D line. The result from the specimen that was tested in the inverted position plots well to the right of the Category C line.

Results from tests where the rivets at the critical detail were judged to be in bearing are shown in Figure 7.2 and cases where the rivets were judged to be free of bearing are shown in Figure 7.3. These judgments were based on whether shear flow (and thus bearing in the rivets) was, theoretically, present at the critical detail. Of course, it is difficult in any test program to determine the degree to which bearing of the rivets may be present. The figures illustrate that the fatigue strength of details where the rivets were in bearing appears to be lower than those where the rivets are not in bearing. When the uncertain nature of the location of the TD series test results is taken into consideration, Category D appears to be generally appropriate for rivets that are in bearing. Category C appears to be appropriate for rivets that are not in bearing, although several of the points fall below the Category C curve. In general, Category D appears to be the most appropriate curve for the evaluation of riveted connections.

7.5 Prediction of Remaining Fatigue Life

Various combinations of parameters for the AREA, Eurocode 3, and Kunz methods have been used to calculate remaining fatigue life of the critical detail of the diagonal at the lower panel point. The program RFL, described in Chapter 6, was used to perform all of the calculations. Each of the three methods use the Miner summation (Equation 2.2) to accumulate fatigue damage, although the damage accumulation calculation is somewhat more complex in the Kunz method. Rainflow counting is used to determine stress ranges for the number and magnitude of stress cycles for all three methods.

The AREA method is somewhat limited because it does not account for the effect of a few large stress cycles mixed with several stress cycles that fall below the constant amplitude fatigue limit. In this situation, the constant amplitude fatigue limit is simply removed as soon as it is exceeded by one cycle, and the slope of the fatigue curve simply becomes three. Also, the effect of the sequence of loading for variable amplitude stress cycles is not considered in the AREA standard. The Eurocode 3 method allows the option of some

improvement over AREA in that a dual slope system may be used to account for the situation in which only a few high stress cycles exist. However, Eurocode 3 does not consider the effect of the order of the applied cycles. The Kunz method accounts for both the order and magnitude of the applied cycles by incorporating a damage limit. The damage limit decreases as the value of the Miner summation increases, and any stress cycle that falls below the damage limit has no effect. The Kunz method also uses a gradual transition region between the damage limit and the descending portion of the fatigue strength curve. Such a transition region is observed in experimental fracture mechanics data and has been explained in Chapter 2. It is expected that, for the same detail category, the AREA method will be the most conservative and the Kunz method will be the least conservative in fatigue life prediction.

The remaining fatigue life calculations show that the AREA Category D and the Eurocode 3, Detail Category 69, with a single slope of three and no constant amplitude fatigue limit and no cut-off limit, predicted the least remaining fatigue life. These methods predicted a remaining life in the order of 260 years for both the *Space Frame* and *Simple Truss* models, referenced from the time the bridge was disassembled in 1992. All of the other methods predicted remaining lives longer than these, and several were greater than 1000 years. It is not possible to judge or to make a worthwhile comparison of the methods of evaluation or the parameters used in the calculations because these calculated fatigue lives are so long. However, it can be concluded that the amount of fatigue damage in the diagonals of the Miette River Bridge was negligible at the time it was disassembled.

Table 7.1 Prediction of Fatigue Test Results by AREA and Kunz Methods

	Specimen	Stress Range (MPa)	Experimental Results (cycles)	AREA Category D (cycles)	Kunz Method (cycles)
	BD1	73	2 401 580	1 690 000	1 840 000
	BD2	69	3 958 270	2 000 000	2 210 000
	BD3	73	2 273 500*	1 690 000	1 840 000
	BD4	66	5 250 610	2 290 000	2 580 000
Option 1 $A_{net}=12\,554\text{ mm}^2$	TD1	64	1 944 670	2 510 000	2 870 000
	TD2	62	2 415 840	2 760 000	3 210 000
	TD3	58	2 415 140	3 370 000	4 120 000
Option 2 $A_{net}=11\,042\text{ mm}^2$	TD1	72.5	1 944 670	1 724 000	1 880 000
	TD2	70.5	2 415 840	1 875 037	2 070 000
	TD3	66	2 415 140	2 285 311	2 580 000

*Represents severing of one angle only.

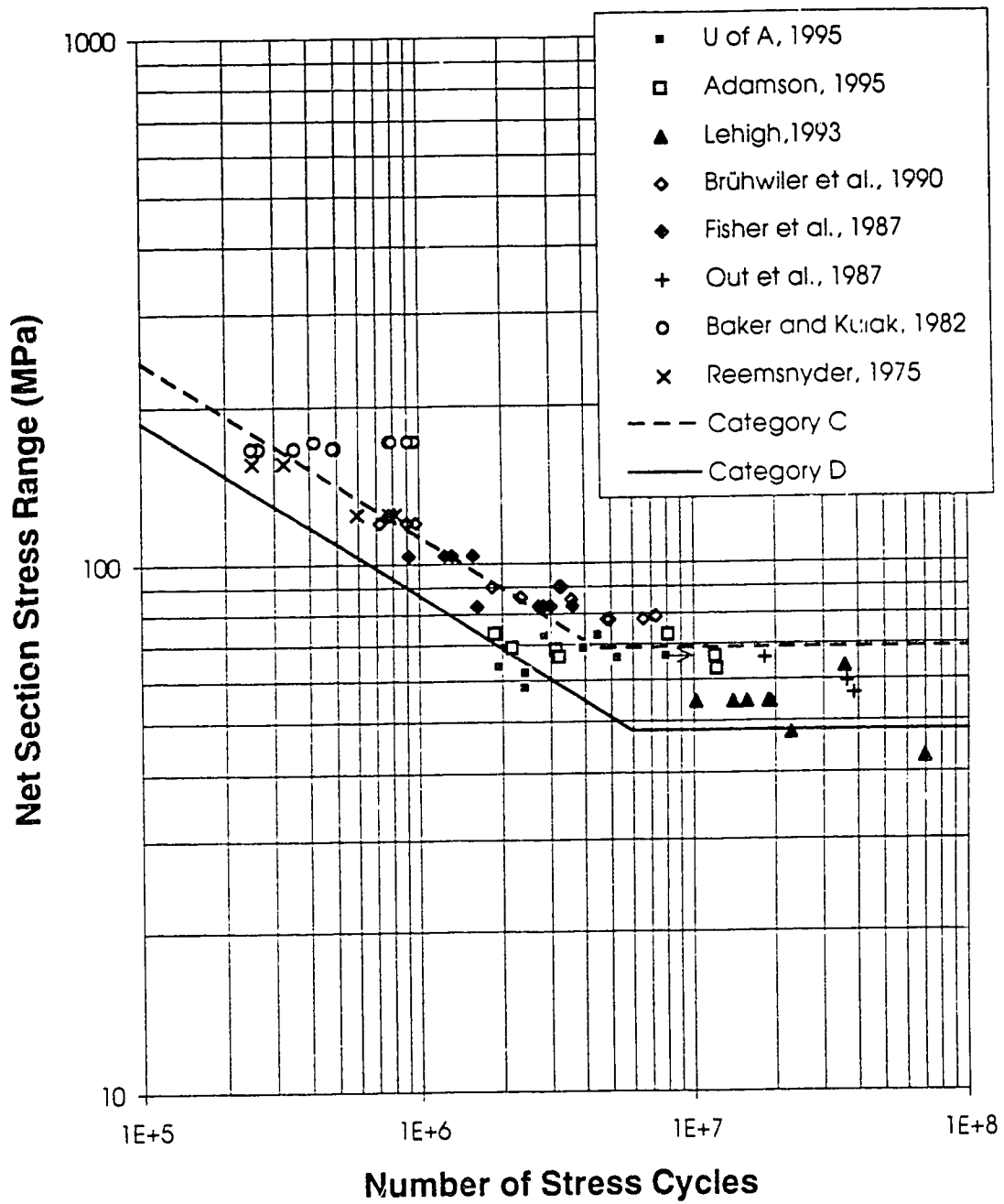


Figure 7.1 Results from Literature Survey and Experimental Program

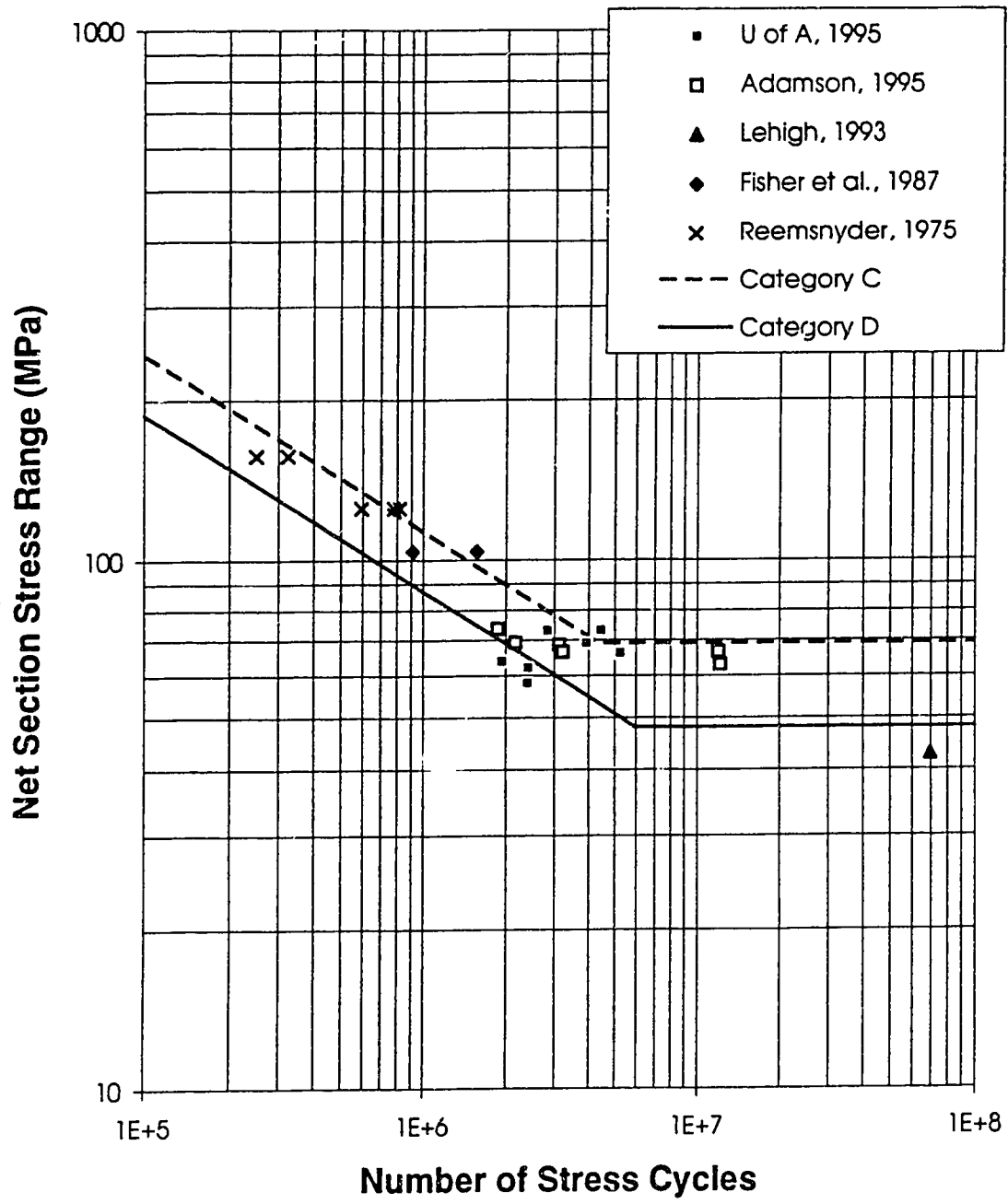


Figure 7.2 Results of Connections with Rivets Theoretically in Bearing

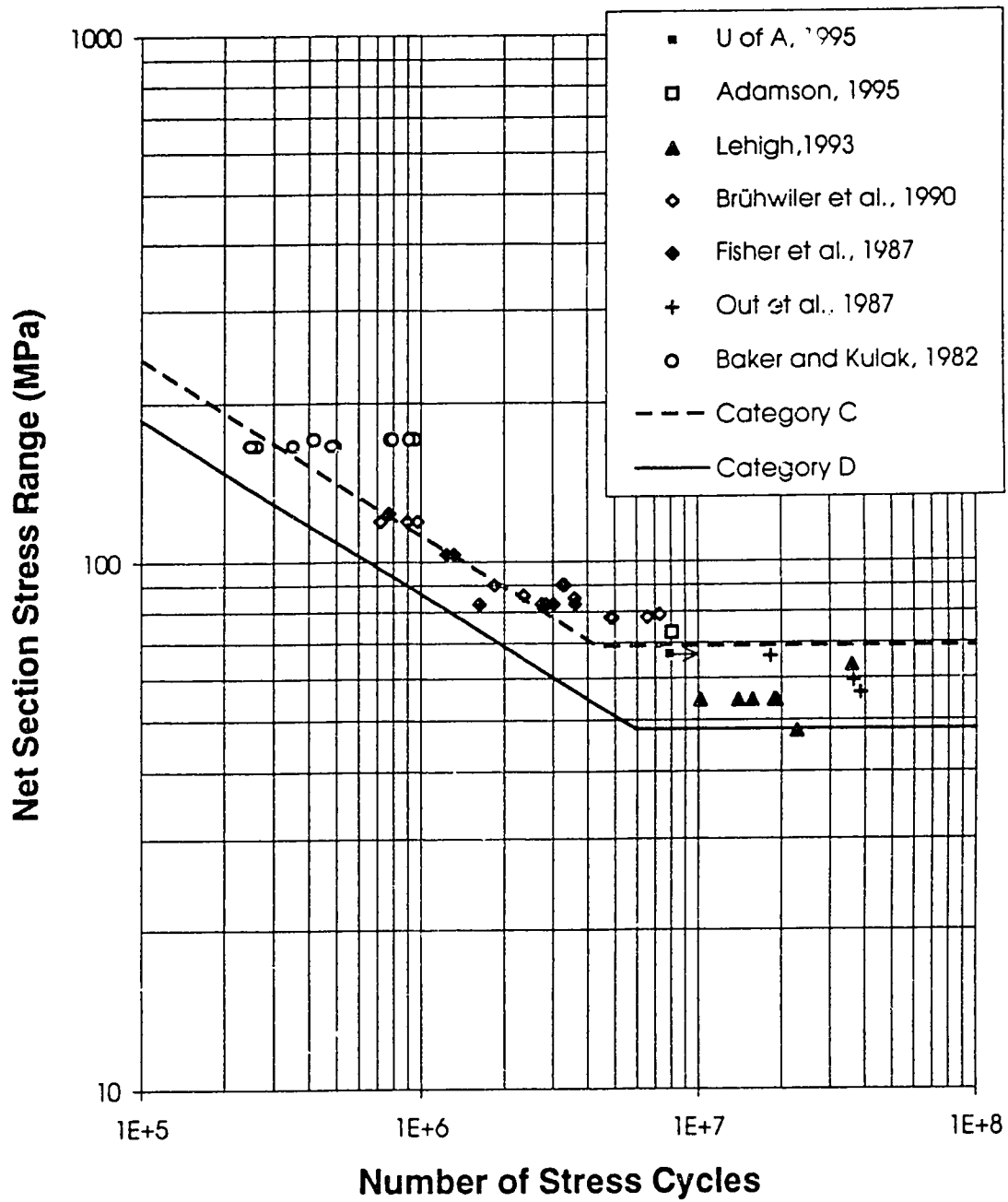


Figure 7.3 Results of Connections with Rivets Theoretically not in Bearing

8. Summary, Conclusions, and Recommendations

8.1 Summary

Service load strain measurements were taken from a tension diagonal and a stringer of the Miette River Bridge in 1992. The bridge was dismantled shortly thereafter and the four main diagonals and ten stringers were obtained by the University of Alberta. These members became part of an ongoing experimental program to explore the fatigue strength of full-scale riveted members.

As part of this study, the diagonals were tested in uniaxial tension fatigue. The critical detail in these tests was the riveted shear splice end connection of the diagonal to the gusset plate. The failure criterion for the tests was defined as severing of one element of the built-up cross-section and the detection of a crack in a second element. In one case, the specimen was repaired after an element had severed and the test was allowed to continue. This was done in order to evaluate the effectiveness of a repair technique and to obtain information on the strength of riveted details that are not subject to bearing stresses. The results from the tests are used to supplement the existing database of results from full-scale fatigue tests, and are compared to strength predictions by AREA [1994] and Kunz [1994]. The fatigue cracks that developed during the tests were opened to allow inspection of their surfaces in order to reveal if any unusual circumstances affected the fatigue crack initiation and growth.

In addition to the experimental program, a survey of existing literature was made on structural modelling of bridges, fatigue tests of riveted connections, and methods for the prediction of remaining fatigue life. Two structural models were also developed as part of this study in order to predict the behaviour of the diagonals. The results from these models were compared to the measured strains in order to determine which model best represents the true behaviour of the structure.

A prediction of remaining fatigue life of the critical detail of the diagonals was also made using various combinations of structural models and fatigue evaluation methods. The prediction of remaining fatigue life also served to determine the likelihood of the existence of fatigue damage prior to the experimental program.

8.2 Conclusions

The following conclusions may be drawn based on the results of the work described above. Several conclusions relate specifically to the Miette River Bridge, but may be applicable in some cases to similar through-truss structures.

1. Few studies of full-scale riveted specimens have been conducted, and only two were identified in which the behaviour of full-scale riveted shear splices was investigated. Most of the tests that have been conducted had rivets that were, theoretically, not in bearing and therefore these results may not accurately represent most riveted connections in service.
2. A plane truss analysis with all connections modelled as pinned gave conservative results for the strain in the diagonal as compared to measurements made while the bridge was in service. The development of a space frame model gave improved predictions, but the additional work involved for a minor increase in accuracy was unwarranted.
3. Measured strains in the diagonal, inspection of the crack surfaces and the prediction of remaining fatigue life did not indicate that any fatigue damage existed when the tests began.
4. The fatigue resistance of the diagonals at their connection to the bottom chord panel point exceeded the Category D fatigue strength curve of the American Railway Engineering Association standard.
5. The fatigue resistance of the diagonals at their connection to the top chord panel point fell near or below the Category D fatigue strength curve depending on how the net-

cross sectional area was defined. It appeared that the rivets in these connections had reduced clamping force.

6. The fatigue resistance of riveted connections where the rivets experience significant bearing appears to be lower than that of details where the rivets are not in bearing.
7. The failure criterion selected, in which one element is severed and a crack has appeared in a second element, closely approximated inability of the specimen to carry the applied load.
8. The repair of a cracked tension member to gusset plate connection with pre-tensioned bolted splice plates extended the life of the connection significantly.
9. Various methods for the calculation of remaining fatigue life can give widely variable results. It was not possible to evaluate the fatigue evaluation techniques because in this study all of the methods yielded extremely long predicted lives.

8.3 Recommendations

The structural models developed in Chapter 3 show that a good estimate of stresses at critical details can be obtained analytically. A simple, plane truss with all joints modelled as pinned gives acceptable accuracy for the prediction of stresses in the web members of a through-truss bridge.

More research is required to determine the significance of the differences between connections where the rivets have substantial bearing and those that are free of bearing.

Further testing is required in order to define the location of the transition region in the fatigue life response and to determine the constant amplitude fatigue limit for riveted connections. Preferably, these tests should be conducted on connections where the rivets are in bearing and where the applied stress ranges are below about 75 MPa. The correlation of the fatigue strength of individual details to the fatigue strength of members with a number of identical details should also be explored.

Additional research is required to determine the effect of staggered rivet patterns on the fatigue strength of a riveted detail, so as to determine an appropriate definition of the critical net cross-sectional area. Category D, used in conjunction with the $s^2/4g$ (Cochrane) rule, appears to be the best available method for evaluation of the fatigue strength of riveted members that have staggered rivet patterns.

List of References

- Adamson, D. (1995). Fatigue Tests of Riveted Bridge Girders, Master of Science Thesis, Department of Civil Engineering, University of Alberta, Edmonton, Alberta.
- American Association of State and Highway Transportation Officials, (1990). Guide Specifications for Fatigue Evaluation of Existing Steel Bridges, Washington, D.C.
- American Railway Engineering Association (1994). "Steel Structures," Chapter 15, Manual for Railway Engineering.
- American Society for Testing and Materials, (1992). "A 370 - 92, Standard Test Methods and Definitions for Mechanical Testing of Steel Products."
- Baker, K.A., and Kulak, G.L. (1982). Fatigue Strength of Two Steel Details, *Structural Engineering Report No. 105*, Department of Civil Engineering, University of Alberta, Edmonton, Alberta.
- Baron F., and Larson, E.W. (1953). "The Effect of Grip on the Fatigue Strength of Riveted and Bolted Joints," Proceedings of the American Railway Engineering Association, Vol. 54, pp. 175-190.
- Brühwiler, E., Smith, I.F.C., and Hirt, M.A. (1990). "Fatigue and Fracture of Riveted Bridge Members," Journal of Structural Engineering, ASCE, Vol. 116, No. 11, pp. 198-214.
- Canadian Standards Association (1989). Limit States Design of Steel Structures, CAN/CSA-S16.1-M89, December.
- Center for Advanced Technology for Large Structural Systems (1993). Assessment of Remaining Capacity and Life of Riveted Bridge Members, *Draft Project Report to Canadian National Railways*, Lehigh University, Bethlehem, Pennsylvania.
- Cochrane, V.H. (1922). "Rules for Riveted Hole Deductions in Tension Members," Engineering News-Record, November 16, pp. 847-848.
- Downing, S.D. and Socie, D.F. (1982). "Simple Rainflow Counting Algorithms," International Journal of Fatigue, Vol. 4, No. 1, pp. 31-40.
- European Committee for Standardisation (1992). Eurocode 3: Design of Steel Structures, ENV 1993-1-1, Brussels.
- Fisher, J.W. (1984). Fatigue and Fracture in Steel Bridges, John Wiley and Sons, New York.
- Fisher, J.W. (1977). Bridge Fatigue Guide, American Institute of Steel Construction, New York.

- Fisher, J.W., and Daniels, J.H. (1976). "An Investigation of the Estimated Fatigue Damage in Members of the 380-ft Main Span, Fraser River Bridge," Proceedings of the American Railway Engineering Association, Volume 77, Bulletin 658, pp. 577-597.
- Fisher, J.W., Yen, B.T., and Wang, D. (1990). "Fatigue Strength of Riveted Bridge Members," Journal of Structural Engineering, ASCE, Vol. 116, No. 11, pp. 2968-2981.
- Fisher, J.W., Yen, B.T., Wang, D., and Mann, J.E. (1987). Fatigue and Fracture Evaluation for Rating Riveted Bridges, *National Cooperative Highway Research Program Report 302*, Transportation Research Board, National Research Council, Washington, D.C.
- Fuchs, H.D., and Stephens, R.I. (1980). Metal Fatigue in Engineering, Wiley-Interscience, New York.
- Gordon, J.E. (1978). Structures, Penguin Books, London, Second Edition.
- Kulak, G.L., Fisher, J.W., and Struik, J.H.A. (1987). Guide to Design Criteria for Bolted and Riveted Joints, Second Edition, John Wiley & Sons, Toronto.
- Kulak, G.L., and Smith, I.F.C. (1993). Analysis and Design of Fabricated Steel Structures for Fatigue: A Primer for Civil Engineers, *Structural Engineering Report No. 190*, Department of Civil Engineering, University of Alberta, Edmonton, Alberta.
- Kunz, P.M. (1994). RFL - Remaining Fatigue Life. (Computer Program), Department of Civil Engineering, University of Alberta, Edmonton, Alberta.
- Kunz, P.M. (1992). Probabilistic Method for the Evaluation of Fatigue Safety of Existing Steel Bridges, *Doctoral Thesis No. 1023*, Swiss Federal Institute of Technology, Lausanne, Switzerland, (in German).
- Lenzen, K.H. (1950). "The Effect of Various Fasteners on the Fatigue Strength of a Structural Joint," Proceedings of the American Railway Engineering Association, Vol. 51, pp. 1-28.
- McGuire, W. (1968). Steel Structures, Prentice-Hall, Englewood Cliffs, New Jersey.
- Miner, M.A. (1945). "Cumulative Damage in Fatigue," Journal of Applied Mechanics, September, pp. 159-164.
- Out, J.M.M., Fisher, J.W., and Yen, B.T. (1984). Fatigue Strength of Weathered and Deteriorated Riveted Members, *Transportation Research Record 950*, Transportation Research Board, National Research Council, Washington, D.C., pp. 10-20.

- Parola, J. F., Chesson, E. Jr., and Munse, W. H. (1964). Effect of Bearing Pressure on Fatigue Strength of Riveted Connections, *Bulletin 481*, Engineering Experiment Station, University of Illinois.
- Petroski, H. (1985). To Engineer is Human: The Role of Failure in Successful Design, St. Martin's Press, New York.
- Reemsnyder, H.S. (1975). "Fatigue life Extension of Riveted Connections," Journal of the Structural Division, ASCE, Vol. 101, No ST12, pp. 2591-2608.
- Schilling, C.G., Klippstein, K.H., Barsom, J.M., and Blake, G.T. (1978), Fatigue of Welded Steel Bridge Members under Variable-Amplitude Loadings, *National Cooperative Highway Research Program Report 188*, Transportation Research Board, National Research Council, Washington, D.C.
- Szeliski, Z.L., and Elkholy, I.A. (1984). "Fatigue Investigation of a Railway Truss Bridge," Canadian Journal of Civil Engineering, Volume 11, pp. 625-631.
- Wilson, W.M., and Thomas, F.P. (1938). Fatigue Tests of Riveted Joints, *Bulletin 302*, Engineering Experiment Station, University of Illinois.
- Wilson and Habibullah, (1992). *SAP90, A Series of Computer Programs for the Finite Element Analysis of Structures*, Computers and Structures Incorporated, Berkeley, California.
- Wyly, L.T., and Scott, M.B. (1956). "An Investigation of Fatigue Failures in Structural Members of Ore Bridges Under Service Loadings," Proceedings of the American Railway Engineering Association, Vol. 57, pp. 175-297.

Appendix A

Details of Trains T730, F430, F658, and F717

Axle distances in meters from first axle of Engine 1; Single wheel loads in kilonewtons.

TRAIN T720			AXLE 2	-151.6	132.3	AXLE 4	-328.0	133.4
Engine 1			AXLE 3	-163.8	132.3	Car 17		
AXLE 1	0.0	143.1	AXLE 4	-165.6	132.3	AXLE 1	-330.2	136.8
AXLE 2	-2.0	143.1	Car 8			AXLE 2	-332.0	136.8
AXLE 3	-4.2	143.1	AXLE 1	-167.8	129.0	AXLE 3	-344.2	136.8
AXLE 4	-13.9	143.1	AXLE 2	-169.5	129.0	AXLE 4	-346.0	136.8
AXLE 5	-16.0	143.1	AXLE 3	-181.8	129.0	Car 18		
AXLE 6	-18.0	143.1	AXLE 4	-183.6	129.0	AXLE 1	-348.2	143.5
Engine 2			Car 9			AXLE 2	-350.0	143.5
AXLE 1	-21.7	143.8	AXLE 1	-185.7	130.1	AXLE 3	-362.5	143.5
AXLE 2	-23.8	143.8	AXLE 2	-187.5	130.1	AXLE 4	-364.3	143.5
AXLE 3	-25.9	143.8	AXLE 3	-200.1	130.1	Car 19		
AXLE 4	-33.9	143.8	AXLE 4	-201.8	130.1	AXLE 1	-366.5	101.2
AXLE 5	-36.0	143.8	Car 10			AXLE 2	-368.3	101.2
AXLE 6	-38.0	143.8	AXLE 1	-204.0	109.0	AXLE 3	-380.8	101.2
Car 1			AXLE 2	-205.8	109.0	AXLE 4	-382.6	101.2
AXLE 1	-41.0	143.5	AXLE 3	-218.4	109.0	Car 20		
AXLE 2	-42.7	143.5	AXLE 4	-220.1	109.0	AXLE 1	-384.8	112.3
AXLE 3	-55.0	143.5	Car 11			AXLE 2	-386.6	112.3
AXLE 4	-56.8	143.5	AXLE 1	-222.3	113.4	AXLE 3	-399.1	112.3
Car 2			AXLE 2	-224.1	113.4	AXLE 4	-400.9	112.3
AXLE 1	-58.9	143.5	AXLE 3	-236.6	113.4	Car 21		
AXLE 2	-60.7	143.5	AXLE 4	-238.4	113.4	AXLE 1	-403.1	139.0
AXLE 3	-73.3	143.5	Car 12			AXLE 2	-404.9	139.0
AXLE 4	-75.1	143.5	AXLE 1	-240.6	111.2	AXLE 3	-417.1	139.0
Car 3			AXLE 2	-242.4	111.2	AXLE 4	-418.9	139.0
AXLE 1	-77.2	144.6	AXLE 3	-254.9	111.2	Car 22		
AXLE 2	-79.0	144.6	AXLE 4	-256.7	111.2	AXLE 1	-421.1	137.9
AXLE 3	-91.3	144.6	Car 13			AXLE 2	-422.8	137.9
AXLE 4	-93.0	144.6	AXLE 1	-258.9	126.8	AXLE 3	-435.4	137.9
Car 4			AXLE 2	-260.7	126.8	AXLE 4	-437.2	137.9
AXLE 1	-95.2	133.4	AXLE 3	-272.9	126.8	Car 23		
AXLE 2	-97.0	133.4	AXLE 4	-274.7	126.8	AXLE 1	-439.3	121.2
AXLE 3	-109.5	133.4	Car 14			AXLE 2	-441.1	121.2
AXLE 4	-111.3	133.4	AXLE 1	-276.9	130.1	AXLE 3	-453.7	121.2
Car 5			AXLE 2	-278.7	130.1	AXLE 4	-455.5	121.2
AXLE 1	-113.5	133.4	AXLE 3	-289.7	130.1	Car 24		
AXLE 2	-115.3	133.4	AXLE 4	-291.5	130.1	AXLE 1	-457.6	137.9
AXLE 3	-127.8	133.4	Car 15			AXLE 2	-459.4	137.9
AXLE 4	-129.6	133.4	AXLE 1	-293.6	141.2	AXLE 3	-471.7	137.9
Car 6			AXLE 2	-295.4	141.2	AXLE 4	-473.4	137.9
AXLE 1	-131.8	131.2	AXLE 3	-308.0	141.2	Car 25		
AXLE 2	-133.6	131.2	AXLE 4	-309.8	141.2	AXLE 1	-475.6	122.3
AXLE 3	-145.8	131.2	Car 16			AXLE 2	-477.4	122.3
AXLE 4	-147.6	131.2	AXLE 1	-311.9	133.4	AXLE 3	-489.9	122.3
Car 7			AXLE 2	-313.7	133.4	AXLE 4	-491.7	122.3
AXLE 1	-149.8	132.3	AXLE 3	-326.3	133.4	Car 26		

Axle distances in meters from first axle of Engine 1; Single wheel loads in kilonewtons.

AXLE 1	-493.9	142.3
AXLE 2	-495.7	142.3
AXLE 3	-507.9	142.3
AXLE 4	-509.7	142.3
Car 27		
AXLE 1	-511.9	143.5
AXLE 2	-513.7	143.5
AXLE 3	-525.9	143.5
AXLE 4	-527.7	143.5
Car 28		
AXLE 1	-529.9	143.5
AXLE 2	-531.6	143.5
AXLE 3	-543.9	143.5
AXLE 4	-545.7	143.5
Car 29		
AXLE 1	-547.8	141.2
AXLE 2	-549.6	141.2
AXLE 3	-561.9	141.2
AXLE 4	-563.6	141.2
Car 30		
AXLE 1	-565.8	113.4
AXLE 2	-567.6	113.4
AXLE 3	-580.2	113.4
AXLE 4	-581.9	113.4

Axle distances in meters from first axle of Engine 1; Single wheel loads in kilonewtons.

TRAIN F430			AXLE 1	-218.5	75.6
Engine 1			AXLE 2	-220.3	75.6
AXLE 1	0.0	144.6	AXLE 3	-235.5	75.6
AXLE 2	-2.7	144.6	AXLE 4	-237.3	75.6
AXLE 3	-10.4	144.6	Car 9		
AXLE 4	-13.1	144.6	AXLE 1	-244.5	76.7
Engine 2			AXLE 2	-246.2	76.7
AXLE 1	-18.0	144.6	AXLE 3	-261.4	76.7
AXLE 2	-20.8	144.6	AXLE 4	-263.2	76.7
AXLE 3	-28.4	144.6	Car 10		
AXLE 4	-31.1	144.6	AXLE 1	-270.4	76.7
Car 1			AXLE 2	-272.1	76.7
AXLE 1	-37.2	66.7	AXLE 3	-287.3	76.7
AXLE 2	-39.0	66.7	AXLE 4	-289.1	76.7
AXLE 3	-54.1	66.7	Car 11		
AXLE 4	-55.9	66.7	AXLE 1	-296.3	76.7
Car 2			AXLE 2	-298.1	76.7
AXLE 1	-63.1	66.7	AXLE 3	-313.2	76.7
AXLE 2	-64.9	66.7	AXLE 4	-315.0	76.7
AXLE 3	-80.0	66.7	Car 12		
AXLE 4	-81.8	66.7	AXLE 1	-322.2	81.2
Car 3			AXLE 2	-324.0	81.2
AXLE 1	-89.0	80.1	AXLE 3	-339.1	81.2
AXLE 2	-90.8	80.1	AXLE 4	-340.9	81.2
AXLE 3	-105.9	80.1			
AXLE 4	-107.7	80.1			
Car 4					
AXLE 1	-114.9	76.7			
AXLE 2	-116.7	76.7			
AXLE 3	-131.9	76.7			
AXLE 4	-133.6	76.7			
Car 5					
AXLE 1	-140.8	76.7			
AXLE 2	-142.6	76.7			
AXLE 3	-157.8	76.7			
AXLE 4	-159.5	76.7			
Car 6					
AXLE 1	-166.7	76.7			
AXLE 2	-168.5	76.7			
AXLE 3	-183.7	76.7			
AXLE 4	-185.5	76.7			
Car 7					
AXLE 1	-192.6	76.7			
AXLE 2	-194.4	76.7			
AXLE 3	-209.6	76.7			
AXLE 4	-211.4	76.7			
Car 8					

Axle distances in meters from first axle of Engine 1; Single wheel loads in kilonewtons.

TRAIN 658			AXLE 4	-164.4	34.5	AXLE 1	-331.2	33.4
Engine 1			Car 9			AXLE 2	-333.0	33.4
AXLE 1	0.0	143.8	AXLE 1	-166.6	23.4	AXLE 3	-345.6	33.4
AXLE 2	-2.0	143.8	AXLE 2	-168.4	23.4	AXLE 4	-347.3	33.4
AXLE 3	-4.2	143.8	AXLE 3	-180.9	23.4	Car 19		
AXLE 4	-13.9	143.8	AXLE 4	-182.7	23.4	AXLE 1	-349.5	34.5
AXLE 5	-16.0	143.8	Car 10			AXLE 2	-351.3	34.5
AXLE 6	-18.0	143.8	AXLE 1	-184.9	24.5	AXLE 3	-363.8	34.5
Car 1			AXLE 2	-186.7	24.5	AXLE 4	-365.6	34.5
AXLE 1	-20.3	34.5	AXLE 3	-199.2	24.5	Car 20		
AXLE 2	-22.1	34.5	AXLE 4	-201.0	24.5	AXLE 1	-367.8	34.5
AXLE 3	-34.6	34.5	Car 11			AXLE 2	-369.6	34.5
AXLE 4	-36.4	34.5	AXLE 1	-203.2	33.4	AXLE 3	-382.1	34.5
Car 2			AXLE 2	-205.0	33.4	AXLE 4	-383.9	34.5
AXLE 1	-38.6	33.4	AXLE 3	-217.5	33.4	Car 21		
AXLE 2	-40.4	33.4	AXLE 4	-219.3	33.4	AXLE 1	-386.1	32.2
AXLE 3	-52.9	33.4	Car 12			AXLE 2	-387.9	32.2
AXLE 4	-54.7	33.4	AXLE 1	-221.5	33.4	AXLE 3	-400.4	32.2
Car 3			AXLE 2	-223.3	33.4	AXLE 4	-402.2	32.2
AXLE 1	-56.9	33.4	AXLE 3	-235.8	33.4	Car 22		
AXLE 2	-58.7	33.4	AXLE 4	-237.6	33.4	AXLE 1	-404.4	24.5
AXLE 3	-71.2	33.4	Car 13			AXLE 2	-406.2	24.5
AXLE 4	-73.0	33.4	AXLE 1	-239.8	33.4	AXLE 3	-418.7	24.5
Car 4			AXLE 2	-241.6	33.4	AXLE 4	-420.5	24.5
AXLE 1	-75.2	33.4	AXLE 3	-254.1	33.4	Car 23		
AXLE 2	-76.9	33.4	AXLE 4	-255.9	33.4	AXLE 1	-422.7	32.2
AXLE 3	-89.5	33.4	Car 14			AXLE 2	-424.5	32.2
AXLE 4	-91.3	33.4	AXLE 1	-258.1	24.5	AXLE 3	-437.0	32.2
Car 5			AXLE 2	-259.8	24.5	AXLE 4	-438.8	32.2
AXLE 1	-93.5	34.5	AXLE 3	-272.4	24.5	Car 24		
AXLE 2	-95.2	34.5	AXLE 4	-274.2	24.5	AXLE 1	-441.0	34.5
AXLE 3	-107.8	34.5	Car 15			AXLE 2	-442.7	34.5
AXLE 4	-109.6	34.5	AXLE 1	-276.4	23.4	AXLE 3	-455.3	34.5
Car 6			AXLE 2	-278.1	23.4	AXLE 4	-457.1	34.5
AXLE 1	-111.7	34.5	AXLE 3	-290.7	23.4	Car 25		
AXLE 2	-113.5	34.5	AXLE 4	-292.5	23.4	AXLE 1	-459.3	34.5
AXLE 3	-126.1	34.5	Car 16			AXLE 2	-461.0	34.5
AXLE 4	-127.9	34.5	AXLE 1	-294.6	33.4	AXLE 3	-473.6	34.5
Car 7			AXLE 2	-296.4	33.4	AXLE 4	-475.4	34.5
AXLE 1	-130.0	34.5	AXLE 3	-309.0	33.4	Car 26		
AXLE 2	-131.8	34.5	AXLE 4	-310.8	33.4	AXLE 1	-477.5	34.5
AXLE 3	-144.4	34.5	Car 17			AXLE 2	-479.3	34.5
AXLE 4	-146.1	34.5	AXLE 1	-312.9	34.5	AXLE 3	-491.9	34.5
Car 8			AXLE 2	-314.7	34.5	AXLE 4	-493.7	34.5
AXLE 1	-148.3	34.5	AXLE 3	-327.3	34.5	Car 27		
AXLE 2	-150.1	34.5	AXLE 4	-329.0	34.5	AXLE 1	-495.8	34.5
AXLE 3	-162.7	34.5	Car 18			AXLE 2	-497.6	34.5

Axle distances in meters from first axle of Engine 1; Single wheel loads in kilonewtons.

AXLE 3	-510.2	34.5	Car 37			AXLE 2	-845.1	34.5
AXLE 4	-511.9	34.5	AXLE 1	-678.7	24.5	AXLE 3	-857.7	34.5
Car 28			AXLE 2	-680.5	24.5	AXLE 4	-859.4	34.5
AXLE 1	-514.1	34.5	AXLE 3	-693.1	24.5	Car 47		
AXLE 2	-515.9	34.5	AXLE 4	-694.8	24.5	AXLE 1	-861.6	33.4
AXLE 3	-528.5	34.5	Car 38			AXLE 2	-863.4	33.4
AXLE 4	-530.2	34.5	AXLE 1	-697.0	34.5	AXLE 3	-876.0	33.4
Car 29			AXLE 2	-698.8	34.5	AXLE 4	-877.7	33.4
AXLE 1	-532.4	34.5	AXLE 3	-711.3	34.5	Car 48		
AXLE 2	-534.2	34.5	AXLE 4	-713.1	34.5	AXLE 1	-879.9	34.5
AXLE 3	-546.7	34.5	Car 39			AXLE 2	-881.7	34.5
AXLE 4	-548.5	34.5	AXLE 1	-715.3	34.5	AXLE 3	-894.2	34.5
Car 30			AXLE 2	-717.1	34.5	AXLE 4	-896.0	34.5
AXLE 1	-550.7	34.5	AXLE 3	-729.6	34.5	Car 49		
AXLE 2	-552.5	34.5	AXLE 4	-731.4	34.5	AXLE 1	-898.2	34.5
AXLE 3	-565.0	34.5	Car 40			AXLE 2	-900.0	34.5
AXLE 4	-566.8	34.5	AXLE 1	-733.6	24.5	AXLE 3	-912.5	34.5
Car 31			AXLE 2	-735.4	24.5	AXLE 4	-914.3	34.5
AXLE 1	-569.0	34.5	AXLE 3	-747.9	24.5	Car 50		
AXLE 2	-570.8	34.5	AXLE 4	-749.7	24.5	AXLE 1	-916.5	33.4
AXLE 3	-583.3	34.5	Car 41			AXLE 2	-918.3	33.4
AXLE 4	-585.1	34.5	AXLE 1	-751.9	34.5	AXLE 3	-930.8	33.4
Car 32			AXLE 2	-753.7	34.5	AXLE 4	-932.6	33.4
AXLE 1	-587.3	33.4	AXLE 3	-766.2	34.5	Car 51		
AXLE 2	-589.1	33.4	AXLE 4	-768.0	34.5	AXLE 1	-934.8	24.5
AXLE 3	-601.6	33.4	Car 42			AXLE 2	-936.6	24.5
AXLE 4	-603.4	33.4	AXLE 1	-770.2	24.5	AXLE 3	-949.1	24.5
Car 33			AXLE 2	-772.0	24.5	AXLE 4	-950.9	24.5
AXLE 1	-605.6	24.5	AXLE 3	-784.5	24.5	Car 52		
AXLE 2	-607.3	24.5	AXLE 4	-786.3	24.5	AXLE 1	-953.1	33.4
AXLE 3	-619.9	24.5	Car 43			AXLE 2	-954.9	33.4
AXLE 4	-621.7	24.5	AXLE 1	-788.5	34.5	AXLE 3	-967.4	33.4
Car 34			AXLE 2	-790.2	34.5	AXLE 4	-969.2	33.4
AXLE 1	-623.9	34.5	AXLE 3	-802.8	34.5	Car 53		
AXLE 2	-625.6	34.5	AXLE 4	-804.6	34.5	AXLE 1	-971.4	34.5
AXLE 3	-638.2	34.5	Car 44			AXLE 2	-973.1	34.5
AXLE 4	-640.0	34.5	AXLE 1	-806.8	34.5	AXLE 3	-985.7	34.5
Car 35			AXLE 2	-808.5	34.5	AXLE 4	-987.5	34.5
AXLE 1	-642.1	34.5	AXLE 3	-821.1	34.5	Car 54		
AXLE 2	-643.9	34.5	AXLE 4	-822.9	34.5	AXLE 1	-989.7	33.4
AXLE 3	-656.5	34.5	Car 45			AXLE 2	-991.4	33.4
AXLE 4	-658.3	34.5	AXLE 1	-825.0	34.5	AXLE 3	-1004.0	33.4
Car 36			AXLE 2	-826.8	34.5	AXLE 4	-1005.8	33.4
AXLE 1	-660.4	34.5	AXLE 3	-839.4	34.5	Car 55		
AXLE 2	-662.2	34.5	AXLE 4	-841.2	34.5	AXLE 1	-1008.0	24.5
AXLE 3	-674.8	34.5	Car 46			AXLE 2	-1009.7	24.5
AXLE 4	-676.5	34.5	AXLE 1	-843.3	34.5	AXLE 3	-1022.3	24.5

Axle distances in meters from first axle of Engine 1; Single wheel loads in kilonewtons.

AXLE 4	-1024.1	24.5	AXLE 1	-1190.9	34.5
Car 56			AXLE 2	-1192.6	34.5
AXLE 1	-1026.2	34.5	AXLE 3	-1205.2	34.5
AXLE 2	-1028.0	34.5	AXLE 4	-1207.0	34.5
AXLE 3	-1040.6	34.5	Car 66		
AXLE 4	-1042.4	34.5	AXLE 1	-1209.1	33.4
Car 57			AXLE 2	-1210.9	33.4
AXLE 1	-1044.5	34.5	AXLE 3	-1223.5	33.4
AXLE 2	-1046.3	34.5	AXLE 4	-1225.3	33.4
AXLE 3	-1058.9	34.5	Car 67		
AXLE 4	-1060.6	34.5	AXLE 1	-1227.4	34.5
Car 58			AXLE 2	-1229.2	34.5
AXLE 1	-1062.8	34.5	AXLE 3	-1241.8	34.5
AXLE 2	-1064.6	34.5	AXLE 4	-1243.5	34.5
AXLE 3	-1077.2	34.5	Car 68		
AXLE 4	-1078.9	34.5	AXLE 1	-1245.7	34.5
Car 59			AXLE 2	-1247.5	34.5
AXLE 1	-1081.1	33.4	AXLE 3	1260.1	34.5
AXLE 2	-1082.9	33.4	AXLE 4	-1261.8	34.5
AXLE 3	-1095.4	33.4	Car 69		
AXLE 4	-1097.2	33.4	AXLE 1	-1264.0	34.5
Car 60			AXLE 2	-1265.8	34.5
AXLE 1	-1099.4	34.5	AXLE 3	-1278.3	34.5
AXLE 2	-1101.2	34.5	AXLE 4	-1280.1	34.5
AXLE 3	-1113.7	34.5			
AXLE 4	-1115.5	34.5			
Car 61					
AXLE 1	-1117.7	33.4			
AXLE 2	-1119.5	33.4			
AXLE 3	-1132.0	33.4			
AXLE 4	-1133.8	33.4			
Car 62					
AXLE 1	-1136.0	34.5			
AXLE 2	-1137.8	34.5			
AXLE 3	-1150.3	34.5			
AXLE 4	-1152.1	34.5			
Car 63					
AXLE 1	-1154.3	33.4			
AXLE 2	-1156.1	33.4			
AXLE 3	-1168.6	33.4			
AXLE 4	-1170.4	33.4			
Car 64					
AXLE 1	-1172.6	34.5			
AXLE 2	-1174.3	34.5			
AXLE 3	-1186.9	34.5			
AXLE 4	-1188.7	34.5			
Car 65					

Axle distances in meters from first axle of Engine 1; Single wheel loads in kilonewtons.

TRAIN 717			AXLE 1	-237.7	67.8	AXLE 3	-515.3	64.5
Engine 1			AXLE 2	-239.4	67.8	AXLE 4	-517.1	64.5
AXLE 1	0.0	145.7	AXLE 3	-257.5	67.8	Car 18		
AXLE 2	-2.7	145.7	AXLE 4	-259.3	67.8	AXLE 1	-524.2	64.5
AXLE 3	-10.4	145.7	Car 9			AXLE 2	-525.9	64.5
AXLE 4	-13.1	145.7	AXLE 1	-266.3	73.4	AXLE 3	-544.0	64.5
Engine 2			AXLE 2	-268.1	73.4	AXLE 4	-545.8	64.5
AXLE 1	-18.0	145.7	AXLE 3	-286.1	73.4	Car 19		
AXLE 2	-20.8	145.7	AXLE 4	-287.9	73.4	AXLE 1	-552.8	75.6
AXLE 3	-28.4	145.7	Car 10			AXLE 2	-554.6	75.6
AXLE 4	-31.1	145.7	AXLE 1	-295.0	73.4	AXLE 3	-572.6	75.6
Car 1			AXLE 2	-296.7	73.4	AXLE 4	-574.4	75.6
AXLE 1	-37.1	61.2	AXLE 3	-314.8	73.4	Car 20		
AXLE 2	-38.9	61.2	AXLE 4	-316.6	73.4	AXLE 1	-581.5	55.6
AXLE 3	-56.9	61.2	Car 11			AXLE 2	-583.2	55.6
AXLE 4	-58.7	61.2	AXLE 1	-323.6	84.5	AXLE 3	-601.3	55.6
Car 2			AXLE 2	-325.4	84.5	AXLE 4	-603.0	55.6
AXLE 1	-65.8	63.4	AXLE 3	-343.4	84.5	Car 21		
AXLE 2	-67.5	63.4	AXLE 4	-345.2	84.5	AXLE 1	-610.1	90.1
AXLE 3	-85.6	63.4	Car 12			AXLE 2	-611.9	90.1
AXLE 4	-87.4	63.4	AXLE 1	-352.3	81.2	AXLE 3	-629.9	90.1
Car 3			AXLE 2	-354.0	81.2	AXLE 4	-631.7	90.1
AXLE 1	-94.4	64.5	AXLE 3	-372.1	81.2	Car 22		
AXLE 2	-96.2	64.5	AXLE 4	-373.9	81.2	AXLE 1	-638.8	87.8
AXLE 3	-114.2	64.5	Car 13			AXLE 2	-640.5	87.8
AXLE 4	-116.0	64.5	AXLE 1	-380.9	80.1	AXLE 3	-658.6	87.8
Car 4			AXLE 2	-382.7	80.1	AXLE 4	-660.3	87.8
AXLE 1	-123.1	67.8	AXLE 3	-400.7	80.1	Car 23		
AXLE 2	-124.8	67.8	AXLE 4	-402.5	80.1	AXLE 1	-667.4	87.8
AXLE 3	-142.9	67.8	Car 14			AXLE 2	-669.2	87.8
AXLE 4	-144.7	67.8	AXLE 1	-409.6	75.6	AXLE 3	-687.2	87.8
Car 5			AXLE 2	-411.3	75.6	AXLE 4	-689.0	87.8
AXLE 1	-151.7	63.4	AXLE 3	-429.4	75.6	Car 24		
AXLE 2	-153.5	63.4	AXLE 4	-431.2	75.6	AXLE 1	-696.1	84.5
AXLE 3	-171.5	63.4	Car 15			AXLE 2	-697.8	84.5
AXLE 4	-173.3	63.4	AXLE 1	-438.2	75.6	AXLE 3	-715.9	84.5
Car 6			AXLE 2	-440.0	75.6	AXLE 4	-717.6	84.5
AXLE 1	-180.4	73.4	AXLE 3	-458.0	75.6	Car 25		
AXLE 2	-182.1	73.4	AXLE 4	-459.8	75.6	AXLE 1	-724.7	87.8
AXLE 3	-200.2	73.4	Car 16			AXLE 2	-726.5	87.8
AXLE 4	-202.0	73.4	AXLE 1	-466.9	79.0	AXLE 3	-744.5	87.8
Car 7			AXLE 2	-468.6	79.0	AXLE 4	-746.3	87.8
AXLE 1	-209.0	83.4	AXLE 3	-486.7	79.0	Car 26		
AXLE 2	-210.8	83.4	AXLE 4	-488.5	79.0	AXLE 1	-753.4	87.8
AXLE 3	-228.8	83.4	Car 17			AXLE 2	-755.1	87.8
AXLE 4	-230.6	83.4	AXLE 1	-495.5	64.5	AXLE 3	-773.2	87.8
Car 8			AXLE 2	-497.3	64.5	AXLE 4	-774.9	87.8

Axle distances in meters from first axle of Engine 1; Single wheel loads in kilonewtons.

Car 27		
AXLE 1	-782.0	90.1
AXLE 2	-783.8	90.1
AXLE 3	-801.8	90.1
AXLE 4	-803.6	90.1
Car 28		
AXLE 1	-810.7	89.0
AXLE 2	-812.4	89.0
AXLE 3	-830.5	89.0
AXLE 4	-832.2	89.0
Car 29		
AXLE 1	-839.3	87.8
AXLE 2	-841.1	87.8
AXLE 3	-859.1	87.8
AXLE 4	-860.9	87.8
Car 30		
AXLE 1	-868.0	87.8
AXLE 2	-869.7	87.8
AXLE 3	-887.8	87.8
AXLE 4	-889.5	87.8
Car 31		
AXLE 1	-896.6	87.8
AXLE 2	-898.4	87.8
AXLE 3	-916.4	87.8
AXLE 4	-918.2	87.8
Car 32		
AXLE 1	-925.3	87.8
AXLE 2	-927.0	87.8
AXLE 3	-945.1	87.8
AXLE 4	-946.8	87.8
Car 33		
AXLE 1	-953.9	75.6
AXLE 2	-955.7	75.6
AXLE 3	-973.7	75.6
AXLE 4	-975.5	75.6
Car 34		
AXLE 1	-982.6	73.4
AXLE 2	-984.3	73.4
AXLE 3	-1002.4	73.4
AXLE 4	-1004.2	73.4
Car 35		
AXLE 1	-1011.2	90.1
AXLE 2	-1013.0	90.1
AXLE 3	-1031.0	90.1
AXLE 4	-1032.8	90.1

Appendix B
Space Frame Model Details

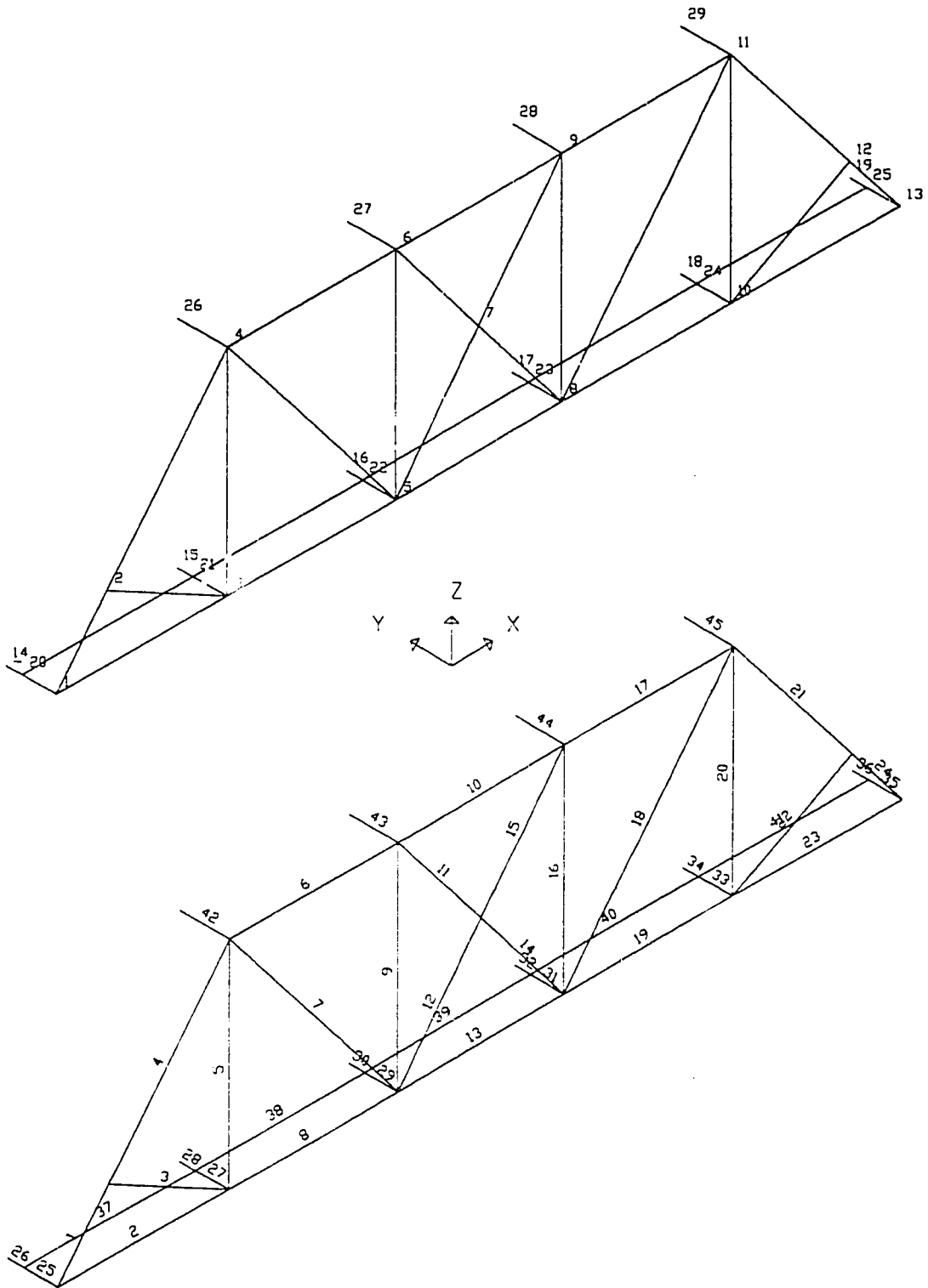


Figure B.1 Node and Element Numbers

SAP90 INPUT FILE for Miette River Bridge, Space Frame
SYSTEM

L=1

JOINTS

1	X=0	Y=0	Z=0
2	X=2262	Y=0	Z=2895.6
3	X=7620	Y=0	Z=0
4	X=7620	Y=0	Z=9753.6
5	X=15240	Y=0	Z=0
6	X=15240	Y=0	Z=9753.6
7	X=19050	Y=0	Z=4876.8
8	X=22860	Y=0	Z=0
9	X=22860	Y=0	Z=9753.6
10	X=30480	Y=0	Z=0
11	X=30480	Y=0	Z=9753.6
12	X=35838	Y=0	Z=2895.6
13	X=38100	Y=0	Z=0
14	X=0	Y=2262	Z=0
15	X=7620	Y=2262	Z=0
16	X=15240	Y=2262	Z=0
17	X=22860	Y=2262	Z=0
18	X=30480	Y=2262	Z=0
19	X=38100	Y=2262	Z=0
20	X=0	Y=1524	Z=0
21	X=7620	Y=1524	Z=0
22	X=15240	Y=1524	Z=0
23	X=22860	Y=1524	Z=0
24	X=30480	Y=1524	Z=0
25	X=38100	Y=1524	Z=0
26	X=7620	Y=2262	Z=9753.6
27	X=15240	Y=2262	Z=9753.6
28	X=22860	Y=2262	Z=9753.6
29	X=30480	Y=2262	Z=9753.6

RESTRAINTS

1	R=0,1,1,0,0,0
13	R=1,1,1,0,0,0
14 19 1	R=0,1,0,1,0,1
26 29 1	R=0,1,0,1,0,1

FRAME

NM=9 NSEC=50

1	A=13632	J=543933	I=295E6,58E6	E=208000	:DIAGONAL (U1-L2)
2	A=20406	J=709E6	I=21E6,580E6	E=208000	:TOP CHORD (U1-U2,U2-U2)
3	A=21690	J=709E6	I=21E6,580E6	E=208000	:BOT. CHORD (L0-L1,L1-L2,L2-L2)
4	A=30169	J=1672E6	I=194E6,944E6	E=208000	:END POST (L0-U1)
5	A=14761	J=590406	I=91E6,335E6	E=208000	:HANGER (U1-L1)
6	A=16445	J=636880	I=134E6,366E6	E=208000	:VERTICAL (U2-L2)
7	A=9787	J=307296	I=11E6,189E6	E=208000	:STRUTS (U2-M1-L2,M1/2-L1)

8	A=31690	J=2.52E6	I=92E6,7895E6	E=208000	:STRINGER (S1R,S1L,S2R,S2L,S3)
9	A=31594	J=1.64E6	I=82E6,12321E6	E=208000	:FLOOR BEAM (FB)
1	1	2		M=4	
2	1	3		M=3	
3	2	3		M=7	
4	2	4		M=4	
5	3	4		M=5	
6	4	6		M=2	
7	4	5		M=1	
8	3	5		M=3	
9	5	6		M=6	
10	6	9		M=2	
11	6	7		M=7	
12	5	7		M=7	
13	5	8		M=3	
14	7	8		M=7	
15	7	9		M=7	
16	8	9		M=6	
17	9	11		M=2	
18	8	11		M=1	
19	8	10		M=3	
20	10	11		M=6	
21	11	12		M=4	
22	10	12		M=7	
23	10	13		M=3	
24	12	13		M=4	
25	1	20		M=9	
26	20	14		M=9	
27	3	21		M=9	
28	21	15		M=9	
29	5	22		M=9	
30	22	16		M=9	
31	8	23		M=9	
32	23	17		M=9	
33	10	24		M=9	
34	24	18		M=9	
35	13	25		M=9	
36	25	19		M=9	
37	20	21		M=8	
38	21	22		M=8	
39	22	23		M=8	
40	23	24		M=8	
41	24	25		M=8	
42	4	26		M=7	
43	6	27		M=7	
44	9	28		M=7	
45	11	29		M=7	

BRIDGE

NL=1
L=1
S=1
F=37,41,1

Appendix C

Train Simulation Algorithm
Effective Strain Range Algorithm

```

C      TRAIN SIMULATION ALGORITHM
C
C      Strain record simulator for passing trains, Miette River Bridge
C      By Jeff DiBattista, April 1994
C
C      This program uses influence lines and data defining the weights
C      and geometries of cars to simulate the crossing of a train over
C      the Miette River Bridge. The program generates a strain record for
C      the tension diagonals.
C
C      The user is asked to input the speed of the train and the duration
C      of the simulation (in case only a partial strain record is desired).
C      The program then asks if the effects of bending are to be included,
C      and if so, if output is to be for the north or south flange.
C
C      Input files are "ILAX" (influence line, axial), "ILBEN" (influence line
C      bending), and "AXLES" (axle locations and wheel loads)
C      Output strain record file is "STRAINS"
C      Influence lines are defined at 246 stations along the bridge
C
C      INTEGER I,N,STATION,NUMAXLES,TSTEPS,TYPE
C      REAL*4 ILAX(300),ILBEN(300),DISTREAL,TIMEREAL,SPEED,AXLEDIST(1000)
C      REAL*4 AXLELOAD(1000),AXLOAD,BENI,OAD,STRAIN,FLANGE
C      OPEN (1,FILE='ILAX')
C      OPEN (2,FILE='AXLES')
C      OPEN (3,FILE='STRAINS')
C      OPEN (4,FILE='ILBEN')
C      PRINT *,'ENTER SPEED IN m/s WITH DECIMAL:'
C      READ *,SPEED
C      PRINT *,'ENTER END TIME IN s WITH DECIMAL:'
C      READ *,ENDTIME
C      PRINT *,'ENTER "1" FOR NO BENDING, "2" FOR BENDING'
C      READ *,TYPE
C      IF (TYPE.EQ.2) THEN
C          PRINT *,'ENTER 1 FOR SOUTH FLANGE, -1 FOR NORTH FLANGE'
C          READ *,FLANGE
C      ENDIF
C      TSTEPS=ENDTIME*10
C      WRITE (3,*) TSTEPS
C
C      **** Read input files ****
C
C      DO 10 I=1,246,1
10      READ (1,100) ILAX(I)
C      DO 12 I=1,246,1
12      ILBEN(I)=0.
C      IF (TYPE.EQ.2) THEN
C          DO 15 I=1,246,1
15      READ (4,100) ILBEN(I)

```

```

ENDIF
READ (2,*) NUMAXLES
DO 20 I=1,NUMAXLES,1
  20   READ (2,*) AXLEDIST(I),AXLELOAD(I)
  C
  C   **** Move train across bridge, looping over 0.1 second increments ****
  C
  TIMEREAL=0.
  STRAIN=0.
  WHILE (TIMEREAL.LT.ENDTIME)
  C
  C   **** At each time increment, loop over all axles ****
  C
  25   DO 30 I=1,NUMAXLES,1
        DISTREAL=SECFD*TIMEREAL+AXLEDIST(I)
  C
  C   **** For each axle, check to see if it is on the bridge ****
  C
        IF (DISTREAL.LT.0.1.OR.DISTREAL.GT.38.1) THEN
          AXLOAD=0.
          BENLOAD=0.
        ELSE
  C
  C   **** Convert distance (m) to integer station number ****
  C
          STATION=DISTREAL*6.456692913
          IF (STATION.EQ.0) THEN
            AXLOAD=0.
            BENLOAD=0.
            GOTO 30
          ENIF
          AXLOAD=AXLELOAD(I)*ILAX(STATION)
          BENLOAD=AXLELOAD(I)*ILBEN(STATION)
        ENDIF
  C
  C   **** Calculate strain contributed by this axle for this time step ****
  C
        STRAIN=STRAIN+AXLOAD/(2.7238)+FLANGE*BENLOAD*0.00301695
  30   CONTINUE
  C
  C   **** Record total strain at this time step ****
  C
        WRITE (3,*) STRAIN
        STRAIN=0.
        TIMEREAL=TIMEREAL+0.1
  ENDWHILE
100  FORMAT (1X,E12.5)
      END

```


C **EFFECTIVE STRAIN RANGE ALGORITHM**

C

C Peak detecting rainflow counting equivalent strain range algorithm

C By Jeff DiBattista, March 1995

C

C This program reads a strain record, finds all minima and maxima,
C and uses a one-pass rainflow counting method (based on Downing and
C Socie) to find strain ranges. To remove small ranges (due to electronic
C noise, vibrations, etc.) from the record, the user is prompted for
C a filter value, below which all strain ranges are deleted. Finally,
C based on the ranges greater than the filter value, the effective
C root-mean-cube strain range is calculated.

C

C ***** Detects peaks and saves them in file "peaks" *****

C

C Input file is "STRAINS"

C Line 1 of "STRAINS" is number of data points

C

```
INTEGER N,SLOPE1,SLOPE2
REAL A,B,C,ALLDATA(1000)
OPEN (1,FILE='STRAINS')
OPEN (2,FILE='PEAKS')
READ (1,*) N
DO 10 I=1,N,1
10  READ (1,*) ALLDATA(I)
   PRINT *, 'CALCULATING PEAKS'
   WRITE (2,*) ALLDATA(I),0
   DO 20 I=1,N-2,1
     SLOPE1=-1
     SLOPE2=-1
     A=ALLDATA(I)
     B=ALLDATA(I+1)
     C=ALLDATA(I+2)
     IF (A.LT.B) THEN
       SLOPE1=1
     ENDIF
     IF (B.LT.C) THEN
       SLOPE2=1
     ENDIF
     IF (SLOPE1.NE.SLOPE2) THEN
       WRITE (2,*) B,0
     ENDIF
20  CONTINUE
   WRITE (2,*) ALLDATA(N),1
   CALL RAINFLOW
   CALL EQUIVALENT
END
```

C

```

C      ***** One-pass rainflow counting of "peaks," saves to "ranges" *****
C
SUBROUTINE RAINFLOW
DIMENSION E(1000)
OPEN (2,FILE='RANGES')
N=2
J=0
ISTART=1
PRINT *,'CALCULATING RANGES'
CALL DATA(E(1),K)
100 CALL DATA(E(2),K)
IF (E(1).EQ.E(2)) GOTO 100
SLOPE=1.
IF (E(1).GT.E(2)) THEN
    SLOPE=-1.
ENDIF
1 CALL DATA(P,K)
IF (K.EQ.1) GOTO 6
N=N+1
SLOPE=SLOPE*(-1.)
E(N)=P
2 IF (N.LT.ISTART+1) GOTO 1
X=SLOPE*(E(N)-E(N-1))
IF (X.IE.0.) GOTO 200
IF (N.LT.ISTART+2) GOTO 1
Y=SLOPE*(E(N-2)-E(N-1))
3 IF (X.LT.Y) GOTO 1
IF (X.EQ.Y.AND.ISTART.EQ.N-2) GOTO 1
IF (X.GT.Y.AND.ISTART.EQ.N-2) GOTO 4
IF (X.GE.Y.AND.ISTART.NE.N-2) GOTO 5
4 ISTART=ISTART+1
GOTO 1
5 RANGE=Y
XMEAN=(E(N-1)+E(N-2))/2.
PRINT *,RANGE
WRITE (2,*) RANGE
N=N-2
E(N)=E(N+2)
GOTO 2
6 J=J+1
IF(J.GT.ISTART) THEN
    WRITE (2,*) 0.000001
    RETURN
ENDIF
N=N+1
SLOPE=SLOPE*(-1.)
E(N)=E(J)
7 IF (N.LT.ISTART+1) GOTO 6
X=SLOPE*(E(N)-E(N-1))

```

```

      IF(X.LE.0.) GOTO 300
      IF (N.LT.ISTART+2) GOTO 6
      Y=SLOPE*(E(N-2)-E(N-1))
8     IF(X.LT.Y) GOTO 6
      IF(X.GE.Y) GOTO 9
9     RANGE=Y
      XMEAN=(E(N-1)+E(N-2))/2.
      PRINT *,RANGE
      WRITE (2,*) RANGE
      N=N-2
      E(N)=E(N+2)
      GOTO 7
200  N=N-1
      E(N)=E(N+1)
      SLOPE=SLOPE*(-1.)
      GOTO 2
300  N=N-1
      E(N)=E(N+1)
      SLOPE=SLOPE*(-1.)
      GOTO 7
      END

C
C     ***** Reads "peaks" file for rainflow subroutine *****
C
      SUBROUTINE DATA(P,K)
      OPEN (1,FILE='PEAKS')
      READ (1,*) P,K
      RETURN
      END

C
C     ***** Calculates equivalent strain range and number of cycles *****
C
      SUBROUTINE EQUIVALENT
      REAL*4 SRI,SRE,FILTER
      OPEN (1,FILE='RANGES')
      N=0.
      SRE=0.
      PRINT *,'ENTER FILTER VALUE WITH DECIMAL POINT:'
      READ *,FILTER
5     READ (1,*) SRI
      IF (SRI.EQ.0.000001) GOTO 10
      IF (SRI.LT.FILTER) GOTO 5
      SRE=SRE+SRI**3.
      N=N+1.
      GOTO 5
10    SRE=(SRE/N)**(1./3.)
      PRINT *,'EFFECTIVE RANGE:                NUMBER OF CYCLES:'
      PRINT *,SRE,N
      END

```

Appendix D
Results of Tension Coupon Tests

Table D.1 Tension Coupon Test Results

Coupon	Elastic Modulus (MPa)	Static Yield Stress (MPa)	Static Ultimate Stress (MPa)	Failure Strain ($\mu\epsilon$)
Web #1	206 000	229	364	341 000
Web #2	210 000	217	375	361 000
Angle #1	210 000	240	387	343 000
Angle #2	210 000	237	389	371 000
Gusset #1	211 000	227	400	332 000
Gusset #2	206 000	221	400	330 000

Appendix E
Crack Tip Location Observations

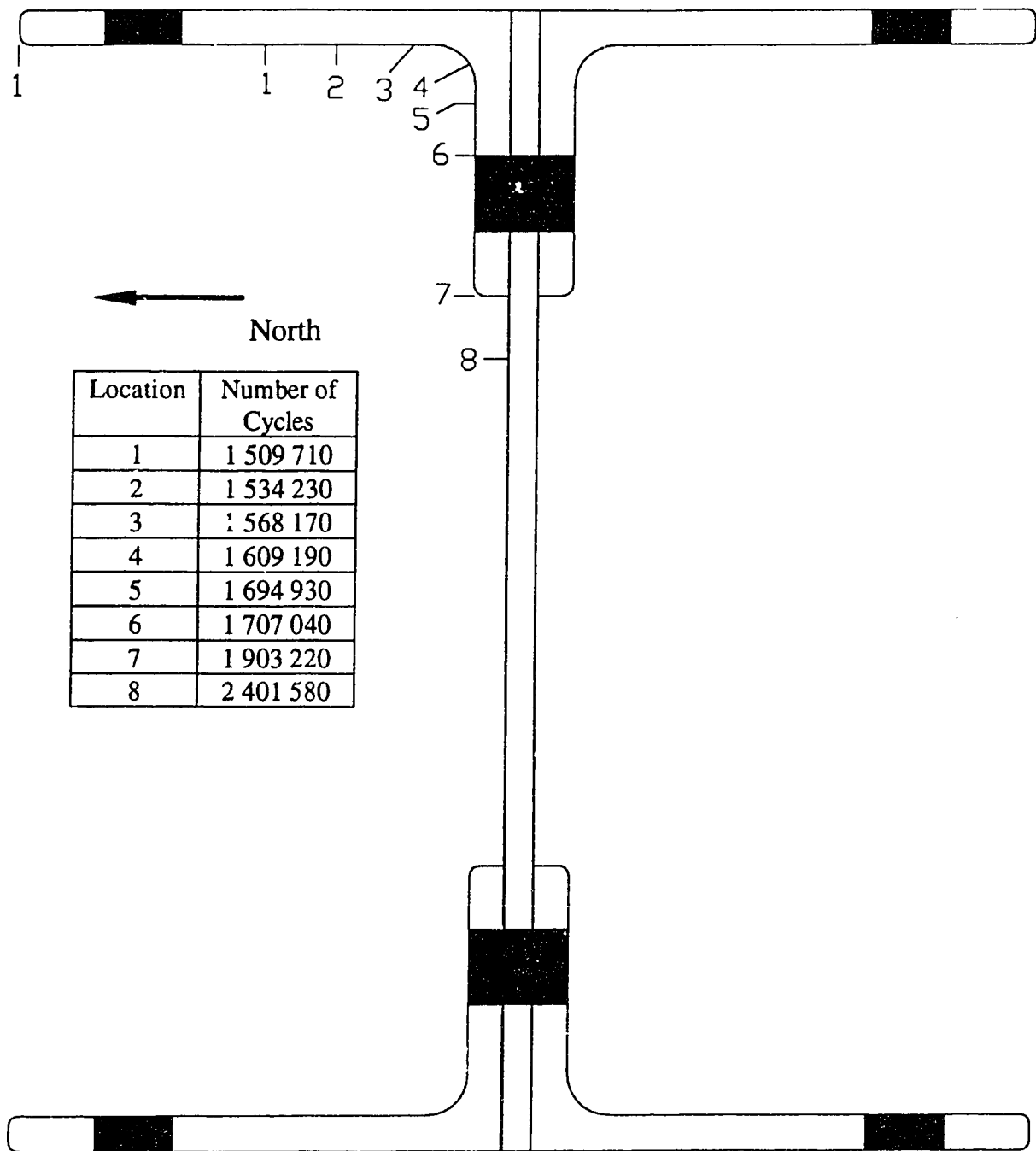


Figure E.1 Specimen BD1
Scale 1:2

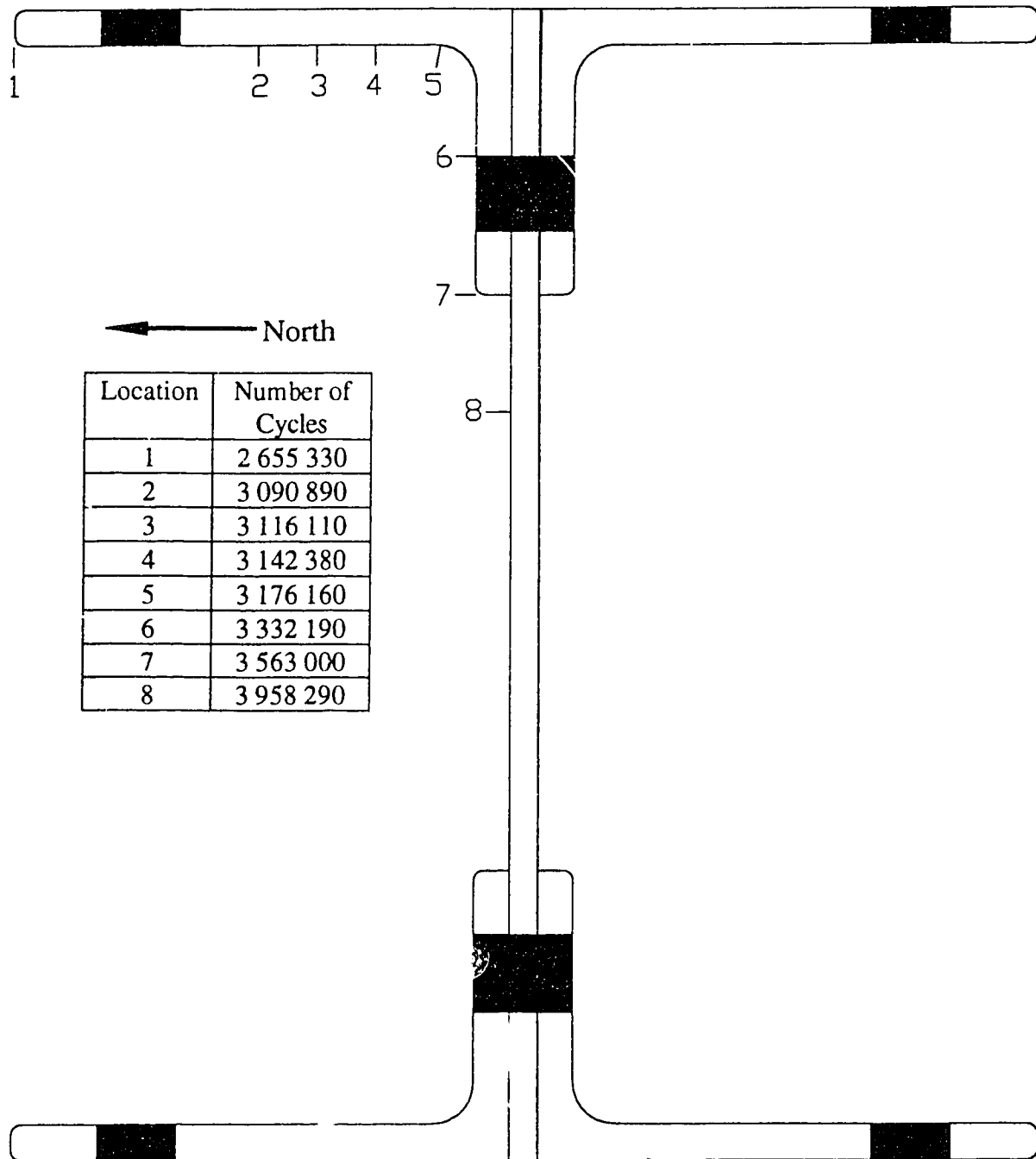


Figure E.2 Specimen BD2
Scale 1:2

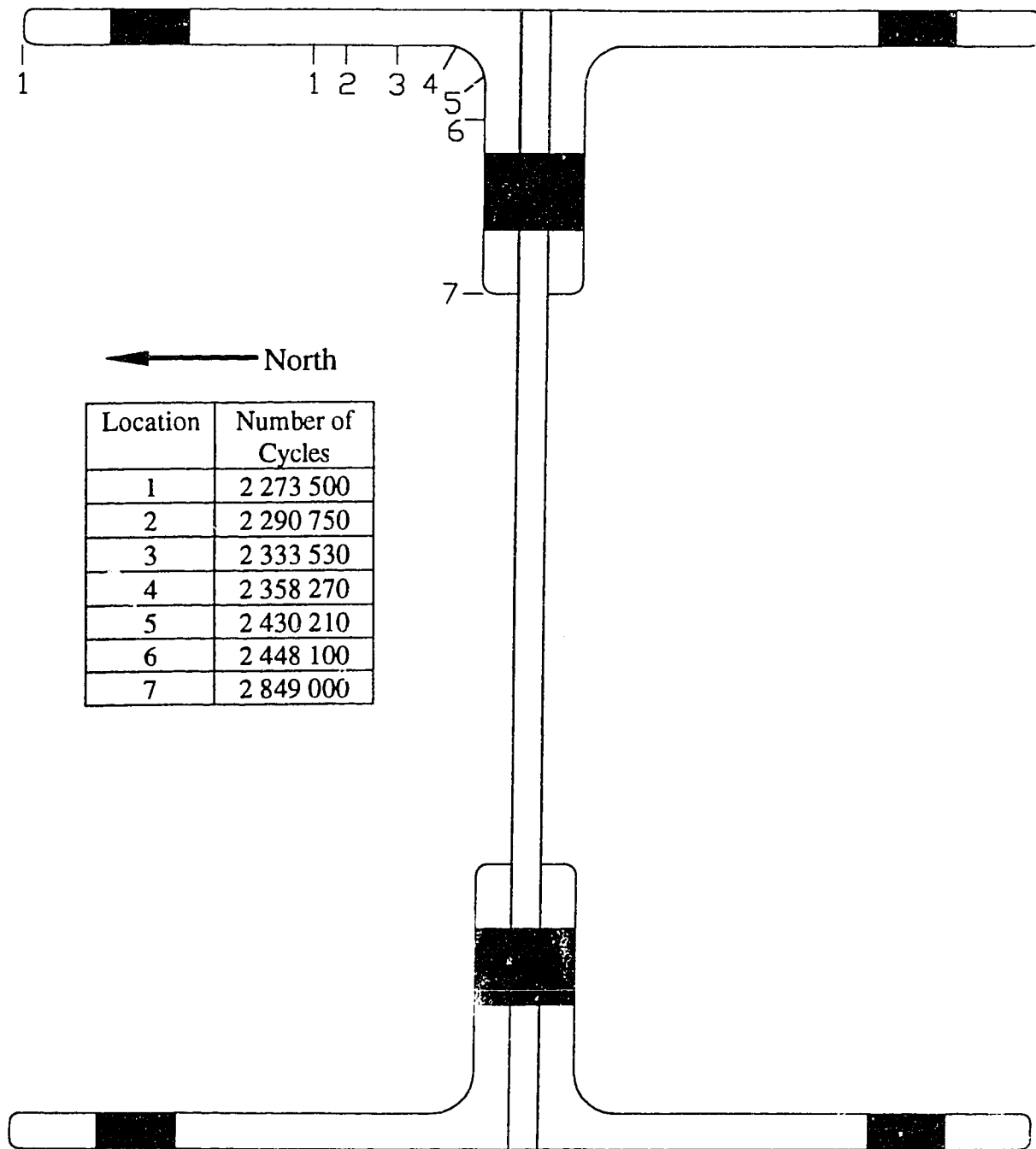


Figure E.3 Specimen BD3

Scale 1:2

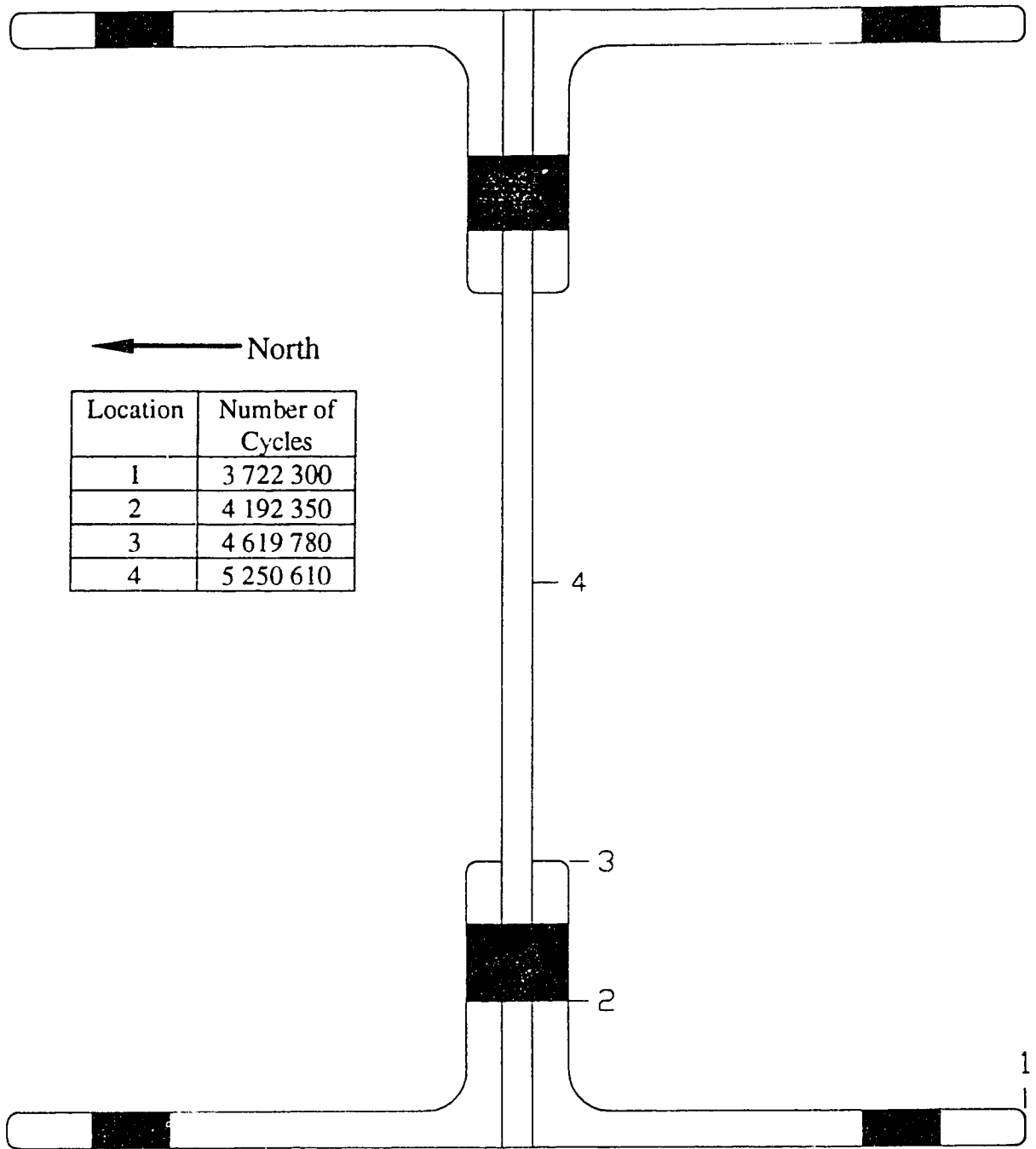


Figure E.4 Specimen BD4

Scale 1:2

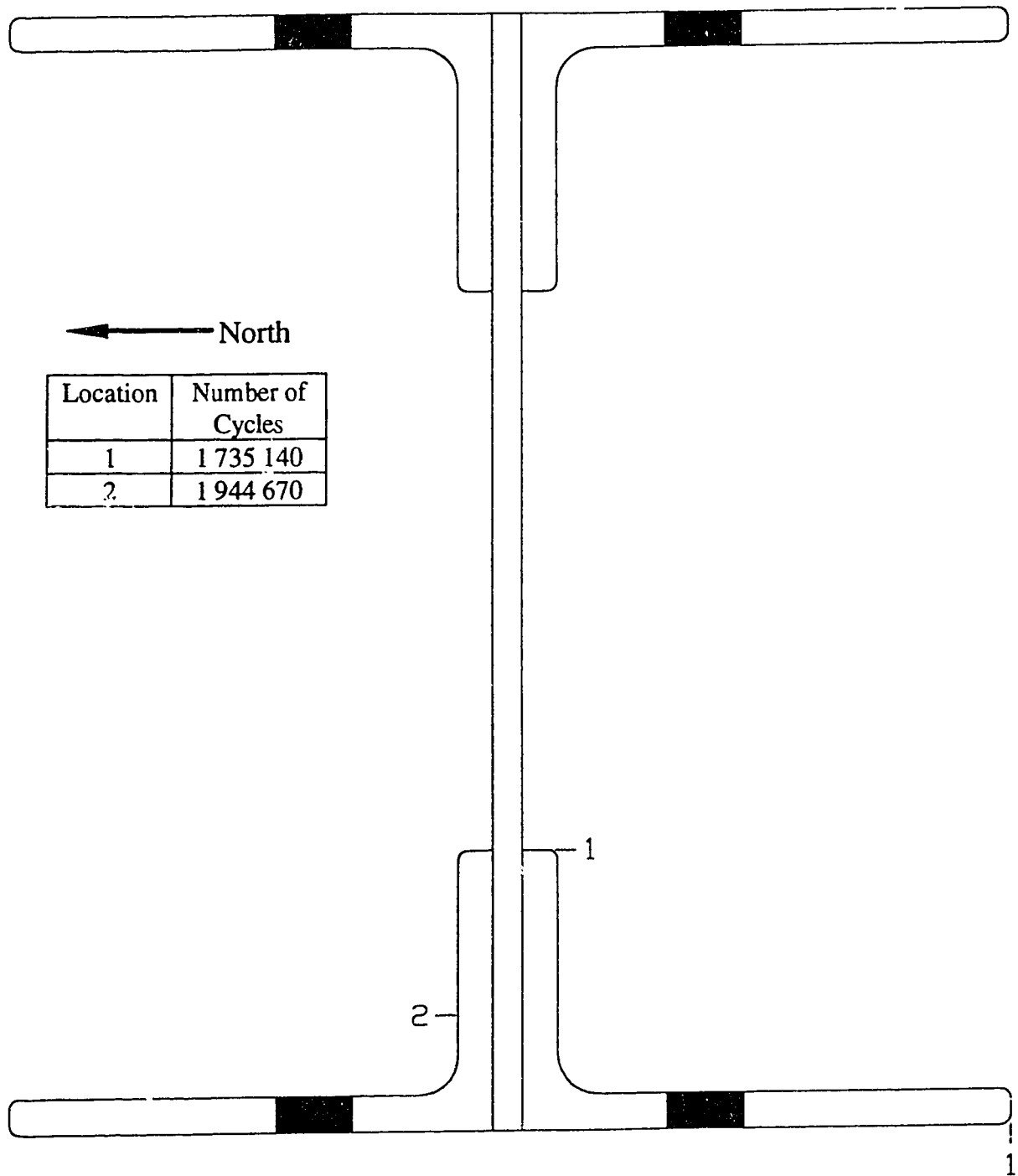


Figure E.5 Specimen TD1

Scale 1:2

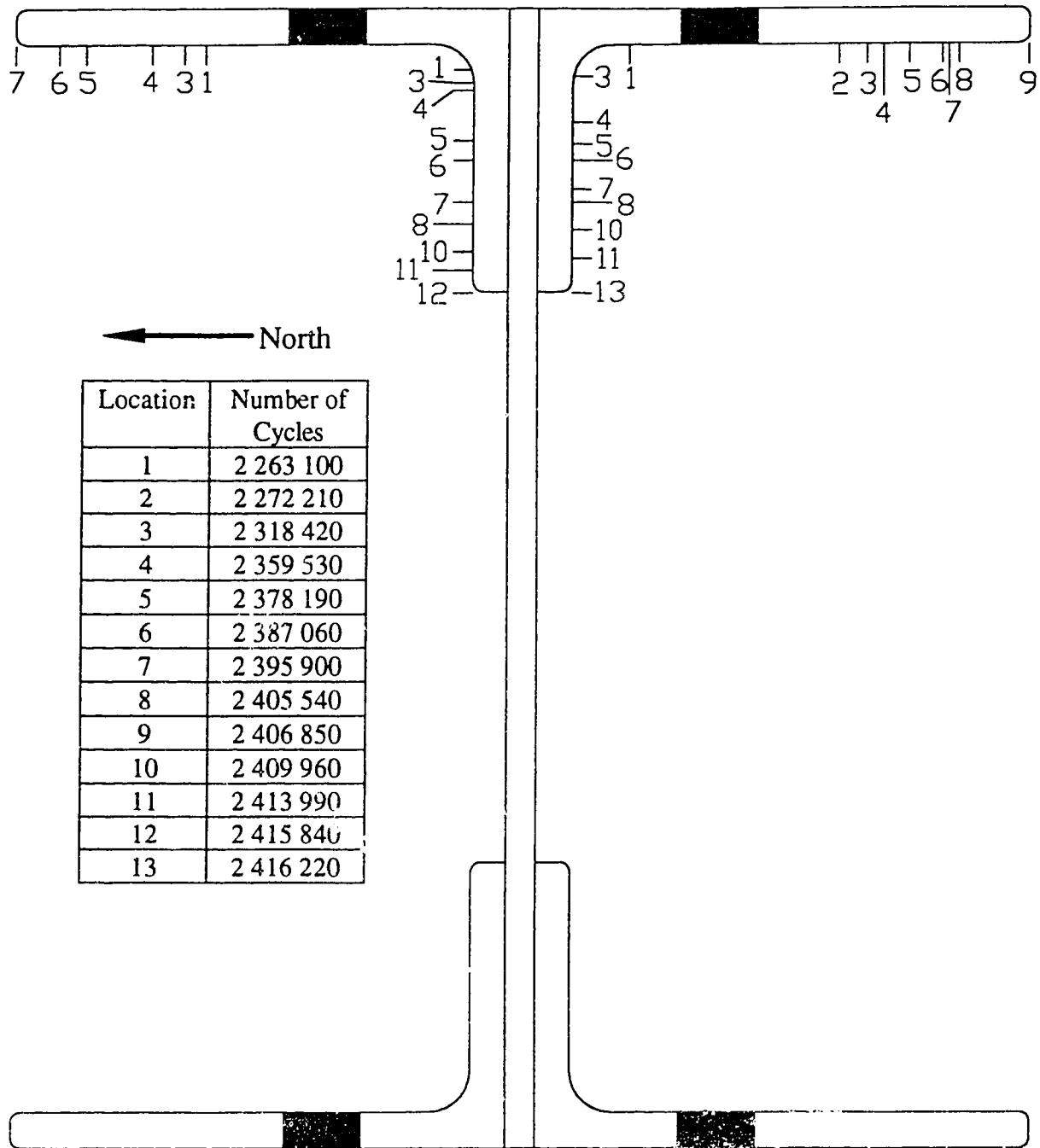


Figure E.6 Specimen TD2

Scale 1:2

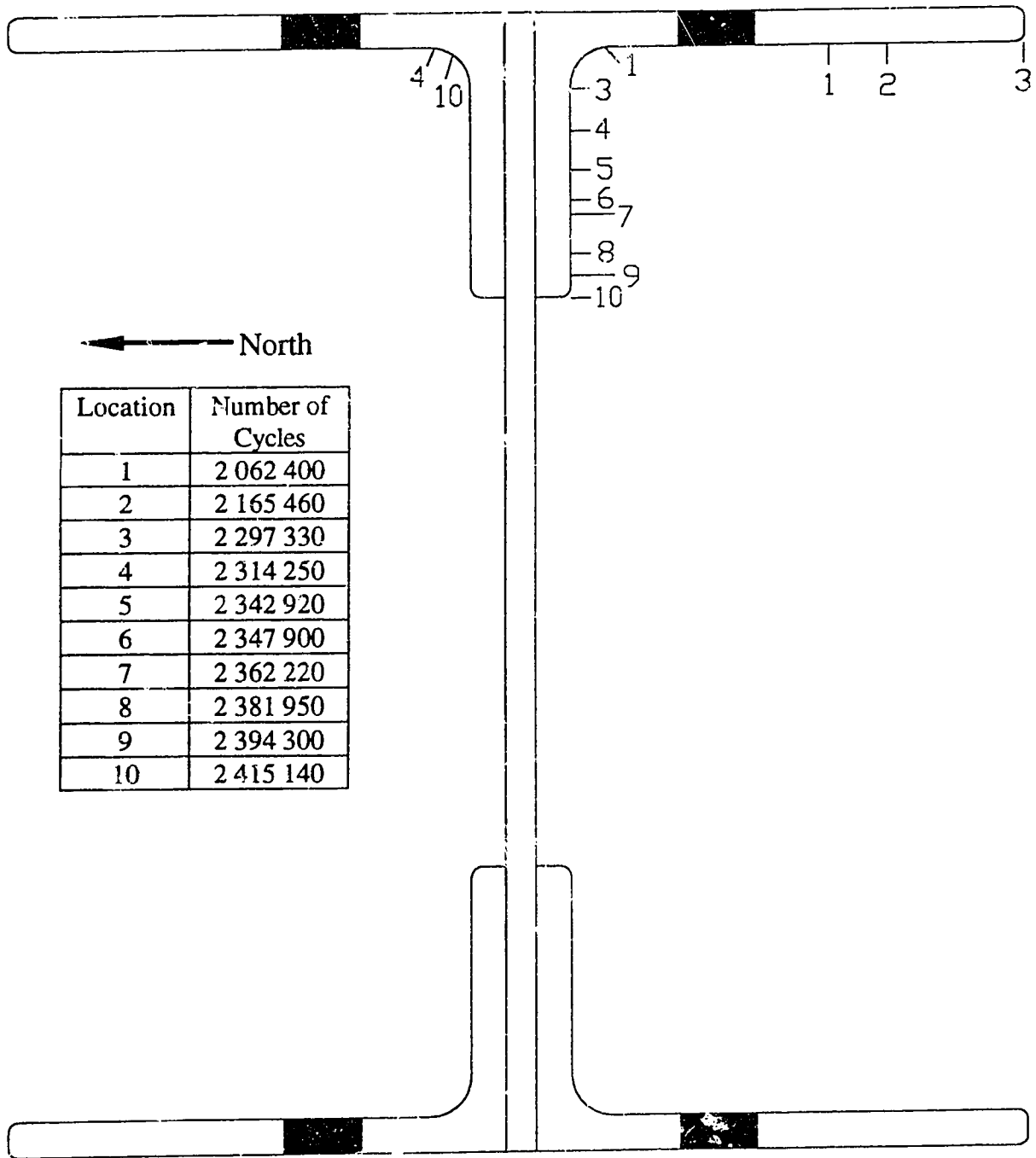


Figure E.7 Specimen TD3

Scale 1:2